TECHNISCHE
UNIVERSITÄT
WIEN
Vienna University of Technology

INSTITUT FÜR
MECHANIK UND
MECHATRONIK
Mechanics & Mechatronics

DISSERTATION

Cooperative fuzzy model predictive control of a multi-zone office building

ausgeführt zum Zwecke der Erlangung des akademischen Grades
eines Doktors der technischen Wissenschaften
unter der Leitung von

Ao.Univ.Prof. Dipl.-Ing. Dr.techn. Martin Kozek

am Institut für Mechanik und Mechatronik
Abteilung für Regelungstechnik und Prozessautomatisierung

eingereicht an der Technischen Universität Wien,
Fakultät für Maschinenwesen und Betriebswissenschaften

von

Dipl.-Ing. Michaela Killian
Hauptstraße 35
2000 Stockerau

Geboren am 14.06.1988
Matr.Nr.: 0625190

Wien, am 7. Januar 2016

Meiner Familie

Danksagung

Leider lässt sich eine wahrhafte Dankbarkeit mit Worten nicht ausdrücken.

Johann Wolfgang von Goethe (1749-1832)

Eidesstattliche Erklärung

Ich erkläre eidesstattlich, dass ich die Arbeit selbständig angefertigt, keine anderen als die angegebenen Hilfsmittel benutzt und alle aus ungedruckten Quellen, gedruckter Literatur oder aus dem Internet im Wortlaut oder im wesentlichen Inhalt übernommenen Formulierungen und Konzepte gemäß den Richtlinien wissenschaftlicher Arbeiten zitiert, durch Fußnoten gekennzeichnet bzw. mit genauer Quellenangabe kenntlich gemacht habe.

Wien, am 7. Januar 2016 Michaela Killian

Kurzfassung

Die vorliegende Dissertation gibt einen Überblick über die Ergebnisse eines Projektes an der Technischen Universität Wien seit 2012. Die enthaltenen Veröffentlichungen sind im Laufe eines Kooperationsprojektes zwischen dem Institut für Mechanik und Mechatronik (Abteilung für Regelungstechnik und Prozessautomatisierung), der FH Joanneum Kapfenberg als Forschungspartner und der evon-automation GmbH, Gleisdorf als Industriepartner entstanden. Das Projekt wurde von der Österreichischen Forschungsförderungsgesellschaft (FFG Nr. 832103) gefördert.

Energieeinsparung in Bürogebäuden ist ein aktuelles Thema, welches in dieser Arbeit behandelt wird. Der Schwerpunkt liegt auf der Entwicklung neuer Methoden für intelligente und energieeffiziente Gebäuderegelungen, welche mit neuen modellprädiktiven Regelungsstrategien umgesetzt wurden. Darüber hinaus konnte die erste Inbetriebnahme in einem realen Gebäude mit sehr guten Ergebnissen abgeschlossen werden.

In dieser Dissertation wird ein nichtlineares modellprädiktives Regelungskonzept für komplexe Bürogebäude präsentiert. Die Auflösung widersprüchlicher Optimierungsziele, wie die Maximierung des Benutzerkomforts und die Minimierung des Energieverbrauchs, stellt in der Gebäudeautomatisierung die größte Herausforderung dar. Modellprädiktive Regelung (MPC) ist in der Lage diese kontroversen Ziele zu lösen, indem sie Wettervorhersagen und/oder Belegungsinformationen berücksichtigt. Da die Dynamik in Gebäuden nichtlinear ist, ist für die Regelung ein geeignetes Modell notwendig. In dieser Arbeit wird das nichtlineare Gebäudemodell durch ein datenbasiertes Black-Box Modell dargestellt, welches direkt für die MPC Auslegung verwendet werden kann. Das komplexe nichtlineare Optimierungsproblem wurde in mehrere weniger komplexe Teilprobleme (Gebäudezonen) aufgeteilt. Jede Zone wird unabhängig von den anderen mit einem individuellen nichtlinearen MPC (Fuzzy MPC - FMPC) geregelt. Wegen einer Betonteilaktivierung im Gebäude existieren Kopplungen zwischen den Zonen, somit ist das globale Ziel, eine kooperative Lösung zwischen den Zonen zu finden. Dieses Problem führt zu einer Kooperation der FMPCs, somit zu einem kooperativen Fuzzy MPC (CFMPC), wobei eine unterliegende Iterationsschleife Konvergenz garantiert. Für den CFMPC wurde Stabilität des geschlossenen Regelkreises und Konvergenz der kooperativen Iterationsschleife nachgewiesen. Darüber hinaus ist dieses Konzept allgemein für komplexe Bürogebäude geeignet, da es in der Lage ist optimal mit Beschränkungen sowie mit Störungen umzugehen.

Abstract

The present PhD Thesis provides an overview on the results of a research project at the Vienna University of Technology since 2012. The publications originated in the course of a cooperation project between the Institute of Mechanics and Mechatronics (Division of Control and Process Automation), the FH Joanneum Kapfenberg (University of applied science) as research partner, and evon-automation GmbH, Gleisdorf as industrial partner. The project has been funded by the Austrian Research Promotion Agency (FFG No. 832103).

A contemporary issue of potentials for saving energy in buildings is discussed in this work. The research was focused on the development of new methodologies for smart and energy-efficient building automation systems. In this context a new nonlinear model predictive control strategy has been developed for a specific building. Moreover, the commissioning in a this real building succeeded with excellent results.

In this PhD Thesis a nonlinear model predictive control (MPC) concept for complex office buildings is presented. Conflicting optimization goals naturally arise in buildings, where the maximization of user comfort versus the minimization of energy consumption poses the main challenge. MPC technologies are able to reduce the energy demand while increasing the user comfort, by taking weather predictions and/or occupancy information into account. Dynamic thermal behavior of buildings is typically nonlinear, thus, for controlling a suitable model is necessary. In this work the overall nonlinear building model is a data-driven black-box model, which can be directly used for controller design. The proposed modeling approach is applicable for other complex buildings. For the demonstration building the complex nonlinear optimization problem has been split into a set of less complex subproblems (different building zones). For each zone an independent nonlinear MPC (fuzzy MPC - FMPC) is designed. Because of an integrated thermal activated building system couplings between different zones occur, thus, the optimization goal is to find a cooperation between the zones. The overall problem formulation leads to a cooperation of the FMPCs, to a cooperative fuzzy MPC (CFMPC), where an underlying cooperative iteration-loop guarantees convergence. Closed-loop stability and convergence of the cooperative iteration-loop has been proven for the CFMPC concept. Additionally, this concept is suitable for complex multi-zone office buildings, as it can optimally deal with input and output constraints as well as with disturbances.

Contents

List of Figures

Chapter 1

Overview

The building sector accounts for a major portion of the world's energy consumption, thus, efficient usage of energy is very important. A model predictive controller scheme has been developed during this work and implemented in a demonstration building.

In Chap. 1 a motivation, the proposed concepts and the related basic research are presented, the first results of the commissioning in the real building are given, and the main contribution of the selected journal articles is described. The publications itself and my own contribution in particular articles can be found in Chap. 2.

1.1 Motivation and problem statement

The global energy consumption of buildings, both residential and commercial, accounts between 20 % and 40 % in developed countries [1]. Thus, efficient usage of energy in buildings is an important task. Conflicting optimization goals naturally arise in buildings, where the maximization of user comfort versus the minimization of energy consumption poses the main challenge. Model predictive control (MPC) is the ideal control strategy to deal with such problems, because both, forecasts of external disturbances as weather (ambient temperature and radiance) and internal disturbances (occupancy) can be explicitly handled by MPCs. Furthermore, MPC is able to deal with input-constraints as well as with output-constraints. The general problem is presented in Fig. 1.1, where ϑ^{ref} represents the reference value for the indoor room temperature and $\vartheta^{\mathrm{act}}_{\mathrm{mean}}$ the actual mean indoor room temperature of the multi-zone office building.

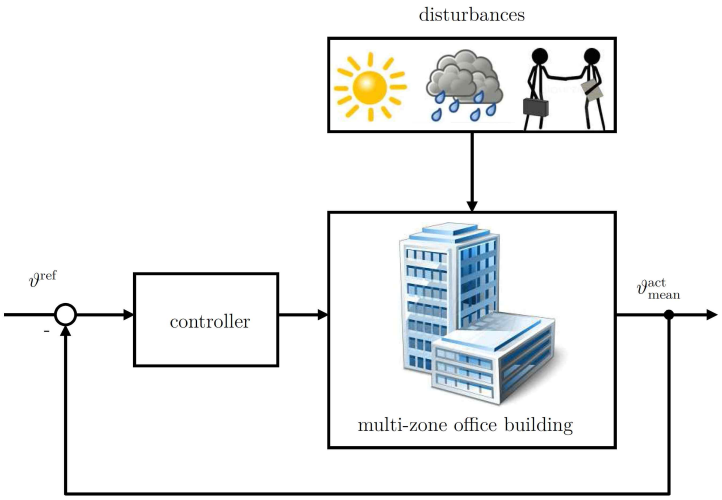

Figure 1.1: General problem scheme of controlling a multi-zone office building with internal and external disturbances.

The controller given in Fig. 1.1 consists of two nonlinear MPCs, on the one hand a cooperative fuzzy MPC and on the other hand a mixed-integer MPC, for details see Sec. 1.1.2.

The main part, presented in this work, is the cooperative fuzzy MPC, which guarantees user comfort in a multi-zone demonstration building: University of Salzburg, Austria.

1.1.1 State-of-the-art review

Classical model predictive control (MPC) approaches are presented in [2, 3]. However, thermal behavior of buildings is typically nonlinear, thus, controlling complex nonlinear dynamic systems with MPC is a challenging upcoming task in the area of building automation. Due to the typically high order, internal and external disturbances, and strong coupling effects in buildings it is difficult, if not impossible, to directly apply nonlinear control design methods.

Two effective methods to deal with this problem are: (i) Splitting the complex nonlinear problem into a set of less complex subproblems, solving the subproblems independently, and finding a cooperation between the set of subproblems. Note that a global optimum and stability may not be guaranteed in this case, [2, 4, 5]. (ii) Using local linear model networks (LLMNs) [6]. This LLMN approach is equivalent to Takagi-Sugeno (TS)-fuzzy modeling, and an effective way to control such systems is given by fuzzy control, [7, 8]. Utilizing the LLMN or TS-fuzzy approach, respectively, the overall complex nonlinear system is represented by a weighted superposition of the local linear models (LLMs).

In the field of building automation recent papers have shown that energy consumption can be reduced significantly with the MPC technology, e. g. [9]. Taking the uncertainty

of disturbances into account either by the use of weather predictions, [10], and/or occupancy information, [11], by using stochastic MPC (SMPC) was found to be superior in terms of comfort violations, [12, 13]. In [14] a two level distributed MPC approach is presented, distinguishing energy conversion and energy distribution without explicit interface between the controllers. The authors of [15] present an energy efficient MPC for temperature control, based on a model from a simulation package. The focus in [15] is on controlling the vapor compression cycle in an air-condition system, which is used for cooling. An MPC only for a building heating system is introduced in [16], in contrast to [14], where only building cooling systems are taken into account. In opposition to [14, 15, 16], in this work the building is controlled for heating and cooling. A fuzzy modeling approach for buildings is given in [17]. Škrjanc et al. [17] compared both: theoretical and experimental modeling. The authors of [18] use fuzzy logic-based advanced on-off control for thermal control in residential buildings. They achieved a reduction of energy consumption while improving the control performance.

In this PhD Thesis, not only a straight-forward FMPC for buildings is shown. A more intelligent algorithm for more than one fuzzy MPC (FMPC) is given, a coordinated FMPC (CFMPC). This problem formulation is similar to distributed MPCs, [19], both leading to a suboptimal solution. The authors of [19] present a distributed MPC structure for thermal regulation in buildings with an inner cooperation-loop. In [19], a simulated building with 3 rooms (one room is one zone) is presented. Moreover, only heating is proposed. In contrast to [19], in this work a real demonstration building with 250 rooms per floor is shown. Therefore, the complexity in the recent work is much higher and the optimization problem for all seasons is more challenging. Furthermore, in [19], only output-coupling is taken into account, which is irrelevant in sense of building temperature control where the room/zone differences are very small. It is much more complex to consider input-coupled systems, as it is presented in the recent work. Furthermore, [4] illustrates the concept of suboptimal MPCs. Scokeart et al. [4] establish conditions under which suboptimal MPCs are stabilizing. The theoretical background of cooperative MPCs is given in [20], where the theoretical assumptions are discussed and proved. Besides the guarantee of user comfort, saving energy and therewith incurred expenses is a current research area for MPC application in building as well, [21]. Therefore, also hybrid MPC for storage tanks in the buildings' supply level, [22] is an important issue in the area of building automation.

In this work however, nonlinear modeling is required for approximating the considered dynamic building behavior. Because of the special nonlinar model approach, a FMPC has been designed, which is completely new in case of fully automated building systems for heating and cooling. Furthermore, CFMPC has been developed in the course of this work, which allows to cooperate between different building zones. For this CFMPC closed-loop stability and convergence has been proven and published. Therefore, a new concept for fuzzy control has been developed.

1.1.2 Problem definition

In case of model predictive control (MPC) of buildings the compensation of disturbances belongs to the most challenging tasks. Both, external disturbances for buildings such as weather (ambient temperature and radiance) and internal disturbances (occupancy) can be explicitly handled by MPCs. Also large time-delays caused by the building's heat capacity, strong couplings between different building zones, and constraints (technical and thermal) in all variables can be incorporated in the MPC optimization. This complete coverage of the overall control problem together with the possibility to directly balance the trade-off between comfort and energy saving makes a strong point for MPC in building automation. Furthermore, the predictions of flexible pricing can also be considered in the MPC optimization problem.

Since one of the most time-consuming parts in the design of model-based controllers is the model design, it is essential to choose the best fitting model structure. Therefore, modeling and zoning has to approximate the nonlinear dynamic behavior of complex buildings. In addition, the building's orientation (because of different radiance impact) and the energy supply shafts are important facts to choose the different buildings zones.

In the specific demonstration building time constants in the user comfort level differ from those of the energy supply level. Therefore, each level needs an appropriate model for the specific nonlinear dynamics. Also in terms of the control purpose different problems occur for each level, thus, the complexity of modeling and controlling is definitely high.

1.2 Goals

The overall goal is to split the global control problem into two less complex optimization problems. On the one hand user comfort has to be guaranteed, and on the other hand the potential of energy savings has to be utilized in the best way. In addition, because of the different dynamical behavior and conflicting optimization goals of each building level (see Sec. 1.1.2) a hierarchical concept has been developed. The hierarchical concept consists of two different nonlinear MPCs, in the user comfort level the user comfort is maximized and in the energy supply level the energy demand is minimized.

Moreover, because of different building zones a cooperation between these zones has to be developed in the user comfort level, which leads to a cooperative nonlinear MPC. The nonlinearity is covered by local linear model networks, and the resulting controller is a so-called fuzzy MPC, thus, a cooperative fuzzy MPC (CFMPC) is developed for guaranteeing comfort under technical and thermal constraints. The complete theory of the CFMPC has been developed, closed-loop stability and convergence of the cooperation has been proven. Furthermore, in the supply level a mixed-integer MPC (MI-MPC) is given to optimize the switching between different supply sources.

Neither the hierarchical concept, nor the different nonlinear MPCs are state-of-the-art controllers in the field of building automation. Using just the CFMPC or the MI-MPC is already a benefit for industry, because the optimization problems are decoupled and are possible to be applied separately. Thus, flexibility for an implementation in real buildings is given.

1.3 Methodology

In this work, two main research results are presented. The first one is the modeling of a nonlinear dynamical building behavior under different assumptions and constraints, which is suitable for MPC. The second one is, based on previously defined models, the design and development of a proper nonlinear MPC concept for a multi-zone building.

1.3.1 General concept

Because of conflicting optimization goals the overall control goal is split into two less complex decoupled optimization goals: 1) maximization of user comfort, and 2) minimization of energy consumption. For both problems nonlinear MPC concepts are used and applied in the real demonstration building. On the one hand a cooperative fuzzy MPC (CFMPC) is developed to guarantee user comfort, and on the other hand a mixed-integer MPC (MI-MPC) was designed as energy management system. Furthermore, the multi-zone office building was split into two different models as well: 1) a model for user comfort called “building”, and 2) a model of the supply level in the basement of the building.

Such a decoupled optimization problem is called hierarchical, because the manipulated variable (energy demand of the building for securing user comfort) of the first MPC, the CFMPC, is the reference value of the second MPC, the MI-MPC. Thus, the energy demand of the building itself is the single communication node between the decoupled MPCs.

The benefit of such a hierarchical concept is the flexible controller structure, which easily allows to add new building zones, see Sec. 1.3.2. In addition, the opportunity for implementing only one MPC is given for industrial partners or owners/operators of buildings as well. One drawback is the loss of the guaranteed global optimum of the whole optimization, which can lead to a suboptimal solution. The developed concept is a hierarchical MPC concept including an CFMPC and an MI-MPC, presented in Fig. 1.2.

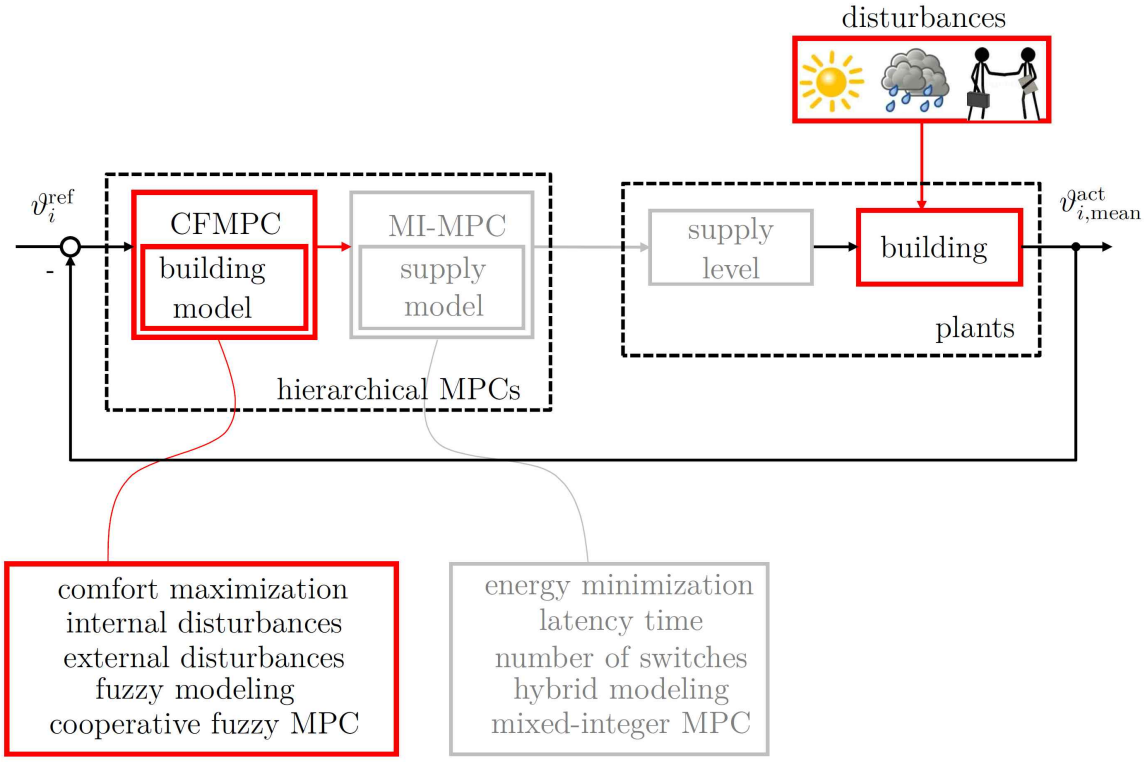

Figure 1.2: Hierarchical MPC scheme consisting of an CFMPC and an MI-MPC. Furthermore, ϑ_i^{ref} is the reference trajectory and $\vartheta_{i,\text{mean}}^{\text{act}}$ the actual mean indoor temperature for each zone i, $i \in \{1, 2, 3, 4\}$, for zoning see Sec. 1.3.2-III. The different colors define the two main research topics of the overall project.

The most important benefits and the main structures of each MPC are listed in Fig. 1.2 and in the following:

1. **c**ooperative **f**uzzy **m**odel **p**redictive **c**ontrol (CFMPC)
   - maximizes user comfort under technical and thermal constraints
   - deals with forecasts of internal and external disturbances (occupancy, radiance, ambient temperature)
   - uses underlying fuzzy models for representing the nonlinear building dynamics
   - is a new concept which has been theoretically developed and proven
2. **m**ixed-**i**nteger **m**odel **p**redictive **c**ontrol (MI-MPC)
   - minimizes energy consumption under technical constraints (latency time, number of aggregate switches)
   - uses linearized hybrid models (piecewise-affine models)

In this research approach the main focus is put on a newly developed CFMPC concept (given in red in Fig. 1.2 and Fig. 1.3). This CFMPC and its necessary conditions are discussed in detail in this work, under the assumption that a perfectly working energy management system (equal to the MI-MPC) exists. This assumption is illustrated in Fig. 1.3 and shows the main research topic of this PhD Thesis in red.

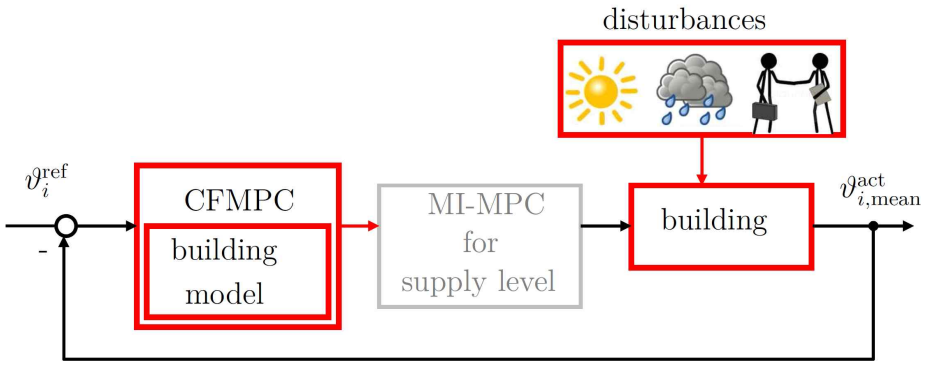

Figure 1.3: The considered scheme for this work is given in red, where the MI-MPC for the supply level is assumed to be perfectly working (grey). For $i = \{1, 2, 3, 4\}$, see Sec. 1.3.2-III.

1.3.2 Modeling and building zones

I. Modeling

In this section the modeling approach for the building based on data-driven black-box models is presented. A nonlinear black-box structure for a dynamical system is a model structure that is adequate to describe the nonlinear building dynamics. The structure is based on local linear model networks (LLMNs), which are equivalent to fuzzy inference-rules, [6, 8]. This local linear model (LLM) approach is an efficient way of model building for complex dynamic systems such as large multi-zone office buildings.

For getting such LLMs the local linear model tree algorithm (LoLiMoT) has been used, which combines a heuristic strategy for partition space decomposition with weighted least squares optimization [6]. It therefore provides an LLM approximation of globally nonlinear dynamic systems.

In LoLiMoT Gaussian Kernel functions are fitted to a rectangular partitioning of the two-dimensional partition space, spanned by (x_1, x_2), performed by a decision tree with axis-orthogonal splits at the internal nodes, see Fig. 1.4.

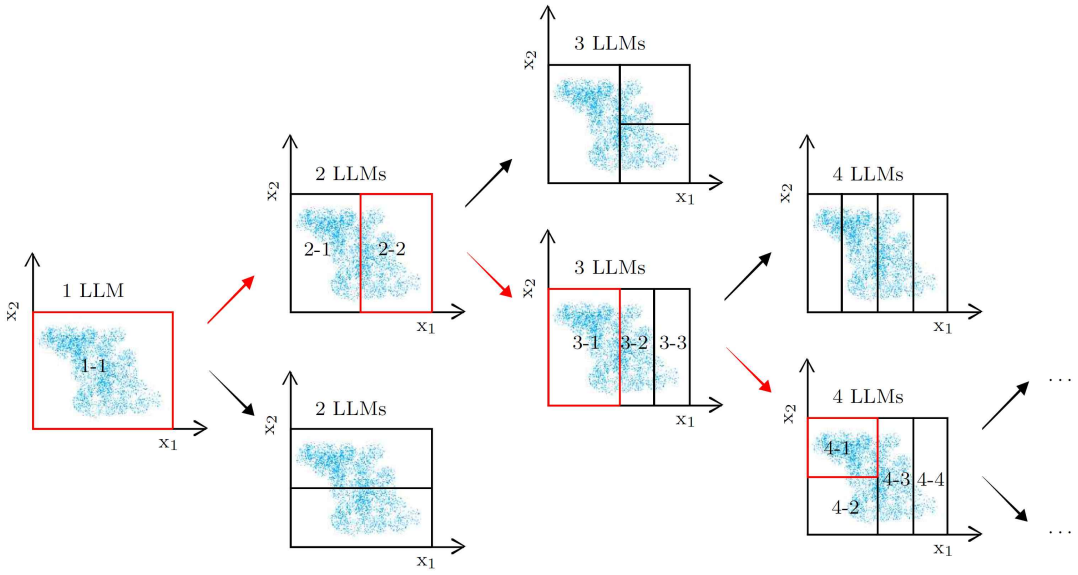

Figure 1.4: First four iterations of LoLiMoT algorithm for a two-dimensional partition space (x_1, x_2).

The selection of the partition space for the LLMs is one of the major tasks, and in many processes it is given by expert knowledge. If this is not the case, it is necessary to analyze the measurements to find the strongest nonlinearities in the process. It is the key point of this algorithm to reach the best results. Note that in Fig. 1.4 the blue dots represent the cloud of measurements, the red boxes define the chosen LLM

for the next split (thus the worst performing LLM) and the black boxes give the LLMs which are kept in the next iteration. Each local model belongs to one hyper-rectangle in which center the fitting point is placed. New hyper-rectangles are found by testing the possible splits in all dimensions and taking the one with the highest performance improvement. The algorithm stops when reaching a predetermined modeling error or maximum size of the tree.
The algorithm is listed in a short summary, see also Fig. 1.4:

1. Start with a global linear model.
2. Perform axis-orthogonal splits on that model.
3. Find the worst LLM by calculating the local loss function for each model.
4. The hyper-rectangle of the worst LLM is split into two halves by doing an axis-orthogonal split. Divisions in all dimensions are tried.
5. Fit LLMs for all possible alternative splits by weighted least squares.
6. Compare these fits and implement the one split with the highest performance improvement.
7. If the termination criterion is met then stop, else go to Step 3.

As shown in [6], two intrinsic features make LoLiMoT extremely fast: First, at each iteration only the worst local model is considered for division. Second, in Step 3 only the parameters of those local models that are newly generated by the division have to be estimated. For the global nonlinearities in the building, the LLMs are blended with mentioned Gaussian Kernel functions, which leads to fuzzy modeling, and subsequently to fuzzy model predictive control (FMPC).

Takagi-Sugeno (TS)-fuzzy models, [7], are suitable for approximating systems by interpolating between local linear, time-invariant auto-regressive models with exogenous inputs (ARX), [8]. The resulting outputs of the LoLiMoT algorithm are parameters for an ARX-model. Therefore, the equivalence to a TS-fuzzy model is obtained, which leads to a resulting fuzzy MPC in Sec. 1.3.3.

II. Building zones

Zoning of the different building zones is one of the major tasks, when talking about a building model. Therefore, four main reasons exist, which lead to multi-zone buildings:

1. More than one supply shaft exists.
2. New buildings contain large glass fronts, thus, the orientation depending on disturbances (radiance) is important.

3. The energy input in the building is based on different sources: thermally activated building system, fan coils, etc.

4. The supply results from combinations of different sources: geothermal energy, free cooling towers, district heating, etc.

In this work two floors including the office rooms have been considered for maximization of the user comfort. The building contains four supply shafts, which connect the piping for the cooling and heating supply and return with the supply level in the basement. The modeling of this specific building is based on these four main shafts, because each of these shafts supplies one building zone. These zones are distributed according to the building's orientation, which is equal to the cardinal direction. This fact makes the modeling more difficult, since the radiance input is given as a mixture of north-east, south-east, south-west and north-west. For control purposes, the building model is split into these four independent zones (red in Fig. 1.5) and one coupling zone (given in blue in Fig. 1.5).

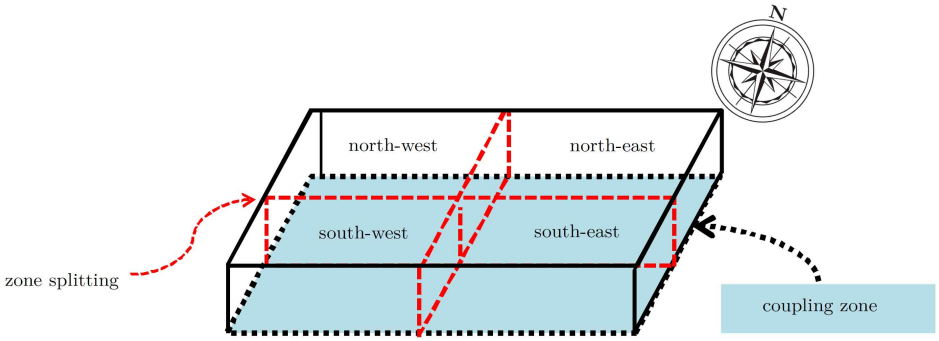

Figure 1.5: Zone splitting for modeling the University building in Salzburg, Austria. This scheme represents one floor of the office rooms, note that the second floor has exactly the same footprint.

III. Model details for specific demonstration building

In the recent approach for the specific building for each zone one LLMN with 3 LLMs was built. Each such TS-fuzzy model is constituted by an LLMN, which consists of LLMs. For each LLMN one FMPC is in use. The 3 LLMs of each FMPC are dedicated to the relevant seasons: winter, transition season (spring and fall), and summer. Overall 13 models were created for control purposes based on historical data and expert knowledge. In addition, one global model for the floor (coupling zone) is designed for a global MPC.

Note that a full cross validation and a 24 hours ahead prediction for all 13 models have been made, and have achieved good results, see Sec. 2.3.

1.3.3 Cooperative fuzzy model predictive control

I. Basic concept

The basic idea of the CFMPC is based on the fact that parallel input-coupled FMPCs are cooperating with each other. It has to be assumed that all FMPCs are parallel and output-blended, additionally an input-coupling between the different FMPCs has to exist.

The cooperative iteration-loop is computed between consecutive time steps and illustrated in Fig. 1.6.

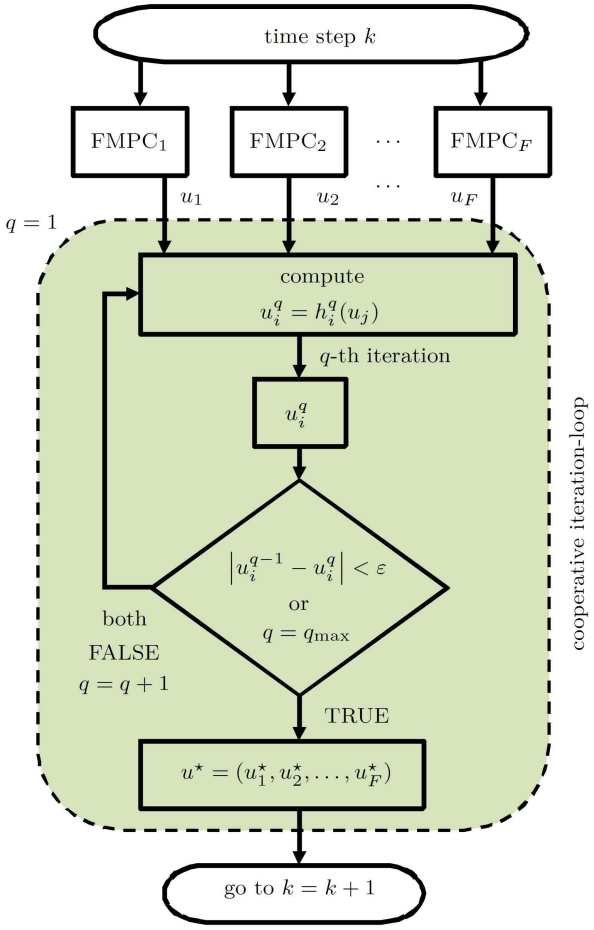

Figure 1.6: Schematic flow-chart of the cooperation iteration-loop between parallel FMPCs. Between consecutive time steps k and $k+1$ the q-th cooperative iteration update $h_i^q(u_j)$ is computed in a loop for the i-th manipulated variable of FMPC$_i$, where $i = \mathbb{F}$ and $j = \mathbb{F} \setminus i$. The resulting cooperative solution for the manipulated variable is given by $u^\star$.

Only u_i for FMPC$_i$,$\forall i \in \mathbb{F} = \{1, 2, \ldots, F\}$, is iteratively updated, all other variables are assumed to be constant during the iteration-loop (e. g. external disturbances). Note that the updated manipulated variables of FMPC$_j$, u_j, $\forall j \in \mathbb{F} \setminus i$ are disturbances for FMPC$_i$. Between consecutive time steps, the cooperative FMPCs perform q iterations of a feasible path algorithm. Let $u^\star$ be the overall blended output after the cooperative iteration-loop. $u^\star$ is computed such that some cost function is minimized and acceptable for each zone. The cooperative iteration-update is given by a function $h_i^q(u_j)$, which calculates the q-th iteration u_i^q. This update is calculated in each iteration step depending on all other manipulated variables u_j. The cooperative iteration-updates are calculated in a loop until a maximal number of iteration steps ($q_{\max}$) is reached or if the increment between the $(q-1)$-th and q-th manipulated variable (for all F variables) is smaller then a given threshold ε. If one of these criteria is fulfilled, the algorithm is advancing to time step $k = k + 1$.

The algorithm is listed in a short summary, see also Fig. 1.6:

1. Start with fixed time step k and iteration step q.
2. Calculate u_i^q for the q-th iteration with the iteration update $h_i^q(u_j)$, $i = \mathbb{F}$ and $j = \mathbb{F} \setminus i$.
3. Check the following criteria:
   a) $\left| u_i^{q-1} - u_i^q \right| < \varepsilon$,
   b) $q = q_{\max}$.
4. If one criterion is TRUE go to time step $k = k + 1$.
5. If both criteria are FALSE go back to 2 and start again with $q = q + 1$.

It is important to note that the individual FMPCs have to be output-blended in this approach. Furthermore, closed-loop stability of the CFMPC has been proven, see Sec. 2.2. Moreover, a convergence proof for the cooperative iteration-loop is presented in Sec. 2.2. In addition, the CFMPC algorithm is able to handle hard constraints as well as unstable LLMs, see Sec. 2.2.

II. Specific CFMPC for building implementation

In this section the CFMPC structure for the specific building is introduced. Note, it is assumed that a suitable energy management system (EMS) exists, which is able to provide the requested energy demand of the CFMPC scheme.

For control purposes, the overall nonlinear building is split into four different zones, see Sec. 1.3.2–II, which are consisting of input-coupled TS-fuzzy models, see Sec 1.3.2–I. The CFMPC is able to control the building over the whole year, because the fuzzy rules are representing the three different seasons, see Sec. 1.3.2–III.

Energy supply in this specific building is provided by a concrete activated floor distributing supply water in a second circuit, which means that this building has a thermally activated buildings system (TABS - coupling zone). Another supply into the building is based on Fan Coils (FC), which are required for the fast dynamics. The time constant of TABS is given by approximately 48 h, in contrast to the time constant for FC which is assumed to be 4 h. The coupling zone is controlled by TABS and each individual zone is managed by FC, which are able to control fast and react to short-term disturbances.

The control of each LLM is realized by MPC, for each building zone the associated MPCs are output-blended by the fuzzy membership functions, which leads to FMPC. In addition to the FMPCs a global MPC is controlling TABS, which affect all other zones. To coordinate the different controllers a cooperative iteration-loop is assumed, which leads to CFMPC. The concept is developed for a specific demonstration building and can be easily adapted for other complex buildings. The CFMPC structure for the specific building is introduced, and in Fig. 1.7 the control concept for 4 FMPCs (FMPC_i, for the specific zone: $i \in \mathbb{F} = \{1, 2, 3, 4\}$ holds) cooperating with 1 global coupling MPC (MPC_T) is illustrated.

The controlled variable is the average indoor room temperature of each zone denoted by $\vartheta^{\text{act}}_{i,\text{mean}}$, $\forall i \in \mathbb{F}$. In Fig. 1.7, $\vartheta^{\text{ref}}_{i}$ describes the reference trajectory for the i-th FMPC of the closed-loop system and $\vartheta^{\text{act}}_{i,\text{mean}}$ represents the actual value. For the coupling zone the mean $\bar{\vartheta}^{\text{ref}}$ of the other 4 reference values is taken, and the actual mean indoor room temperature is given as $\bar{\vartheta}^{\text{act}}$.

The manipulated variables before the cooperative iteration-loop are denoted by u_j, $j = \{T, F_i\}$, $\forall i \in \mathbb{F}$. The "T" denotes "TABS" and "F_i" denotes the control by FC for zone_i. Furthermore, three main disturbances to the building are considered: radiance, ambient temperature, and occupancy.

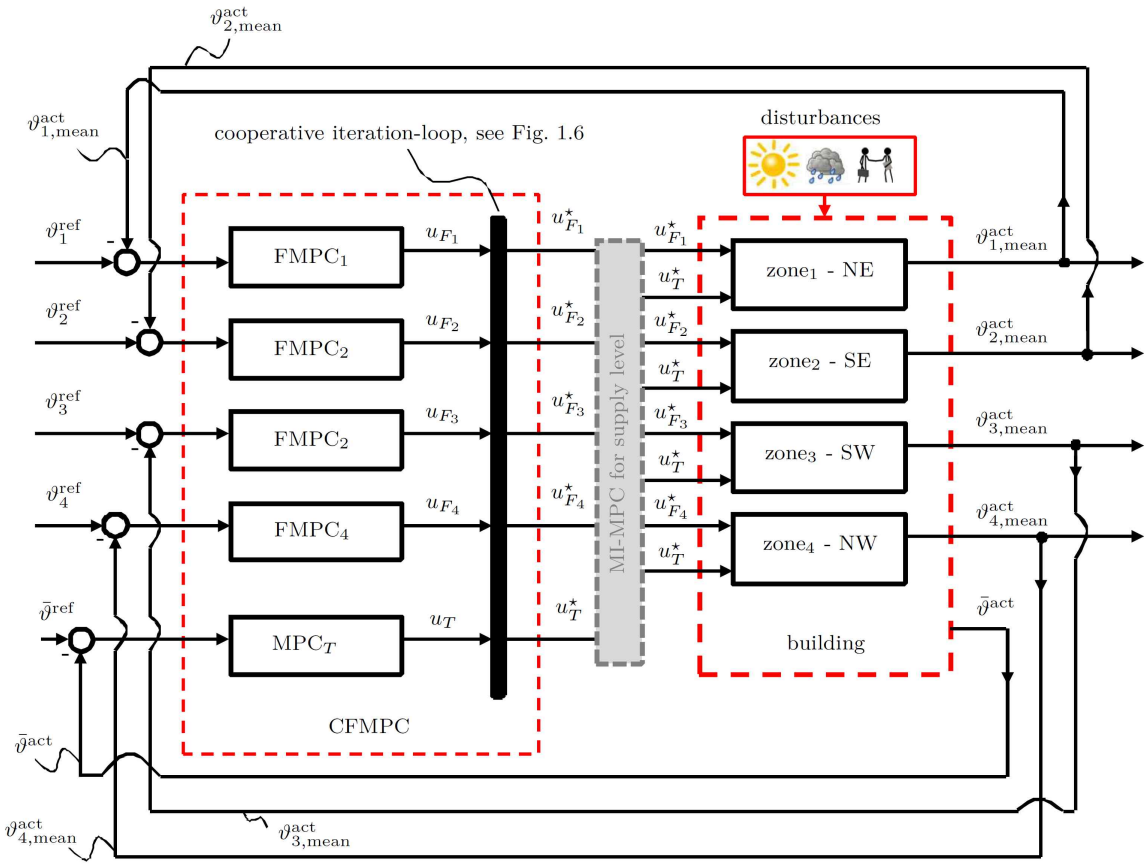

Figure 1.7: CFMPC scheme for the specific building. The scheme shows the structure of a CFMPC, which is used for the demonstration building, with 4 different zones, and the assumption that the supply level is perfectly controlled by an existing energy management system (MI-MPC).

1.4 Summary of scientific approaches

In **Publication A**, see Sec. 2.1, an effective modeling approach for building heating dynamics is presented. The proposed model is a data-driven fuzzy model, which reproduces the nonlinear dynamic behavior of a specific complex building. The fuzzy model is based on LLMs, for which a two-dimensional partition space is obtained. Benefits of this effective modeling are the low complexity by design, and that the fuzzy black-box model is suitable for MPC without any transformations. A full cross-validation highlights the results of such a low-order fuzzy model for buildings. In summary, an effective fuzzy black-box model for building heating dynamics has been presented in this work.

In **Publication B**, see Sec. 2.2, a newly developed CFMPC concept is presented. The overall nonlinear plant is assumed to consist of several parallel input-coupled TS-fuzzy models. Each such TS-fuzzy subsystem is represented in the form of a LLMN. The control of all LLMs in each LLMN is realized by an MPC. For each LLMN the outputs of the associated MPCs are blended by the fuzzy membership functions, which leads to a resulting structure that one FMPC is designed for each LLMN-subsystem. Overall, a parallel combination of FMPCs results, which mutually affects all LLMN-subsystems by their respective manipulated variables. To compensate detrimental cross-couplings in this setup, a cooperation between the FMPCs is introduced.

For this cooperation, convergence is proven and for the closed-loop system a stability proof is given. In addition, it is demonstrated in a simulation example that the proposed input-constraint CFMPC algorithm achieves convergence of the fuzzy LLMNs within few cooperative iteration steps. This work shows theoretically that the CFMPC algorithm is able to handle hard constraints as well as unstable LLMs. Simulations are given to demonstrate the effectiveness of the theoretical results.

In **Publication C**, see Sec. 2.3, the developed CFMPC (Sec. 2.2) is presented to coordinate different input-coupled manipulated variables of buildings (building model is presented in Sec. 2.1). The overall nonlinear building is split into four different zones, which are consisting of input-coupled TS-fuzzy models, and one global coupling zone. The CFMPC concept is able to control both modes, heating and cooling, in contrast to most of the state-of-the-art MPCs in buildings, where just heating or cooling systems are controlled. Thus, the validity over all seasons is one great advantage. The concept is developed for a specific demonstration building and can be easily adapted for other complex buildings. The CFMPC achieves significantly higher control performance with slightly less energy consumption in contrast to state-of-the-art controllers and MPCs in building. The closed-loop simulation examples verify the advantages and effectiveness of the CFMPC in building automation.

In **Publication D**, see Sec. 2.4, for the sake of completeness an excursion to the MI-MPC and the underlying supply level is given. It shows the basic idea of a hybrid energy management system for the supply level in buildings, using an MI-MPC, in a hierarchical control scheme.

1.5 Scientific contributions of this work

The scientific contributions of this work are universally applicable. The developed concept is flexible and easy to extend to additional building zones. However, data-driven modeling depends on specific building measurements, thus, obtaining a valid model is one of the most time-consuming parts. The hierarchical controller concept (consisting of two nonlinear MPCs) leads to a decoupling of conflicting optimization goals. Therefore, the new concept is easy to implement and flexible in the structure. The most theoretical useful contribution is the development of the CFMPC, for which closed-loop stability and convergence has been proven. In addition the commissioning in the real building has already been performed with excellent results in the first month of operation.

The scientific contributions of this work and can be summarized:

- Development of flexible and effective fuzzy black-box models.
  - These models are valid for adoption in various nonlinear processes with nonlinear system behavior.
  - For the specific building a full cross-validation underlines the model quality.
- Flexibility of hierarchical control concept.
  - Decoupling of conflicting optimization problems.
  - Easy to implement and the possibility to use individual MPCs, instead of the overall hierarchy.
  - For the specific building the flexibility for adding new building zones or supply sources is given.
  - The preparation for future integration in Smart Grids and for flexible pricing is given and can be easily added in the specific MPCs.
- Development of CFMPC.
  - The complete theory has been developed with a completely new FMPC.
  - Closed-loop stability has been proven.
  - Convergence has been proven.
  - The CFMPC has been tested for unstable LLMs and oscillating LLMs with input and output constraints.

  - For the specific building a flexibility for adding new building zones is given.
  - The communication between different input-coupled systems has been improved and is easy to handle with the CFMPC.

- Commissioning in the real building.
  - The CFMPC is active in the demonstration building.
  - The concept is easy to implement and flexible.
  - The CFMPC achieves very good results right from the start in the closed-loop on-line run.
  - The proof of concept has passed the commissioning with excellent results.

1.6 Commissioning in a real building

1.6.1 Facts of the demonstration building

The demonstration building in this work is a 27.000 m^2 university building near the center of Salzburg, Austria. It has five floors above ground containing several large and numerous smaller meeting rooms, offices and lecture rooms. In this approach two floors including the office rooms have been considered for maximization of the user comfort. On each floor the building contains 250 office rooms, the footprint of these floors is identical and each has an effective area of about 6.500 m^2. The facade of this special building has a glass ratio of about 70 % and outside blinds extend over 2 floors, see Fig. 1.8.

Figure 1.8: Demonstration building: University building in Salzburg, Austria. ©Luigi Caputo

1.6.2 Simulation setup

The simulation set-up for the demonstration building is given in Sec. 1.3.3-II. In the simulation the developed CFMPC has been compared to historical data of the state-of-the-art PID controller, which was originally implemented in the building. Furthermore, the CFMPC has been compared to a global linear MPC and an FMPC neither with cooperation nor with the knowledge of coupling zones.

The CFMPC concept shows a performance increase of 21.86 % as compared to an FMPC concept without cooperation. Furthermore, the performance of the presented CFMPC

concept provides an improvement of 19.67 % over the rule-based PID controller in the specific demonstration building and 16.17 % against a global linear MPC. The relations of performance are calculated by the mean squared error (MSE).

1.6.3 Results of the commissioning in the real building

In this part the results of the first commissioning with optimal parameters from theoretical calculations is shown, see Fig. 1.9.

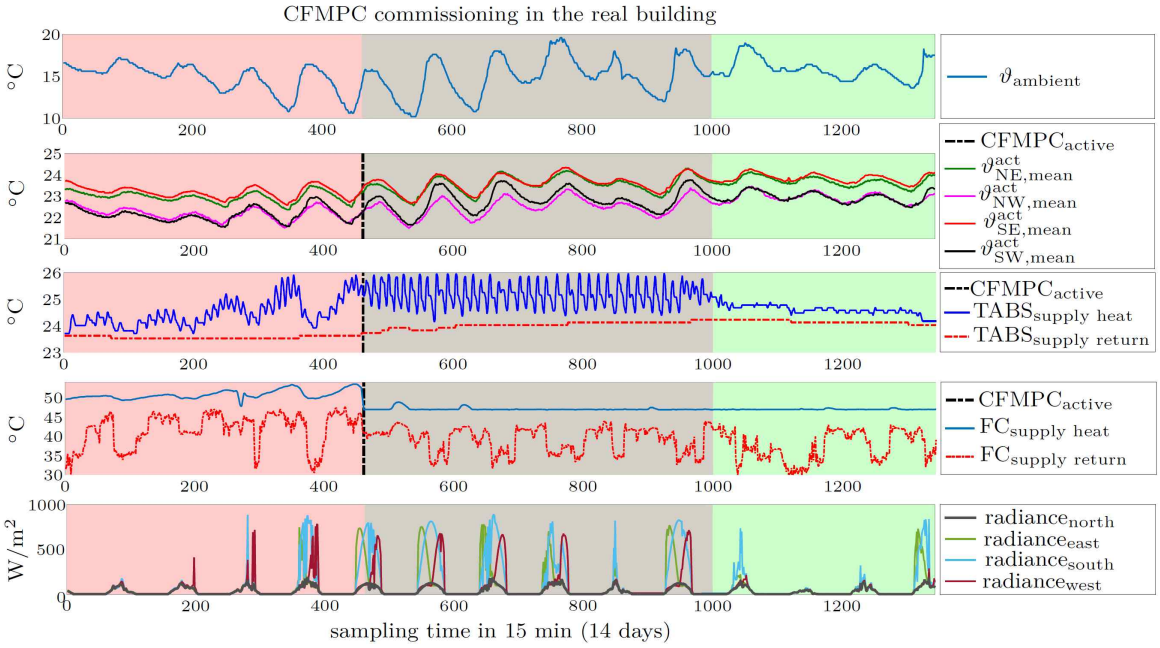

Figure 1.9: First results of the controller commissioning in the real building. In the red area the conventional PID controller is still active, in the gray field the CFMPC becomes active and tuning of an underlying basic PID control loop has been done (three-way valve of heat supply TABS), and in green the work of only the new CFMPC is illustrated.

In Fig. 1.9 the strategy of the conventional PID controller is shown in the red area, activating the CFMPC and tuning an underlying basic PID controller (three-way valve of heat supply TABS) is given in the gray field, and the completely integrated CFMPC in the building is shown with a green background. The whole commissioning with the transition from the conventional strategy to the fully automated CFMPC took only a few days. In Fig. 1.9 the switch from the conventional PID controller to the CFMPC is given. In the first and the last subplot the disturbances ambient temperature $\vartheta_{\text{ambient}}$ and radiance$_j$ are given, $j = \{\text{north, east, south, west}\}$. In the second subplot the mean

indoor room temperatures $\vartheta^{\text{act}}_{i,\text{mean}}$ of the i zones are illustrated, $i = \{\text{NE, NW, SE, SW}\}$. It is obvious, that the mean zone temperatures are strongly correlated with both disturbances, however, the maximal temperature differences during 24 hours in the green area are given in Tab. 1.1.

Zone	**Temperature difference**
zone_{NE}	$\Delta_{\text{NE}} = 0.6386$ °C
zone_{NW}	$\Delta_{\text{NW}} = 0.8142$ °C
zone_{SE}	$\Delta_{\text{SE}} = 0.5652$ °C
zone_{SW}	$\Delta_{\text{SW}} = 0.7359$ °C

Table 1.1: Difference between the maximal and minimal indoor mean room temperature of each zone: $\Delta_i = \max(\vartheta^{\text{act}}_{\text{i,mean}}) - \min(\vartheta^{\text{act}}_{\text{i,mean}}), i = \{\text{NE, NW, SE, SW}\}$ for samples 1000 to 1300 in Fig. 1.9.

In the third and fourth subplot of Fig. 1.9 the heat supplies of TABS and FC are illustrated. In the red field the conventional PID controller was active and the variance of both supply temperatures is high. In subplot three the tuning of an underlying basic PID controller for the TABS supply temperature has been done and is shown in the gray area. Finally in the green field the CFMPC is fully integrated, and in subplot three and four supply temperatures of the new strategy are shown, which are almost constant. Furthermore, it is obvious that the strategy of the CFMPC favors lower supply temperatures. The fourth subplot of Fig. 1.9 illustrates the drop of the average supply temperature of FCs by approximately 10 °C, caused by the energy minimizing CFMPC strategy.

In Tab. 1.2 a comparison over one week based on an equivalent variance in the ambient temperature between the conventional PID controller concept and the newly developed CFMPC concept is given.

Variance of...	**PID controller**	**CFMPC**
$\vartheta_{\text{ambient}}$	3.2418 °C^2	3.4305 °C^2
$\vartheta^{\text{act}}_{\text{NE,mean}}$	0.0860 °C^2	0.1008 °C^2
$\vartheta^{\text{act}}_{\text{NW,mean}}$	0.1163 °C^2	0.1094 °C^2
$\vartheta^{\text{act}}_{\text{SE,mean}}$	0.0909* °C^2	0.1679* °C^2
$\vartheta^{\text{act}}_{\text{SW,mean}}$	0.1510* °C^2	0.2545* °C^2
$\text{TABS}_{\text{supply heat}}$	0.2026* °C^2	0.0562* °C^2
$\text{FC}_{\text{supply heat}}$	6.5384* °C^2	0.0049* °C^2

Table 1.2: Comparison over one week based on an equivalent variance in the ambient temperature. * stands for a significant difference with $\alpha = 2\%$, Levene Test.

The most impressive result is that the variance in supply temperature of both supply sources can be significantly reduced while variance in the mean room temperatures in the different zones is only slightly increased. The control strategy of the CFMPC is more smooth with less supply temperature in °C. No user complaints have been recorded since the commissioning of the CFMPC, due to the small difference in the standard deviations of temperatures (see Tab. 1.3) which always stays below 0.12 °C. Therefore, the standard deviation in °C are given in Tab. 1.3 to underline the results even if a significant difference has been analyzed.

standard deviation of...	**PID controller**	**CFMPC**
$\vartheta_{\text{ambient}}$	1.8005 °C	1.8522 °C
$\vartheta^{\text{act}}_{\text{NE,mean}}$	0.2932 °C	0.3175 °C
$\vartheta^{\text{act}}_{\text{NW,mean}}$	0.3411 °C	0.3308 °C
$\vartheta^{\text{act}}_{\text{SE,mean}}$	0.3015 °C	0.4098 °C
$\vartheta^{\text{act}}_{\text{SW,mean}}$	0.3886 °C	0.5045 °C
$\text{TABS}_{\text{supply heat}}$	0.4501 °C	0.2370 °C
$\text{FC}_{\text{supply heat}}$	4.5005 °C	1.2476 °C

Table 1.3: Comparison of standard deviations depending on Tab. 1.2.

Tab. 1.3 illustrates that the differences between the standard deviations (CFMPC to conventional PID control) in all zones are in the interval [0.0103 °C; 0.1159 °C], where the smallest difference is in zone NW and the biggest in zone SW. However, the difference between the two control strategies is apparently not noticeable for the user. Additionally, Fig. 1.10 illustrates, that the CFMPC is able to minimize the operating range of both supply sources. Note that zero-mean measurements are used based on the data of Tab. 1.2.

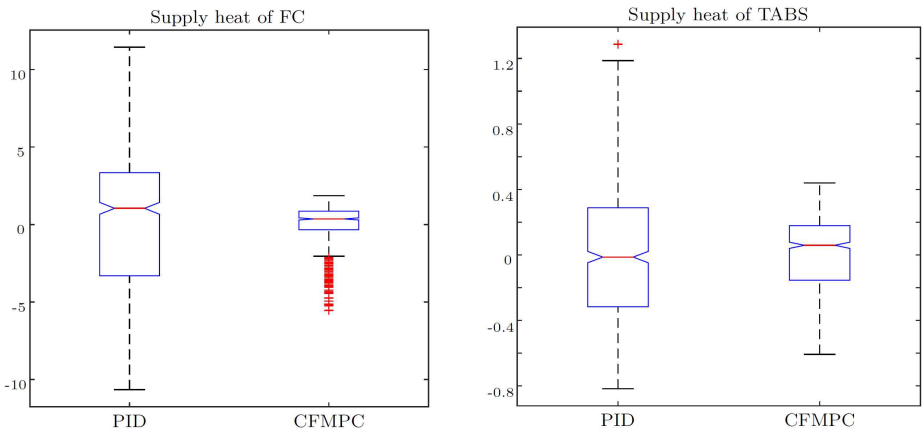

Figure 1.10: Boxplots of zero-mean supply heat temperatures for comparison of the conventional PID controllers with the proposed CFMPC.

1.6.4 Summary of commissioning

To summarize the proof of concept in the real building: The CFMPC achieves excellent performance in the first commissioning, the transition has been smooth and without any complications. Therefore, the developed CFMPC concept is promising to obtain energy savings with equal user comfort, even without an additional energy management system.

Bibliography

[1] L. Pérez-Lombard, J. Ortiz, and C. Pout. A review on buildings energy consumption information. *Energy and Buildings*, 40(3):394 – 398, 2008.

[2] E. F. Camacho and C. Bordons. *Model Predictive Control*. Advanced Textbooks in Control and Signal Processing. Springer London, 2004.

[3] J. B. Rawlings and D. Q. Mayne. *Model Predictive Control: Theory and Design*. Nob Hill Publishing, 2009.

[4] P. Scokaert, D. Q. Mayne, and J. B. Rawlings. Suboptimal model predictive control (feasibility implies stability). *Automatic Control, IEEE Transactions on*, 44(3):648–654, Mar 1999.

[5] Y. L. Huang, H. H. Lou, J. P. Gong, and T. F. Edgar. Fuzzy model predictive control. *Fuzzy Systems, IEEE Transactions on*, 8(6):665–678, Dec 2000.

[6] O. Nelles. *Nonlinear System Identification: From Classical Approaches to Neural Networks and Fuzzy Models*. Engineering online library. Springer, 2001.

[7] T. Takagi and M. Sugeno. Fuzzy identification of systems and its applications to modeling and control. *Systems, Man and Cybernetics, IEEE Transactions on*, SMC-15(1):116–132, Jan 1985.

[8] J. Abonyi. *Fuzzy Model Identification for Control*. Birkhauser Boston, 2002.

[9] J. Široký, F. Oldewurtel, J. Cigler, and S. Prívara. Experimental analysis of model predictive control for an energy efficient building heating system. *Applied Energy*, 88(9):3079 – 3087, 2011.

[10] F. Oldewurtel, A. Parisio, C. N. Jones, D. Gyalistras, M. Gwerder, V. Stauch, B. Lehmann, and M. Morari. Use of model predictive control and weather forecasts for energy efficient building climate control. *Energy and Buildings*, 45(0):15 – 27, 2012.

[11] F. Oldewurtel, D. Sturzenegger, and M. Morari. Importance of occupancy information for building climate control. *Applied Energy*, 101(0):521 – 532, 2013. Sustainable Development of Energy, Water and Environment Systems.

[12] Y. Ma, J. Matusko, and F. Borrelli. Stochastic model predictive control for building HVAC systems: Complexity and conservatism. *Control Systems Technology, IEEE Transactions on*, 23(1):101–116, Jan 2015.

[13] F. Oldewurtel, C. N. Jones, A. Parisio, and M. Morari. Stochastic model predictive control for building climate control. *Control Systems Technology, IEEE Transactions on*, 22(3):1198–1205, May 2014.

[14] Y. Ma, F. Borrelli, B. Hencey, B. Coffey, S. Bengea, and P. Haves. Model predictive control for the operation of building cooling systems. *Control Systems Technology, IEEE Transactions on*, 20(3):796–803, May 2012.

[15] M. Wallace, R. McBride, S. Aumi, P. Mhaskar, J. House, and T. Salsbury. Energy efficient model predictive building temperature control. *Chemical Engineering Science*, 69(1):45 – 58, 2012.

[16] S. Prívara, J. Široký, L. Ferkl, and J. Cigler. Model predictive control of a building heating system: The first experience. *Energy and Buildings*, 43(2–3):564 – 572, 2011.

[17] I. Škrjanc, B. Zupančič, B. Furlan, and A. Krainer. Theoretical and experimental fuzzy modelling of building thermal dynamic response. *Building and Environment*, 36(9):1023 – 1038, 2001.

[18] C. S. Kang, C. H. Hyun, and M. Park. Fuzzy logic-based advanced on–off control for thermal comfort in residential buildings. *Applied Energy*, 155:270 – 283, 2015.

[19] P. D. Moroşan, R. Bourdais, D. Dumur, and J. Buisson. Building temperature regulation using a distributed model predictive control. *Energy and Buildings*, 42(9):1445 – 1452, 2010.

[20] B. T. Stewart, A. N. Venkat, J. B. Rawlings, S. J. Wright, and G. Pannocchia. Cooperative distributed model predictive control. *Systems & Control Letters*, 59(8):460 – 469, 2010.

[21] H. Huang, L. Chen, and E. Hu. A new model predictive control scheme for energy and cost savings in commercial buildings: An airport terminal building case study. *Building and Environment*, 89:203 – 216, 2015.

[22] F. Berkenkamp and M. Gwerder. Hybrid model predictive control of stratified thermal storages in buildings. *Energy and Buildings*, 84:233 – 240, 2014.

Chapter 2

Publications

List of selected journal publications:

Publication A

Michaela Killian, Barbara Mayer, and Martin Kozek.
Effective fuzzy black-box modeling for building heating dynamics.
Energy and Buildings, Volume 96, 2015, pages 175–186, ISSN: 0378-7788.
DOI: 10.1016/j.enbuild.2015.02.057

Publication B

Michaela Killian, Barbara Mayer, Alexander Schirrer, and Martin Kozek.
Cooperative Fuzzy Model Predictive Control.
Fuzzy Systems, IEEE Transactions on, 2015, ISSN: 1063-6706, article in press.
DOI: 10.1109/TFUZZ.2015.2463674

Publication C

Michaela Killian, Barbara Mayer, and Martin Kozek.
Cooperative fuzzy model predictive control for heating and cooling of buildings.
Energy and Buildings, Volume 112, 2016, pages 130–140, ISSN: 0378-7788.
DOI: 10.1016/j.enbuild.2015.12.017

Publication D

Barbara Mayer, Michaela Killian, and Martin Kozek.
Management of hybrid energy supply systems in buildings using mixed-integer model predictive control.
Energy Conversion and Management, Volume 98, 2015, pages 470–483, ISSN: 0196-8904.
DOI: 10.1016/j.enconman.2015.02.076

2.1 Publication A

Michaela Killian, Barbara Mayer, and Martin Kozek.
Effective fuzzy black-box modeling for building heating dynamics.
Energy and Buildings, Volume 96, 2015, pages 175–186, ISSN: 0378-7788.
DOI: 10.1016/j.enbuild.2015.02.057

Own contribution
Problem analysis, selection of methods, execution of the solution, development and programming of algorithms, consideration of implementation aspects, performing simulation studies, and structuring, writing and editing of the manuscript was done by the applicant. Providing raw data, discussion of methodology, and editing of the manuscript was done by the second author. Problem statement, discussion and editing was done by the third author.

Energy and Buildings 96 (2015) 175–186

Contents lists available at ScienceDirect

Energy and Buildings

journal homepage: www.elsevier.com/locate/enbuild

Effective fuzzy black-box modeling for building heating dynamics

M. Killian[a,*], B. Mayer[b], M. Kozek[a]

[a] Vienna University of Technology, Institute of Mechanics and Mechatronics, Getreidemarkt 9, 1060 Vienna, Austria
[b] FH Joanneum, Werk-VI-Strasse 46, 8605 Kapfenberg, Austria

ARTICLE INFO

Article history:
Received 16 December 2014
Received in revised form 13 February 2015
Accepted 25 February 2015
Available online 6 March 2015

Keywords:
Building modeling
Black-box modeling
Nonlinear dynamic model
Local linear models (LLM)

ABSTRACT

In this paper an effective modeling approach for building heating dynamics is presented. The proposed model is a so-called fuzzy black-box model. This data-based model is able to reproduce the nonlinear dynamic behavior of a complex office building split into different zones. The fuzzy black-box model is based on local linear models (LLM), for which a 2-dimensional *partition space* is obtained. In the proposed work data pre-processing is one of the most important tasks and thus extensively explained. This includes the selection of suitable input and output data and selection of appropriate model orders. Furthermore, it is presented that even with a small amount of data good models can be achieved. The output of this LLM algorithm is an autoregressive model with exogenous input (ARX). The resulting model is specifically tailored for model-based control design. The uniqueness of the presented work lies not only in the low-order of the building model, but also in the way of retrieving a model in the most effective and time-saving way.

1. Introduction

1.1. Motivation

Energy efficient climate control is an important current task, hence there has been a growing rethinking in energy savings. The building sector accounts for about 40% of the total energy consumption [1]. In order to guarantee indoor environmental quality (IEQ) while minimizing building energy consumption, it is necessary to both invest in passive energy saving measures (isolation, external shading, freecooling, etc.) and in intelligent automation schemes [2]. Energy savings must be carefully assessed with respect to the consequences in IEQ, which is not only affected by thermal quality but also by air quality, lighting, sound, odor, and vibration. It is known, that model predictive control (MPC) is able to reduce this energy consumption in an efficient way [3]. However, it is also common knowledge that modeling is crucial for a well operating controller. Therefore, this work shows a new effective approach for creating a dynamical nonlinear building model. This model on the one hand is able to represent the important nonlinear effects of a specific building and on the other hand is well suited for control purposes.

An *effective modeling* approach for building heating systems is introduced by identifying a fuzzy black-box model. A local linear model tree (LoLiMoT) algorithm is proposed for creating an efficient building model [4,5]. This fuzzy black-box algorithm uses local linear models (LLM), a so-called *partition space*, and different parameters for training based on measurement data. In this work a 2-dimensional partition space is used, this space is given from expert knowledge or it is manually chosen, it represents the most important nonlinearities in the process to be modeled. One highlight of this work is, that within the whole building dynamics each building-zone can have different dynamics. Therefore, the whole building is split into zones, which are modeled separately.

1.2. State-of-the-art MPC

Since the specific MPC formulation is an important driver for the building model structure, a short overview on MPC and building applications is given.

Classical linear model predictive control (MPC) approaches are presented in [6]. However, thermal behavior of buildings is typically nonlinear, which leads to a nonlinear MPC (NMPC) approach.

In terms of buildings the authors of [3] present an MPC for an energy efficient building heating system, based on RC models. These models are based on the description of heat transmission between nodes that are representing temperatures, whereas the present approach is based on LLMs suitable for a specific NMPC. A comparison between different control strategies of thermal

* Corresponding author. Tel.: +43 1 58801 325522.
E-mail addresses: michaela.killian@tuwien.ac.at (M. Killian), barbara.mayer@fh-joanneum.at (B. Mayer), martin.kozek@tuwien.ac.at (M. Kozek).

http://dx.doi.org/10.1016/j.enbuild.2015.02.057
0378-7788/

Nomenclature

ARX	autoregressive model with exogenous input
FC	fan coil
FMPC	fuzzy MPC
k_σ	steepness of the membership function
LLM	local linear model
LLMN	local linear model network
LoLiMoT	local linear model tree
$\dot{m}$	mass flow in kg s^{-1}
MPC	model predictive control
NE	north-east
NMPC	nonlinear MPC
NW	north-west
occ_i	occupancy of zone i in %
$\dot{Q}$	heat flow in J
rad_i	radiance of zone i in W/m^2
SE	south-east
SW	south-west
TABS	thermal activated building system
TS	Takagi–Sugeno
$t_{90\%}$	90% value of step-response in %
$\vartheta_{\text{ambient}}$	ambient temperature in K
ϑ_{FC}	heat supply FC in K
$\vartheta_{\text{indoor}}$	indoor room temperature in K
$\vartheta_{\text{indoor}}^{\text{mean},i}$	mean indoor temperature of zone i in K
ϑ_{TABS}	heat supply TABS in K

comfort in buildings is presented in [7]. The results clearly indicate that the best control strategy for the building in [7] is an MPC controller. Another advantage of MPC is the effective compensation of disturbances. For a detailed discussion about MPC dealing with disturbances in buildings see [8,9]. For MPC dealing with weather forecasts see [8], different occupancy patterns are presented in [9].

An advantageous model for MPC is the Takagi–Sugeno (TS) fuzzy model [10,4,11], which is used in the presented approach. The resulting NMPC is a so-called fuzzy MPC (FMPC), [11,10]. Nelles et al. [4] discussed the identification of dynamical nonlinear processes with a fuzzy black-box approach, and the equivalence between LLMs and TS-fuzzy models is shown.

FMPC is able to deal with overall nonlinear systems by controlling LLMs and produce the global nonlinear output by blending the LLMs with membership functions. In [12–14] the FMPC concept with underlying TS-fuzzy models is presented, both in practice and theory.

1.3. State-of-the-art system identification

For system identification different basic approaches are common. The classical linear system identification is described in [15]. In this work the superior performance of nonlinear over linear model structure is shown utilizing LLM identification techniques [4,11]. Privara et al. [16] have shown that the time and effort for modeling a building is much larger than for the consecutive control design. In [17,16] the relevance of models for MPCs is presented, as well as an overview and an analysis of different identification tools, most importantly deterministic-physical modeling or probabilistic semi-physical modeling. The problem of probabilistic semi-physical modeling, mentioned in [16] is the high computational demand, therefore it is suitable only for a smaller set of measured variables. For deterministic semi-physical modeling least squares (LS) are used for solving the parameter estimation problem. The possible advantage is an efficient solver with guaranteed global optimum of the parameter estimates, however, the physical model part requires expert knowledge and an incorrect model structure will inevitably lead to biased parameters. In the proposed work a fuzzy black-box algorithm is used for identifying the utilized ARX, furthermore, a low-order model is assumed by design. This approach relief's the user of physical modeling and is computationally efficient.

In [18] a building model suitable for MPC based on RC models is presented. The main limitation of the model is the focuses on a single room, thus neglecting thermal couplings between neighboring zones. In contrast, the proposed method utilizes an effective low order model for two floors of a building (250 rooms), which is suitable for MPC design.

Black-box modeling for buildings has been presented earlier. In [19,20] black-box modeling of buildings has been reported, however, in [19] subspace identification is used, and in [20] input\output data are generated by using co-simulation between EnergyPlus and Matlab. The presented subspace approach, presented in [19] uses orthogonal and oblique projections to find Kalman state sequences for obtaining then system matrices, while in the proposed work local linear ARX models are identified by using only orthogonal splits in the partition space, which leads to time-variant system matrices. In contrast to [20] in the recent approach real measurements are chosen for the identification. In [21] a gray-box model is has been presented, where system identification is used to identify reduced-order models. White-box modeling is also common in building modeling. This approach gives nearly perfect physical models of a building, but these highly complex models are not suitable for control design. Therefore, they are used for reproducing missing measurements, for validation, or to simulate open-loop cases. However, in this approach fuzzy black-box modeling is used for defining the global nonlinear thermal behavior on buildings, subjected to the condition that the system has a manageable amount on states, inputs and outputs.

In [22] a Heating, Ventilation and Air Condition (HVAC) system of a building is controlled with fuzzy control, therefore a TS-fuzzy model for the building dynamics is used. The authors of [22] achieved a more effective and more energy-efficient control strategy in contrast to the conventional PI controller. In that as well as in [22,23] Gaussian Kernel functions are used for the membership functions.

The main difference between these approaches and the present one is, that in the current work a dynamical nonlinear model is identified, whereas in [23] a static model is assumed. Furthermore, the partition space in [23] is chosen as the whole input space, while in this paper a 2-dimensional partition space is. In addition, in the approach proposed here a fuzzy black-box model for a heating is presented, whereas in [23] only illuminance is considered.

In modern buildings Thermal Activated Building Systems (TABS) and Fan Coils (FC) are the major supply for building heating and cooling control. In [24] a fuzzy model for FC is given and described. The main advantage of the fuzzy controller for FC is not mainly given in performance, but in the easiness of understanding and including fuzzy linguistic logic. In the approach proposed here a fuzzy model for the whole building heating dynamics is presented (two floors, each including 250 rooms).

Another common approach in data-driven modeling is using neural networks (NN) [4,5]. In [25] an energy analysis of a building using two different types of artificial neural networks (ANN) is presented. Least squares and back propagation algorithms are used in [25], demonstrating that ANNs outperform linear models over large time frames. In [26] a neural-network based MPC for HVAC systems using predicted mean vote (PMV) index is given. In [26] the PMV index depends on six factors: metabolic rate, clothing insulation, air temperature and humidity, air velocity, and the mean radiant temperature. Utilizing a neural-network based MPC significant energy savings from approximately 50% are reported.

Fig. 1. Photo of the University building in Salzburg, Austria.

The remainder of this work is structured as follows: In Section 2 a general description of the demonstration building is given. The methodology of fuzzy black-box modeling is outlined in Section 3. The following section contains the building identification and the specific model structure. Simulation and validation results are presented in Section 5, and Section 6 summarizes the results.

2. Building description

The building which is presented in this work is a 27.000 m^2 University building in the center of Salzburg, Austria. It has five floors above ground containing several large and numerous smaller meeting rooms, offices and lecture rooms. There are six atriums within the building complex (see Fig. 2), which are additional disturbances, because of incident radiation. The facade of this special building has a glass ratio of about 70% and outside blinds, see Fig. 1. In this paper the modeling is limited to the second and third floor, where the offices of the building are located (in Fig. 1 these zones are shown with the wooden blinds). In each of these floors the building contains 250 office rooms, the footprint of these floors is identical and each has an effective area of about 6.500 m^2. For the layout see Fig. 2. The building contains five shafts nearby the side staircases. In four of these shafts, the piping for the (cooling and) heating supply and return are installed, connecting the supply level in the basement to all floors. The modeling of this specific building is based on these four main shafts (see Fig. 2), because each of these shafts supplies one building-zone. These zones are chosen according to the building's orientation, which is equal to the cardinal direction. This fact makes the modeling more difficult, since the radiance input is given as a mixture from North-East (NE), South-East (SE), South-West (SW) and North-West (NW), see Fig. 2. In this work zone NE and zone SW are considered to be identified by a fuzzy black-box algorithm. Zone SW is affected by radiance the most, in contrast to zone NE, which is affected by radiance the least. For zone SE and zone NW the same method is used, but in this work only the modeling of zone NE and zone SW are demonstrated.

In this approach an effective fuzzy black-box model for heating is presented and validated. In this specific building energy input is provided by a concrete activated floor distributing supply water in a second circuit, which means that this building has a Thermal Activated Buildings System (TABS). The supply into the building of this resource is based on Fan Coils (FC). The supply heat temperatures are denoted by $\vartheta_{\mathrm{TABS}}$ and ϑ_{FC}. Both, district heating and heat pumps, can contribute to the supply temperature in the building. More specifically, Fig. 3 presents the inputs and output in an example of one single-room. Note, that $\vartheta_{\mathrm{ambient}}$ denotes the ambient temperature and $\vartheta_{\mathrm{indoor}}$ denotes the output, the averaged indoor room

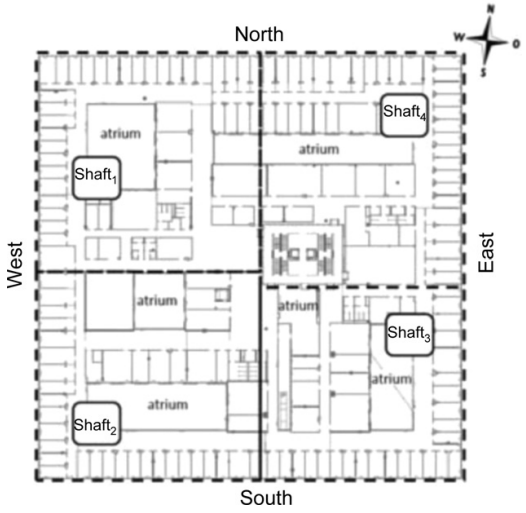

Fig. 2. Layout of the second floor, which is identically partitioned as the third floor. In this picture the atriums and the four main shafts are shown. Furthermore, the orientation and the layout of the rooms is given.

temperature for one room. Note that a "generic indoor temperature" $\vartheta_{\mathrm{indoor}}^{\mathrm{mean}}$ can be assumed for one building zone, because of the fact that inside the building only insignificant temperature differences occur. The walls in all rooms of one zone have approximately the same temperature and the temperature distribution is assumed to be homogeneous. Hence, radiation of opaque walls is neglected and the mean of all indoor air temperatures as measured by the automation system. Temperature sensors are integrated in the room operating system, and the mounting height is handicapped accessible based on DIN18040, approximately between 85 cm and 105 cm. The sensors have a measuring range of 273.15–323.15 K, and an accuracy of ±0.1 K. External radiance is measured by four mono-crystal silicon cells, oriented in the cardinal directions. These sensors have a measuring range of 0–1200 W/m^2, an accuracy of 5% (ISO 9060), and a long-term stability of <1%/year.

3. Black-box model

3.1. General black-box modeling aspects

In this approach a fuzzy black-box model for buildings is presented. It is to note, that for a nonlinear dynamical black-box model

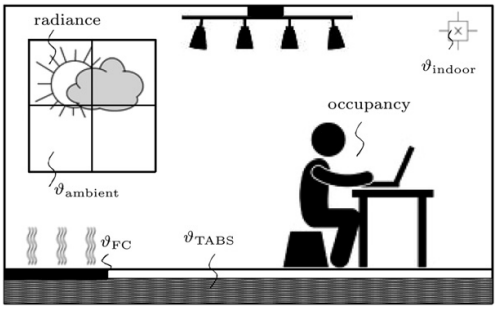

Fig. 3. Inputs and output for the specific black-box model shown in an example. The supply heats are denoted by $\vartheta_{\mathrm{TABS}}$ and ϑ_{FC}.

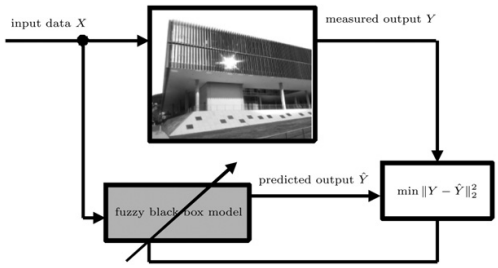

Fig. 4. Schematic work flow of data-driven black-box model.

many measurements of the process are needed. These measurements should include the typical behavior of the building heating dynamics, and also contain stronger excitation of the heat supply than during the normal process. However, for a good and realistic black-box model these measurements have to describe the main nonlinear ties in the process (building dynamics).

In Fig. 4 it is shown how a data-driven black-box model in general works. For modeling with a black-box, input- and output-data are required [15]. The matrix of input-data X is inserted in the real process (building itself) and in the black-box model of this process. From the real process the outputs Y are measured. The model simulates a so-called predicted output $\hat{Y}$. The goal is to minimize the error between the predicted output of the model $\hat{Y}$ and the real measured output of the process Y. This leads to minimize the error $\|Y - \hat{Y}\|_2^2$, and to update the model parameters, symbolized in Fig. 4 with the diagonal arrow through the black-box modeling box. In this approach for the black-box a local linear model tree (LoLiMoT) algorithm is used and presented in Section 3.2 [4,5]. After showing the main details of the algorithm in an overview, the mathematical formulation of the extracted so-called Takagi–Sugeno (TS) fuzzy models for representation of the local linear models (LLM) is presented in Section 3.3.

3.2. Black-box modeling with local linear model trees (LoLiMoT)

The LoLiMoT algorithm combines a heuristic strategy for partition space decomposition with weighted least squares optimization [4]. It therefore provides an LLM approximation of globally nonlinear dynamic systems.

In LoLiMoT Gaussian Kernel functions are fitted to a rectangular partitioning of the m-dimensional input or *partition space* (for details see Section 4.2) performed by a decision tree with axis-orthogonal splits at the internal nodes (Fig. 5). Note that in Fig. 5 the gray boxes define the chosen LLM for the next split (thus the worst performing LLM) and the white boxes give the LLMs which are kept in the next iteration. Each local model belongs to one hyper-rectangle in which center the fitting point is placed.

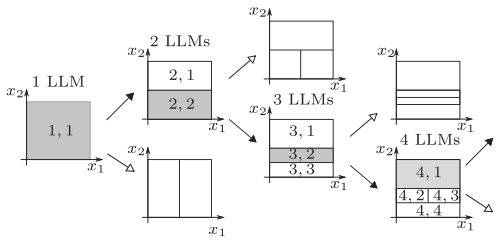

Fig. 5. First four iterations of LoLiMoT algorithm for a two-dimensional input space ($m = 2$).

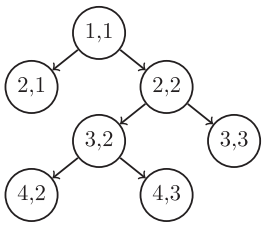

Fig. 6. Interpretation of Fig. 5 as a decision tree.

New hyper-rectangles are found by testing the possible splits in all dimensions and taking the one with the highest performance improvement. The algorithm stops when reaching a predetermined modeling error or maximum size of the tree (Fig. 6). Note that the partition space need *not* be identical to the input space of the local models, and that the choice of partition variables allows for incorporation of expert knowledge. The partition space is the key point of this algorithm, it should describe the strongest non-linearities during the process to reach the best results. The algorithm is listed in a short summary, see also Fig. 5:

1. Start with a global linear model.
2. Perform axis-orthogonal splits on that model.
3. Find the worst LLM by calculating the local loss function for each model.
4. The hyper-rectangle of the worst LLM is split into two halves by doing an axis-orthogonal split. Divisions in all dimensions are tried.
5. Fit LLMs for all possible alternative splits by weighted least squares.
6. Compare these fits and implement the one split with the highest performance improvement.
7. If the termination criterion is met then stop, else go to Step 3.

As shown in [4], two intrinsic features make LoLiMoT extremely fast: First, at each iteration only the worst local model is considered for division. Second, in Step 3 only the parameters of those local models that are newly generated by the division have to be estimated.

The calculation of the error in Step 3 is based on the local sum of squared error loss function and not their mean. Thus, the local model quality critically depends on the distribution of the training data and hence also of the partitioning data.

3.3. Takagi–Sugeno (TS)-fuzzy models

TS-fuzzy models are suitable for approximating systems by interpolating between local linear, time-invariant autoregressive models with exogenous inputs (ARX), [11]. The resulting output of the LoLiMoT algorithm, see Section 3.2, are parameters for an ARX-model. Therefore, the equivalence to a TS-fuzzy model is obtained [4].

The basic element of a TS-fuzzy system is a set of fuzzy inference rules. In general, each inference rule consists of two elements: the IF-part (antecedent) and the THEN-part (consequent) [10], the set of rules is given by $\mathcal{R}$ in this work.

Here $\zeta = [\zeta_1, \zeta_2, \ldots, \zeta_p] \in \mathbb{R}^p$ is the vector of input fuzzy variables. The elements of the fuzzy vector are usually a subset of the past input and outputs [11]. This vector is defined as:

$$\zeta \in \{y(k), \ldots, y(k - n_a + 1), u_l(k - \tau), \ldots, u_l(k - n_b - \tau + 1)\} \in \mathbb{R}^p, \quad (1)$$

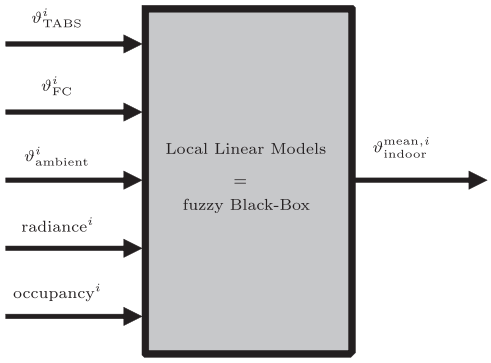

Fig. 7. Inputs and outputs for the specific black-box model of zone i, $i = \{\text{NE, SW}\}$. The first two inputs are supply heat temperatures and the third is the ambient temperature, all in K.

where y is the output, u_l is the input l where l denotes the specific input parameter or number of input, n_a is the maximum lag considered for the output and n_b is the maximum lag considered for the input terms. Furthermore, τ is the discrete dead time.

The overall system is approximated by a collection of coupled multiple-input single-output (MISO) discrete-time TS-fuzzy models of the input–output nonlinear ARX (NARX) type

$$y^{k+1} = \sum_{j=1}^{r} \Phi_j(\zeta) y_j^{k+1}, \tag{2}$$

where r denotes the global number of rules. The degree of fulfillment of the specific jth rule can be computed using the product operator $\mu_j(\zeta) = \prod_{i=1}^{p} \mu_{j,\Xi_i}(\zeta_i)$, where Ξ_i are the antecedent fuzzy set or regions for the jth rule $\mathcal{R}^j$. Furthermore, the normalized degree of fulfillment can be computed as

$$\Phi_j(\zeta) = \frac{\mu_j(\zeta)}{\sum_{i=1}^{r} \mu_i(\zeta)}. \tag{3}$$

The membership function is parametrized improperly through the centers, the spreads and the steepness value k_σ, [4,11,10].

Note, that Φ_j denotes the fuzzy membership function in the operating point ζ, for LLM$_i$, $i = 1, \ldots, r$. In this work, *blended* describes the mixture between LLMs, where $\sum_{i=1}^{r} \Phi_i = 1$ holds. *Blended zones* are the areas in the partition space, where the LLMs are overlapping each other. Note, that the approach of Section 3.2 is equivalent to the mathematical representation in this section, Section 3.3, therefore $p \equiv r$ holds.

4. Fuzzy black-box model for building heating dynamics

In this section the work flow of the effective fuzzy black-box model for the specific building in Austria is presented. In Fig. 7 the specific input/output collection of the black-box model is presented. The overall output is given by the mean of the indoor room temperature $\vartheta^{\text{mean},i}_{\text{indoor}}$ of each zone i. The model inputs are given by two heat supply, one for TABS $\vartheta^{\text{mean},i}_{\text{indoor}}$ and one for FC ϑ^i_{FC}, the ambient temperature $\vartheta^i_{\text{ambient}}$, the radiance^i for each orientation and the occupancy^i profile, depending on each zone i. The data for the data-driven black-box model are taken from an open-loop step-test during 29th of April 2014–5th of May, 2014. The test was done during a holiday and an ensuring weekend. Therefore, occupancy is insignificant during the duration of the open-loop step-test. Note, that for complete identification additional data are needed. Thus, closed-loop data are also used for the identification.

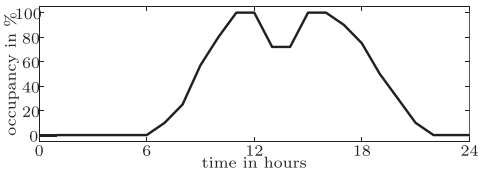

Fig. 8. Generic occupancy profile for offices in University buildings, adapted from [9], pattern 3.

For the closed-loop data and the validation period the occupancy profile is one of the most important disturbances for modeling proper thermal behavior.

4.1. Selection of input and output data

Selecting input and output data for system identification is an important pre-processing step in case of data-based modeling. It is obvious to choose the output based on the associated control variable of the MPC. For reconstructing the strongest nonlinear building behavior it is important to choose the minimum number of uncorrelated inputs. Therefore, only the variables are chosen which are affecting the model output. Note, that for heat flow $\dot{Q}^i_j$ of TABS and FC the following relation holds:

$$\dot{Q}^i_j = \underbrace{\dot{m}^i_j}_{const.} \cdot \vartheta^i_j \cdot \underbrace{c^i_p}_{const.}, \tag{4}$$

where c_p, the specific heat capacity of water, is assumed to be constant and has no sub fix j. Also the mass flows $\dot{m}^i_j$ are assumed to be constant, further $i = \{\text{NE, SW}\}$ and $j = \{\text{TABS, FC}\}$. Because of Eq. (4) the heat supplies are given in K in the remainder of this work. The following list specifies the model inputs:

- supply heat of TABS for each zone i in K, denoted by $\vartheta^i_{\text{TABS}}$,
- supply heat of FC for each zone i in K, denoted by ϑ^i_{FC},
- ambient temperature in K, denoted by $\vartheta_{\text{ambient}}$,
- radiance in W/m^2,
- a generic occupancy profile for each zone i in %,

$i = \{\text{NE, SW}\}$. The output of the model is the mean of the indoor room temperatures in one zone, denoted by $\vartheta^{\text{mean,i}}_{\text{indoor}}$.

As such models are attractive for all kinds of controller design, because of their low order, see Section 3, the goal is to obtain a model which is able to reproduce the main dynamics of the whole building and not to represent each single room perfectly. Utilizing analytical modeling tools, often a high-order model is obtained and afterwards the reduced order model is used for model-based control.

The utilized generic occupancy, adapted from pattern 3 of [9], is presented in Fig. 8. This is a special profile for offices in an University building.

4.2. Selection procedure for choice of partition space

As introduced in Section 3.2, selection of the partition space for the LLMs is one of the major tasks. In many processes the partition space is given by expert knowledge. If this is not the case, it is necessary to analyze the measurements to find the strongest nonlinearities in the process. In Fig. 9 the exemplary plotmatrix for zone north-east is given. The procedure is as follows: (1) search for a data-distribution/data-cloud which cannot be mapped by linear correlations; (2) if (1) leads to no result, search for the data-cloud with the largest spread; (3) if (1) and (2) did not succeed, start trial and error procedure or incorporate expert knowledge. In this

specific plotmatrix for zone north-east, which shows step-test measurements from one week of the University Salzburg, see Fig. 9, the problem is that only a small amount of data are measured, to be specific 168 hours (1 hour = 1 sample). Therefore, according to case (3) the suitable partition space for this specific building was selected by know-how of the building operators.

In the University building in Salzburg, Austria, a 2-dimensional partition space is chosen for presenting the strongest nonlinear effects in this building. Therefore, an input–input partition space is chosen: $\vartheta^i_{\text{TABS}} \times \vartheta^i_{\text{ambient}}$, $i = \{\text{NE, SW}\}$. Past analysis has shown that these are the most important variables within building heating control.

4.3. Selection procedure for choice of model order

The *orders* n_a and n_b (see Section 3.3) in the LoLiMoT algorithm have to be chosen manually. If order = 1 is chosen, the input–output model from this algorithm is static. Therefore, with a higher order it is possible to make the model dynamic and also represent dead time. There is no strict rule to choose the order of each input and output. Eq. (5) shows a general pulse transfer function for a discrete-time transfer function representation:

$$G(z) = \frac{b_0 z^{-\tau} + b_1 z^{-1-\tau} + \cdots + b_n z^{-n_b-\tau}}{1 + a_1 z^{-1} + \cdots + a_n z^{-n_a}} = \frac{Y(z)}{U(z)}. \tag{5}$$

This equation gives the relation between input $U(z)$ (numerator) and output $Y(z)$ (denominator), see Eq. (1). Note, that for each building zone *only one* common denominator is identified. Therefore, the dynamics of each input to the overall output is specifically given by the numerator.

For linear system identification different algorithms are state-of-the-art for parameter identification, see [15]. The orders of the fuzzy black-box model of this specific building, are chosen as shown in Table 1. The acronyms "rad" stand for radiance and "occ" for occupancy, respectively. For details, see Sections 4.5 and 5.2.

Table 1
Orders for inputs and output of both zones.

$\vartheta^{\text{mean,NE}}_{\text{indoor}}$	$\vartheta^{\text{NE}}_{\text{TABS}}$	$\vartheta^{\text{NE}}_{\text{FC}}$	$\vartheta^{\text{NE}}_{\text{ambient}}$	rad^{NE}	occ^{NE}
4	3	3	1	2	1
$\vartheta^{\text{mean,SW}}_{\text{indoor}}$	$\vartheta^{\text{SW}}_{\text{TABS}}$	$\vartheta^{\text{SW}}_{\text{FC}}$	$\vartheta^{\text{SW}}_{\text{ambient}}$	rad^{SW}	occ^{SW}
3	2	2	2	1	1

4.4. Selection procedure for choice of number of LLMs

In Section 3.2 it is shown, that the number of LLMs is essential for the quality of the model. This quality is measured with two different statistical criterions: (1) the coefficient of determination R^2 and (2) the root-mean-square error (RMSE). These statistical tools are computed as:

$$R^2 \equiv 1 - \frac{\sum_t^n \|Y_t - \hat{Y}_t\|_2^2}{\sum_t^n \|Y_t - \overline{Y}\|_2^2}, \tag{6}$$

$$\text{RMSE} \equiv \sqrt{\frac{\sum_{t=1}^n \|\hat{Y}_t - Y_t\|_2^2}{n}}, \tag{7}$$

where $\overline{Y}$ is the mean of the measured output values, calculated as $\overline{Y} = 1/n \sum_{t=1}^n Y_t$ and n is the number of measurements for Y.

The steepness k^i_σ, $i = \{\text{NE, SW}\}$ of the Gaussian-membership functions is considered to be $k^{\text{NE}}_\sigma = 1/2$ and $k^{\text{SW}}_\sigma = 1/3$, illustrated in Figs. 10 and 11 [4]. This steepness determines whether the blending between different LLMs is hard or soft. A smaller value for k^i_σ, $i = \{\text{NE, SW}\}$ presents a harder crossover between models than a larger value. As it is presented in Figs. 10 and 11, the membership functions of zone north-east have a larger value for $k^i_\sigma, i = \{\text{NE, SW}\}$, than those of zone south-west. The work flow is given as: (1) first optimize k_σ, this could be done with trial and error or an nonlinear optimization; (2) optimize the number of LLMs.

In Table 2 a comparison between the number of LLMs and the model fit is presented for both zones, the chosen orders for inputs and output is taken from Section 4.3.

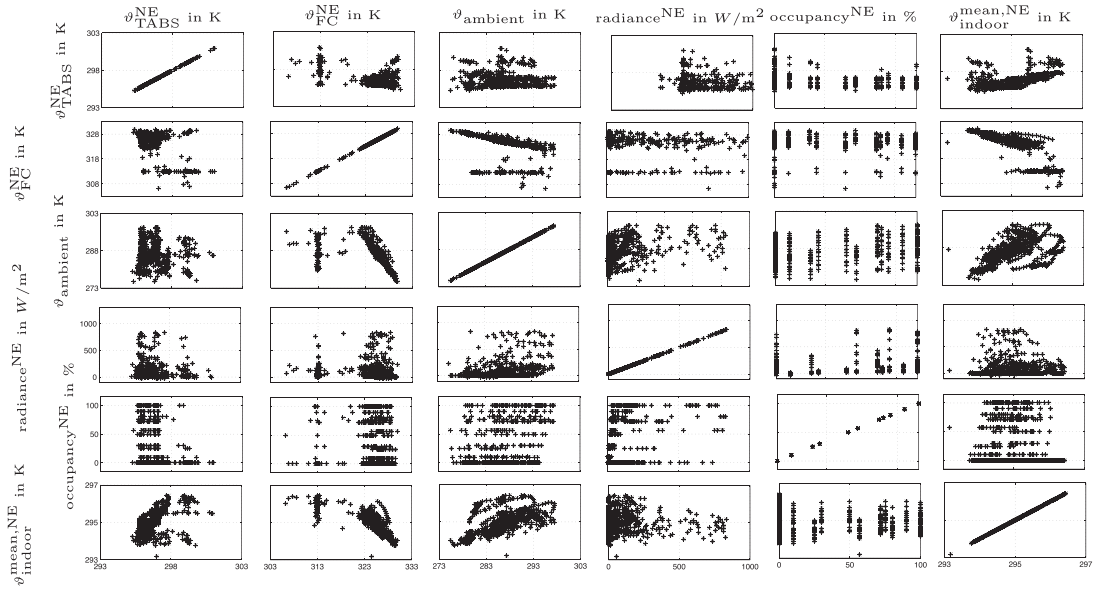

Fig. 9. The plotmatrix for zone north-east is shown in this figure. In the main diagonal the distribution from all variables against their selves is shown.

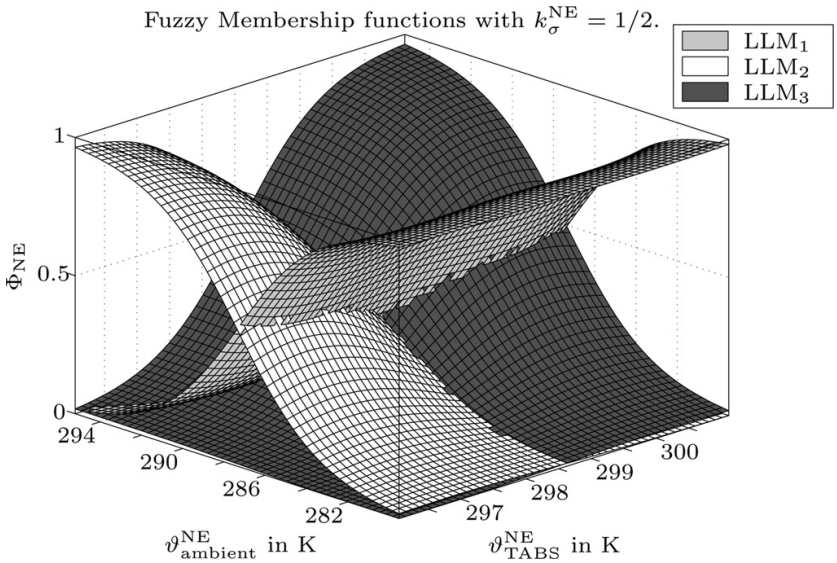

Fig. 10. Fuzzy membership functions for zone north-east.

For both zones three LLMs are selected. Note, that the higher the number of LLMs the better the model fit will be. Therefore, the first significant increase (R^2) or decrease (RMSE) in the statistical values indicates the optimal number of LLMs. Fig. 12 presents Table 2 in a graphical form.

The diamond shows a possible number of LLMs for R^2 and the circle shows the possible number of LLMs for the RMSE. Note, that R^2 converges faster than the RMSE. The possible-best number of LLMs for R^2 in both zones is 2, for the RMSE is 4. Therefore, the chosen number in this specific building model is given by 3 in both zones. If the number of LLMs is too high, it can occur that some LLMs are so-called off-equilibrium LLMs [27,28].

Note that an alternative approach is the use of the Akaike information criterion (AIC), leading to similar results. In the AIC the model performance is balanced against the number of parameters. In the presented criterions the number of parameters is not considered inherently (but the mentioned balance is done by using Fig. 12).

In Fig. 10 the fuzzy membership function for zone north-east is shown, and in Fig. 13(a) the 2-dimensional partition space with the axis orthogonal splits is shown. Furthermore, the

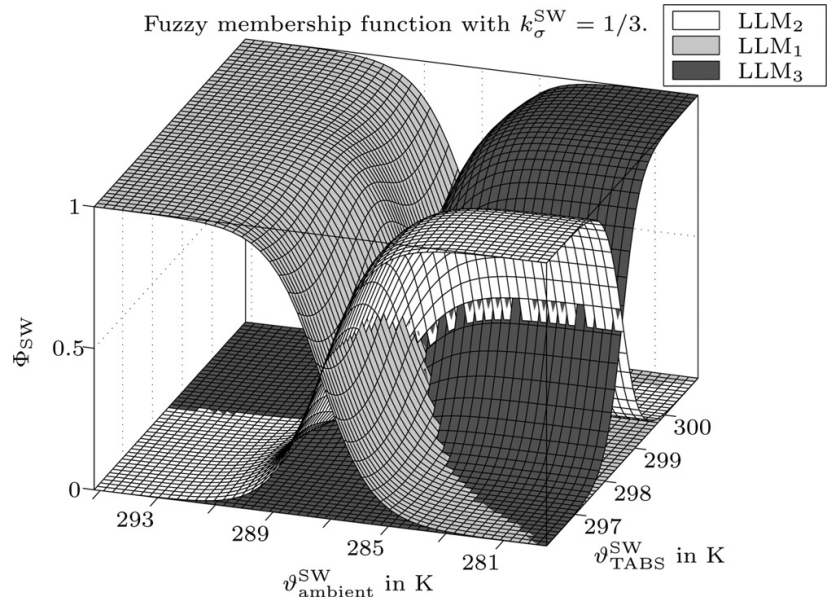

Fig. 11. Fuzzy membership functions for zone south-west.

Table 2
Comparison of model performance of zone north-east depending on the number of LLMs and zone south-west, respectively.

#LLMs	R^2_{NE}	$RMSE_{NE}$	R^2_{SW}	$RMSE_{SW}$
1	0.877	0.262	0.827	0.297
2	0.915	0.217	0.887	0.241
3	0.930	0.196	0.917	0.207
4	0.940	0.182	0.928	0.192
5	0.945	0.175	0.937	0.179
6	0.948	0.164	0.939	0.177

fuzzy membership function for zone south-west is presented in Fig. 11. Moreover the 2-dimensional partition space is illustrated in Fig. 13(b).

4.5. Final TS-fuzzy building model

The final model of this specific University building in Austria is parametrized as discussed in Sections 4.1–4.4. In this section the nonlinear step-responses are shown as well as the linear step-responses of representative LLMs. Also the value when 90% of the steady state step-response are reached are given in the specific subplots. In Fig. 14 the partition space from zone north-east is shown once again. In this plot the diamond gives the steady state value and the cross denotes the input step (the dashed line shows the change over different LLMs). The corresponding nonlinear step-response shown in Fig. 15. Note, that only a step in the ambient temperature input can directly cause a nonlinear step-response. Furthermore, the resulting $t_{90\%}$ value of the nonlinear step-response from $\vartheta^{NE}_{ambient}$ is presented. Note that the $t_{90\%}$ value for the transient between those two LLMs is actually an average value between $t_{90\%}$ values of the individual LLMs (Fig. 16). The local linear step-responses of each input to the overall output for LLM_1 (from the final model) in zone north-east is shown in Fig. 16. For zone south-west LLM_2 is chosen and presented in Fig. 17. Note, that instead of a unit step, a step is chosen which is in a well defined temperature range for buildings. All steps are simulated based on the fact that the system

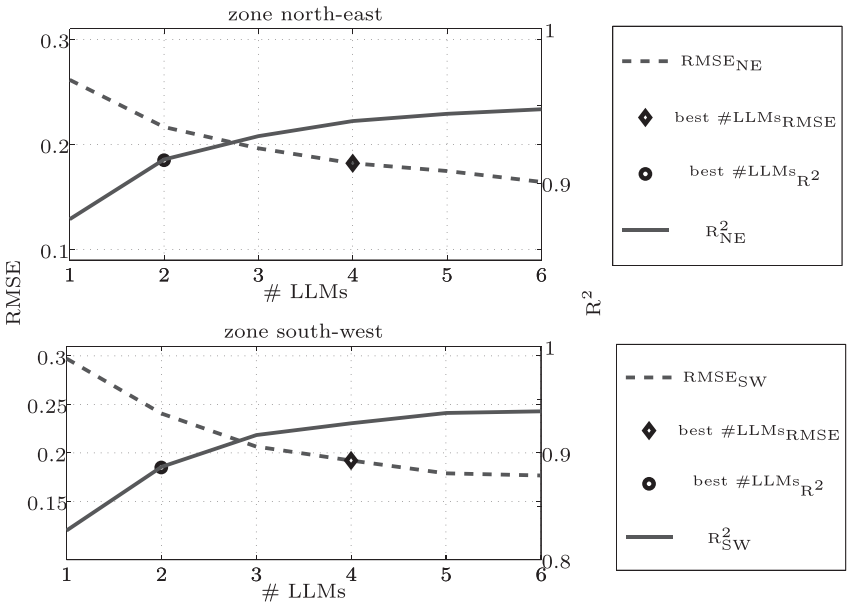

Fig. 12. These subplots show the number of LLMs against the RMSE (on the left *y*-axes) and R^2 (on the right *y*-axes) for both zones. On the top the plot shows the values for zone north-east and on the bottom the same for zone south-west. The diamond shows the chosen number of LLMs in case of the best RMSE fit for this specific case. The same is shown with the circle for R^2.

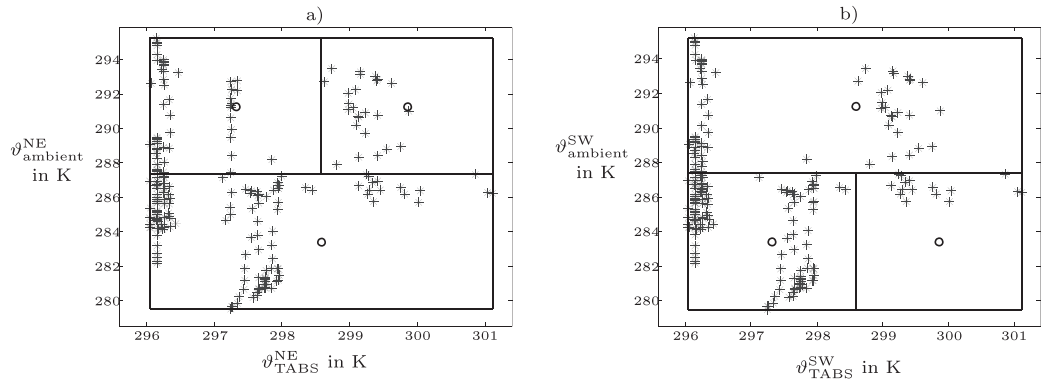

Fig. 13. In (a) the 2-dimensional partition space for zone north-east with local model centers and spreads is shown. The same is presented in (b) for zone south-west.

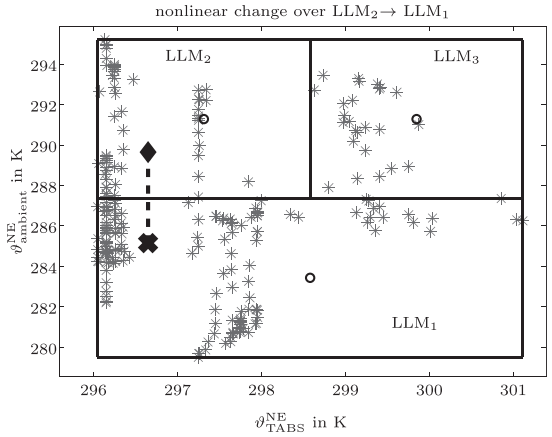

Fig. 14. Partition space of zone north-east with change over different LLMs, this leads to a nonlinear step-response. The diamond represents the start in the steady state and the cross represents the final step value.

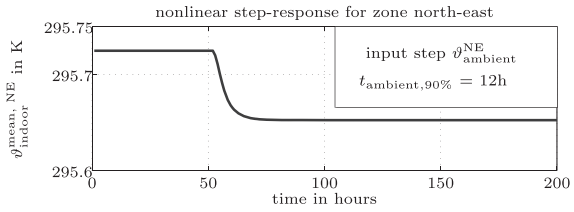

Fig. 15. Nonlinear step-response for $LLM_2 \rightarrow LLM_1$ of zone north-east with $t_{90\%}$ values.

Table 3
Statistical values for validation of both zones for 21.04.2014–28.04.2014.

R^2_{NE}	$RMSE_{NE}$	R^2_{SW}	$RMSE_{SW}$
0.632	0.265	0.746	0.279

dynamics are steady state at this moment. In Figs. 16 and 17 the different time constants are presented. For input $\vartheta^i_{ambient}$, $i = \{NE, SW\}$, a step from 286.15 K to 278.15 K is chosen, which is normal for Salzburg at this season. Note, that in Fig. 16 and 17 $t_{j,90\%}$ stands

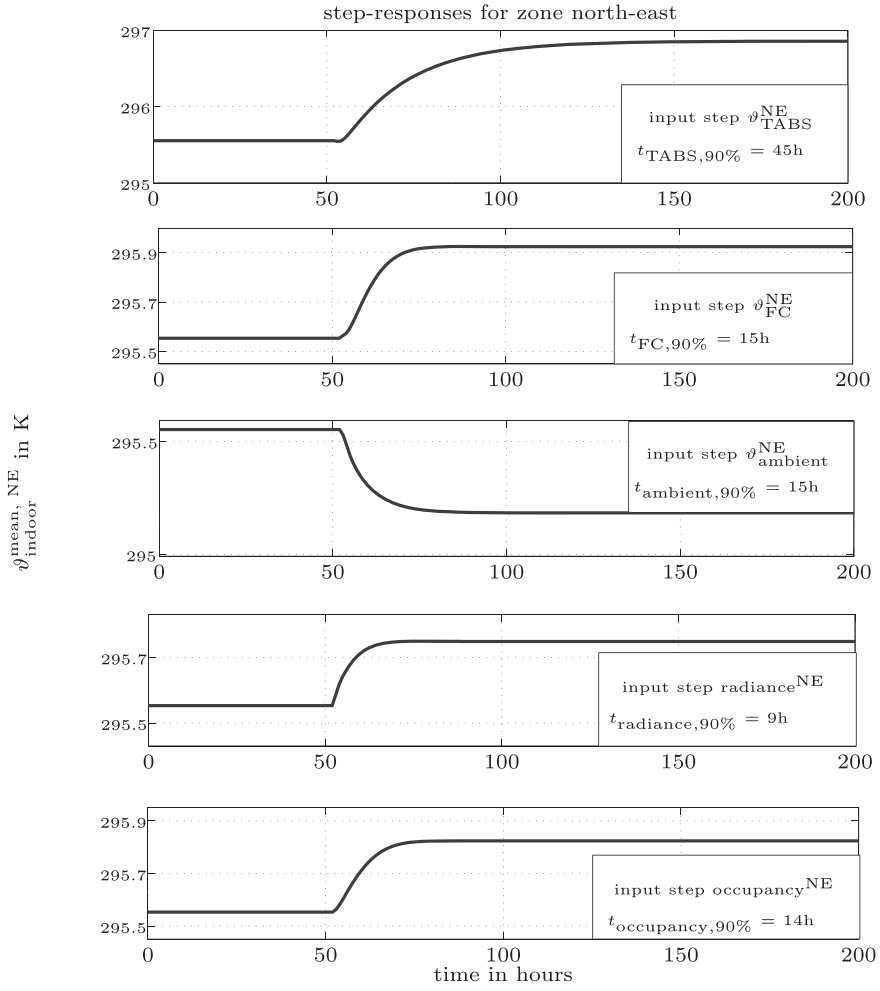

Fig. 16. Step-responses for LLM_1 of zone north-east with $t_{90\%}$ values.

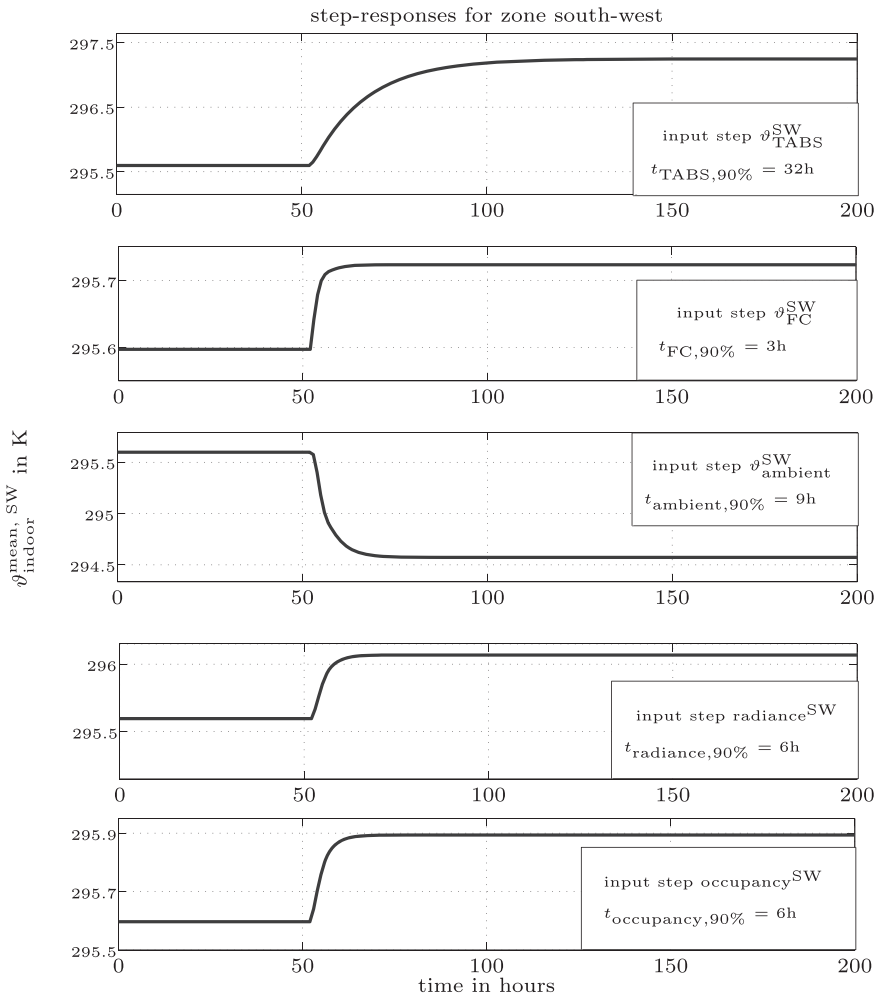

Fig. 17. Step-responses for LLM_2 of zone south-west with $t_{90\%}$ values.

for the time when 90% of a steady state is reached, for specific input j. The fuzzy black-box model is able to correctly reproduce the time constants according to expert knowledge. Note, that because of structural and physical differences between zone north-east and zone south-west it is plausible, that the time constants are smaller in zone south-west than in zone north-east. This could be due to the fact that zone south-west is elevated on columns (see Fig. 1) and has a much larger contact area to the ambiance than zone north-east, which is integrated in the main building. The main statement is, that the effective fuzzy black-box model is able to represent the nonlinear dynamical behavior of the University building, see following Section 5.

5. Simulation and validation results

A full cross validation is shown in this section. Data from one week before the step test were used for validation. In this specific building all relevant variables are directly measured (ambient temperature, radiance, indoor room temperature and both supply heats are measured). Only for occupancy a generic profile is used, see Fig. 8. The demonstration building is equipped with an Distributed Control System (DCS) with an integrated historical database (XAM-Control, [29]). Therefore all sensors (room temperature, ambient temperature, radiation,...) and actors (valves, motors,...) are directly connected (analog or digital signal) to the I/O modules of the DCS. These modules are connected via an Transmission Control Protocol/Internet Protocol (TCPIP) connection to the controllers, using an internal http based protocol. Besides that the meters (energy consumption) are connected via M-Bus to the DCS.

5.1. Model validation

In Fig. 18 the measured and predicted output values for both zones during one week in April 2014 are shown. In Fig. 18 the solid-black line gives the measured values (data) and the dashed-gray line gives the model output from the specific zone obtained from the fuzzy black-box model. Note, that during the validation weeks normal occupancy profiles are in effect. In Table 3 the statistical criterions for both zones are given. It is to mention, that the absolute maximal temperature prediction error in zone north-east is smaller than 0.72 K and the maximal temperature difference in zone south-west is smaller than 0.76 K. The maximum resolution of the indoor

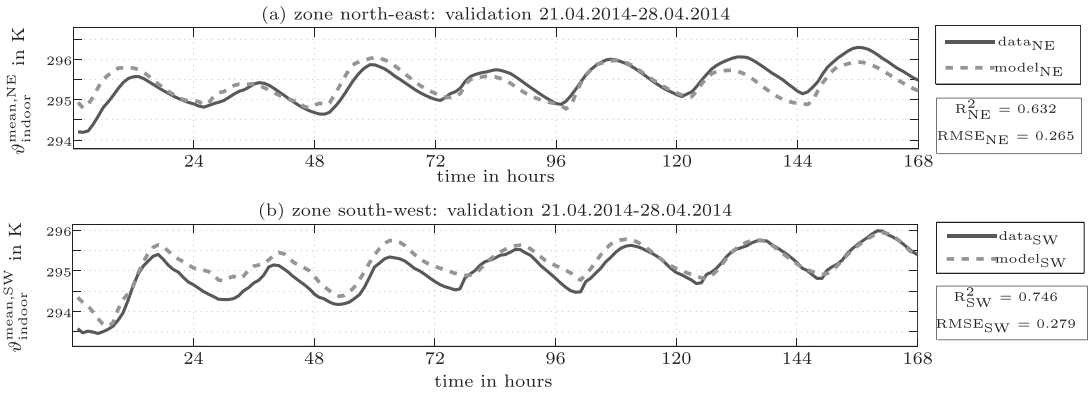

Fig. 18. In subplot (a) the validation for zone north-east is presented. In subplot (b) zone south-west is shown. Statistical values R^2 and RMSE are also shown in the subplots.

air temperature sensors is 0.1 K, see Section 2. Nevertheless, computational results have been given up to three decimal points, such as the model output θ^i_{mean}, which is an averaged value over several rooms.

Note that the model is utilized in an MPC for predicting the output over a prediction horizon. The FMPC starts calculating the prediction from an accurate measure and computes for a prediction horizon from about 12 hours to a maximum of 36 hours. Even if the underestimation trend is present in the model it will hardly compromise the validity of the FMPC prediction.

5.2. Discussion

As it has already been mentioned, that the overall dynamic behavior is given good in both models. It must be considered, that the duration for the open-loop step-test and the resulting measurements cover only a duration of one week with a sampling-time of 1 hour. Therefore, only 168 data-points were available for system-identification. This small amount of training data yields a surprisingly good nonlinear dynamic building model. The resulting RMSE of 0.27 and 0.28 K, respectively, for a prediction horizon of a whole week is a clear proof of the suitability for model based controller design.

Another issue in this specific building is the disturbances of the so-called blinds. The position of these blinds (see Fig. 1) is not measurable. Unfortunately, the important information is missing in the system identification, but as it is shown in Section 5.1 the models are performing quite well without this information. The reason is that the black-box model inherently contains the average user behavior of a zone in terms of setting the blinds' position for a specific radiation intensity. Furthermore, the output $\vartheta^{mean}_{indoor}$ of each zone is given by the mean of 40 rooms per zone, which partly compensates for deviations in the behavior of an individual user. Nevertheless, the model for zone south-west may still include systematic errors, which cannot be currently eliminated.

As it is mentioned in the Introduction, this specific building has different dynamics associated to the different zones (defined by the individual supply zones and geographic orientation). Hence, different time constants and different mean values are plausible and coincide with existing expert knowledge. Furthermore, structural and physical differences between the zones exist. In spite of these complications, the full cross validation (see Fig. 18) gives fine results for a suitable model for an MPC design.

In Fig. 16 and 17 the local linear step-responses from selected LLMs of both models are shown. Here it is to mention that the different $t_{90\%}$ constants are coming from the fact mentioned in Section 4.5.

Note, that the effort in the work flow of data-driven modeling versus white-box modeling is significantly different. For a black-box model no perfect plan-data are needed and no algorithm for order reduction is necessary. It should be noted, that there are only few parameters for optimizing such a complex nonlinear dynamical building behavior. To specify them: (1) k_σ and the spreads of the membership-functions and (2) the ARX-parameters for the transfer functions.

The main purpose of the presented model (plant model for controller design) is therefore given, as a good generalization is achieved with minimum modeling effort.

6. Conclusion

An effective fuzzy black-box model approach was introduced and applied to a specific building. The data-based model makes use of all relevant input and output measurements from an open-loop step-test. Benefits of this effective modeling are the low complexity by design, and that the fuzzy black-box model is suitable for MPC, without any transformations. Another benefit is, that the effective data-based model is able to represent the strongest nonlinear effects in building heating dynamics. The process for getting such models is shown in details. A full cross validation highlights the results of such low-order fuzzy black-box model for buildings. Beside a full cross validation, nonlinear step-responses and local linear step-responses for both zones are shown. The associated time constants also coincide with expert knowledge. In summary, an effective fuzzy black-box model for building heating dynamics has been presented in this article.

Acknowledgements

This work was supported by the project "SMART MSR" (FFG, No. 832103) in cooperation with evon GmbH. We are grateful for the support of University Salzburg.

References

[1] L. Pérez-Lombard, J. Ortiz, C. Pout, A review on buildings energy consumption information, Energy Build. 40 (3) (2008) 394–398, http://dx.doi.org/10.1016/j.enbuild.2007.03.007.
[2] F.R. d'Ambrosio Alfano, B.W. Olesen, B.I. Palella, G. Riccio, Thermal comfort: design and assessment for energy saving, Energy Build. 81 (0) (2014) 326–336, http://dx.doi.org/10.1016/j.enbuild.2014.06.033.

[3] J. Široký, F. Oldewurtel, J. Cigler, S. Prívara, Experimental analysis of model predictive control for an energy efficient building heating system, Appl. Energy 88 (9) (2011) 3079–3087, http://dx.doi.org/10.1016/j.apenergy.2011.03.009.
[4] O. Nelles, Nonlinear System Identification: From Classical Approaches to Neural Networks and Fuzzy Models, Engineering Online Library, Springer, 2001.
[5] M. Killian, S. Grosswindhager, M. Kozek, B. Mayer, Pre-processing of partition data for enhancement of LOLIMOT, in: Proceedings of the 2013 8th EUROSIM Congress on Modelling and Simulation, EUROSIM '13, IEEE Computer Society, Washington, DC, USA, 2013, pp. 271–275, http://dx.doi.org/10.1109/EUROSIM.2013.56.
[6] E. Camacho, C. Bordons, Model Predictive Control, Advanced Textbooks in Control and Signal Processing, Springer, London, 2004.
[7] M. Castilla, J. Álvarez, M. Berenguel, F. Rodríguez, J. Guzmán, M. Pérez, A comparison of thermal comfort predictive control strategies, Energy Build. 43 (10) (2011) 2737–2746, http://dx.doi.org/10.1016/j.enbuild.2011.06.030.
[8] F. Oldewurtel, A. Parisio, C.N. Jones, D. Gyalistras, M. Gwerder, V. Stauch, B. Lehmann, M. Morari, Use of model predictive control and weather forecasts for energy efficient building climate control, Energy Build. 45 (0) (2012) 15–27, http://dx.doi.org/10.1016/j.enbuild.2011.09.022.
[9] W.-K. Chang, T. Hong, Statistical analysis and modeling of occupancy patterns in open-plan offices using measured lighting-switch data, Build. Simul. 6 (1) (2013) 23–32, http://dx.doi.org/10.1007/s12273-013-0106-y.
[10] T. Takagi, M. Sugeno, Fuzzy identification of systems and its applications to modeling and control, IEEE Trans. Syst. Man Cybern. SMC-15 (1) (1985) 116–132, http://dx.doi.org/10.1109/TSMC.1985.6313399.
[11] J. Abonyi, Fuzzy Model Identification for Control, Birkhauser, Boston, 2002.
[12] J. Roubos, S. Mollov, R. Babuska, H. Verbruggen, Fuzzy model-based predictive control using Takagi–Sugeno models, Int. J. Approx. Reason. 22 (12) (1999) 3–30, http://dx.doi.org/10.1016/S0888-613X(99)00020-1.
[13] M. Killian, B. Mayer, M. Kozek, Hierarchical fuzzy MPC concept for building heating control, in: Proceedings of the 19th World Congress of the International Federation of Automatic Control (IFAC'14), 2014, pp. 12048–12055, http://dx.doi.org/10.3182/20140824-6-ZA-1003.00772.
[14] B. Mayer, M. Killian, M. Kozek, Cooperative and hierarchical fuzzy MPC for building heating control, in: IEEE International Conference on Fuzzy Systems (FUZZ-IEEE), 2014, pp. 1054–1059, http://dx.doi.org/10.1109/FUZZ-IEEE.2014.6891573.
[15] L. Ljung, System Identification: Theory for the User, Prentice-Hall information and System Sciences Series, Prentice Hall PTR, 1999.
[16] S. Prívara, J. Cigler, Z. Váňa, F. Oldewurtel, C. Sagerschnig, E. Žáčeková, Building modeling as a crucial part for building predictive control, Energy Build. 56 (0) (2013) 8–22, http://dx.doi.org/10.1016/j.enbuild.2012.10.024.
[17] S. Prívara, Z. Váňa, E. Žáčeková, J. Cigler, Building modeling: selection of the most appropriate model for predictive control, Energy Build. 55 (Cool Roofs, Cool Pavements, Cool Cities, and Cool World) (2012) 341–350, http://dx.doi.org/10.1016/j.enbuild.2012.08.040.
[18] B. Lehmann, D. Gyalistras, M. Gwerder, K. Wirth, S. Carl, Intermediate complexity model for model predictive control of integrated room automation, Energy Build. 58 (2013) 250–262.
[19] S. Prívara, Z. Vana, D. Gyalistras, J. Cigler, C. Sagerschnig, M. Morari, L. Ferkl, Modeling and identification of a large multi-zone office building, in: IEEE International Conference on Control Applications (CCA), 2011, pp. 55–60, http://dx.doi.org/10.1109/CCA.2011.6044402.
[20] T.T.M.P. Sullivan Royer, Stephane Till Black-box modeling of buildings thermal behavior using system identification, in: Proceedings of the 19th World Congress of the International Federation of Automatic Control (IFAC'14), 2014, pp. 10850–10855, http://dx.doi.org/10.3182/20140824-6-ZA-1003.01519.
[21] G. Reynders, J. Diriken, D. Saelens, Quality of grey-box models and identified parameters as function of the accuracy of input and observation signals, Energy Build. 82 (0) (2014) 263–274, http://dx.doi.org/10.1016/j.enbuild.2014.07.025.
[22] A. Preglej, J. Rehrl, D. Schwingshackl, I. Steiner, M. Horn, I. Škrjanc, Energy-efficient fuzzy model-based multivariable predictive control of a {HVAC} system, Energy Build. 82 (0) (2014) 520–533, http://dx.doi.org/10.1016/j.enbuild.2014.07.042.
[23] V. Logar, I. Živa Kristl, Škrjanc, Using a fuzzy black-box model to estimate the indoor illuminance in buildings, Energy Build. 70 (0) (2014) 343–351, http://dx.doi.org/10.1016/j.enbuild.2013.11.082.
[24] C. Ghiaus, Fuzzy model and control of a fan-coil, Energy Build. 33 (6) (2001) 545–551, http://dx.doi.org/10.1016/S0378-7788(00)00097-9.
[25] R. Kumar, R. Aggarwal, J. Sharma, Energy analysis of a building using artificial neural network: a review, Energy Build. 65 (0) (2013) 352–358, http://dx.doi.org/10.1016/j.enbuild.2013.06.007.
[26] P. Ferreira, A. Ruano, S. Silva, E.C. Conceicao, Neural networks based predictive control for thermal comfort and energy savings in public buildings, Energy Build. 55 (0) (2012) 238–251, http://dx.doi.org/10.1016/j.enbuild.2012.08.002.
[27] R. Murray-Smith, T.A. Johansen, R. Shorten, On transient dynamics, off-equilibrium behaviour and identification in blended multiple model structures, in: European Control Conference, 1999, p. 14.
[28] T. Johansen, R. Shorten, R. Murray-Smith, On the interpretation and identification of dynamic Takagi–Sugeno fuzzy models, IEEE Trans. Fuzzy Syst. 8 (3) (2000) 297–313, http://dx.doi.org/10.1109/91.855918.
[29] Evon automation, The software, XAMControl. Available from: http://evon-automation.com/index.php/en/products/xamcontrol (accessed 05.01.15).

2.2 Publication B

Michaela Killian, Barbara Mayer, Alexander Schirrer, and Martin Kozek.
Cooperative Fuzzy Model Predictive Control.
Fuzzy Systems, IEEE Transactions on, 2015, ISSN: 1063-6706, article in press.
DOI: 10.1109/TFUZZ.2015.2463674

Own contribution
Problem analysis, advancement of methods, development of theoretical results, proofs of developed concepts, execution of the solution, development and programming of algorithms, consideration of implementation aspects, performing simulation studies, and structuring, writing and editing of the manuscript was done by the applicant. Discussion of methodology, and editing of the manuscript was done by the second author. Problem statement, development of theoretical results, discussion and editing was done by the third author. Problem statement, discussion and editing was done by the third author.

Cooperative Fuzzy Model Predictive Control

Michaela Killian, Barbara Mayer, Alexander Schirrer, and Martin Kozek.

***Abstract*—In this paper a cooperative fuzzy model predictive control (CFMPC) is presented. The overall non-linear plant is assumed to consist of several parallel input-coupled Takagi-Sugeno (TS) fuzzy models. Each such TS-fuzzy subsystem is represented in the form of a local linear model network (LLMN). The control of each local linear model (LLM) in each LLMN is realized by model predictive control (MPC). For each LLMN the outputs of the associated MPCs are blended by the fuzzy membership functions, which leads to a fuzzy model predictive controller (FMPC). The resulting structure is one FMPC for each LLMN-subsystem. Overall, a parallel combination of FMPCs results, which mutually affects all LLMN-subsystems by their respective manipulated variables. To compensate detrimental cross-couplings in this setup, a cooperation between the FMPCs is introduced. For this cooperation, convergence is proven and for the closed-loop system a stability proof is given. It is demonstrated in a simulation example that the proposed input-constraint CFMPC algorithm achieves convergence of the fuzzy LLMNs within few cooperative iteration steps. Simulations are given to demonstrate the effectiveness of the theoretical results.**

***Index Terms*—cooperative MPC, fuzzy MPC, fuzzy control, stability, Takagi-Sugeno model.**

I. INTRODUCTION

Controlling complex non-linear dynamic systems is a challenging task in the area of process control. Due to the typically high order and strong coupling effects it is difficult, if not impossible, to directly apply non-linear control design methods. Two effective methods to circumvent this problem are: (i) Splitting the complex non-linear problem into a set of less complex sub-problems, solving the sub-problems independently, and finding a cooperation between the set of sub-problems. Note that a global optimum and stability may not be guaranteed in this case, [1], [2], [3]. (ii) Using LLMNs [4]. This LLMN approach is equivalent to Takagi-Sugeno (TS) fuzzy modeling, and an effective way to control such systems is given by fuzzy control, [5], [6]. Utilizing the LLMN or TS-fuzzy approach, respectively, the overall complex non-linear system is represented by a weighted superposition of the LLMs.

However, if the system to be controlled is non-linear *and* of high order, none of the two before mentioned approaches may be feasible. Nevertheless, many large complex systems can be divided into several LLMN-subsystems, where each of these LLMN-subsystems is less complex but may still exhibit non-linear behavior. In this paper an effective method to solve such a control problem is given, where a combination of the two mentioned approaches is proposed, and a set of input-coupled LLMN-subsystems constitutes the global plant. Utilizing MPC, the resulting structure is a CFMPC.

One main advantage of this CFMPC concept is the simplification from one global FMPC optimization problem to multiple local optimization problems. Furthermore, the smaller number of manipulated variables also significantly reduces computational complexity. The CFMPC algorithm optimizes several local less complex optimization problems, hence, if convergence occurs, a solution exists which can only be suboptimal, but the implementation is inherently distributed and local optimizations can run in parallel. Furthermore, tractability is much more likely than for the global FMPC problem. Another benefit is the expandable structure of the controller scheme. If one new subsystem and a resulting FMPC is added to the CFMPC concept, only the new controller has to be designed and all other controllers in the system only have to incorporate an additional further disturbance signal (the input signal of the new subsystem).

MPC is a well-established and effective method for process control, [7]. The merging of TS-fuzzy modeling and MPC leads to a so-called FMPC strategy, which can be considered a powerful design tool on its own, [8], [3], [9], [10]. This control concept is also utilized in this work because of efficient constraint handling, its decoupling characteristics, and inherent robustness properties, [2].

Cooperative MPC (CMPC) has been developed for both non-linear and linear plants, and respective proofs of convergence and stability are available, [11], [12]. Note, however, that the CMPC concept does not guarantee global optimality. Nevertheless, for complete convergence Pareto-optimality of the plant-wide feedback control has been shown. For the combination with LLMs the linear version of CMPC is the natural choice [11]. Hence, the concept proposed here utilizes cooperative control for several coupled fuzzy MPCs. The main contributions of this work are as follows:

- A CFMPC concept for cooperative control of fuzzy MPCs is presented.
- A CFMPC optimization algorithm is derived based on [11].
- Based on a fixed-point theorem a proof of convergence for the cooperative iteration loop is given.
- Stability of the resulting CFMPC is proven.

Cooperation between individual FMPCs is constituted by an inner iteration-loop, see Fig. 1, which is executed within consecutive time steps k and $k+1$. At each cooperative iteration q an improved solution of the cooperative manipulated variable u^q is computed by the q-th iteration update $h^q(\cdot,\cdot)$. The solution $u^\star$ is obtained when the iterate u^q converges to

This work was supported by the project "SMART MSR" (FFG, No. 832103) in cooperation with evon GmbH.

M. Killian, M. Kozek, and A. Schirrer are with the Institute of Mechanics and Mechatronics, Vienna University of Technology, Vienna, 1060 Austria e-mail: michaela.killian@tuwien.ac.at, martin.kozek@tuwien.ac.at, alexander.schirrer@tuwien.ac.at.

B. Mayer is with the Institute of Industrial Management, FH Joanneum Kapfenberg, Austria e-mail: barbara.mayer@fh-joanneum.at

Manuscript revised May 06, 2015; accepted July 25, 2015.

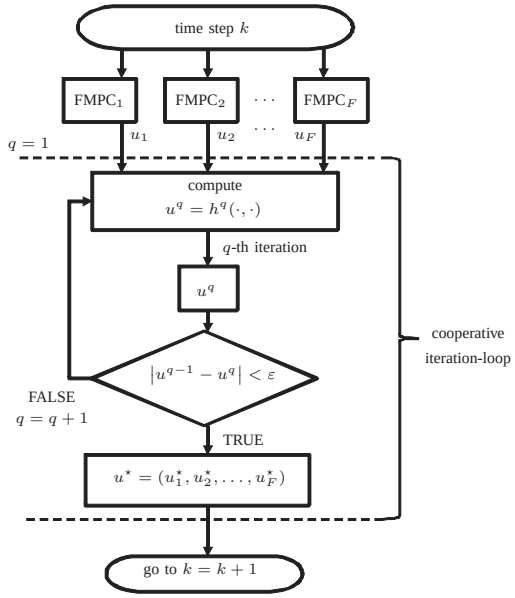

Fig. 1. Schematic flow-chart of CFMPC. Between consecutive time steps k and $k+1$ the q-th cooperative iteration update $h^q(\cdot,\cdot)$ is computed in a loop. The resulting cooperative solution for the manipulated variable is given by $u^\star$.

a fixed value. Note that in contrast to the original manipulated variable u from the individual FMPCs, the final cooperative manipulated variable is denoted by $u^\star$. A fast cooperation (as it is demonstrated in Sec. VI) is not guaranteed in general, it strongly depends on the system behavior. The whole CFMPC scheme in general is illustrated in Fig. 2.

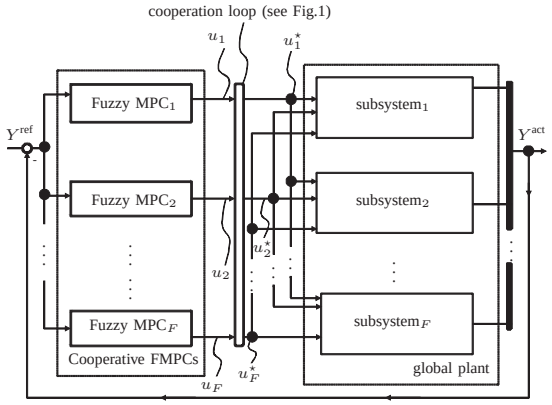

Fig. 2. Concept of Cooperative FMPCs for $\mathbb{F} = \{1, 2, \ldots, F\}$.

Note that Y^{ref} gives the reference values and Y^{act} represents the actual output value. Furthermore, the manipulated variables u_i, $\forall i \in \mathbb{F}$ represent the manipulated variables before the cooperative iteration update, $u_i^\star$, $\forall i \in \mathbb{F}$ in contrast denote the manipulated variables after the cooperative iteration update.

The TS-fuzzy models utilized here have been extensively applied in the area of MPC, [5], [9], [13], [14], [15]. This type of underlying models leads to a specific class of controllers – the class of fuzzy model predictive controllers (FMPC) [3], [10], [16], [17]. Furthermore, controlling linear processes by MPC is widespread because of its mature stability theory, the inherent robustness, and handling of constraints [2], [7], [18]. One major advantage of TS-fuzzy models is given by the possibility of their direct identification from measurement data; one of the published methods is the local linear model tree algorithm (LOLIMOT), [4], [19]. This identification method leads to LLMs as well and can be used to approximate TS-fuzzy models for control design. In [5] the fundamental TS-fuzzy concepts can be found.

In [13] an output-feedback predictive controller, based on TS-fuzzy models, is presented. The control law depends on the membership functions, and stability is ensured by quadratic boundedness. [20] introduces robust stability constraints for MPC, the underlying model being also based on TS-fuzzy models. The MPC presented in [21] solves a $\min - \max$ optimization of a quasi-worst-case infinite horizon objective function. Applications of FMPC schemes are given in [16], [17], which cover the application of building heating control. In [9], [10] an efficient way for using TS-fuzzy models in MPC theory is given. Structure and controller design of an MPC for TS-fuzzy models can be partly adopted from [9], [10].

Stability for FMPC is presented in different approaches, [22], [23], [24], [25], [26], [20]. A global analytic proof of stability for FMPC does not exist, but several stability conditions have been derived: (i) using linear-matrix inequalities (LMI) is a common approach for showing stability [23], [26], (ii) the so-called non-quadratic membership-dependent Lyapunov function is also used in literature [22]; (iii) other types of Lyapunov functions are the common-quadratic Lyapunov function, the piecewise-quadratic Lyapunov function or the fuzzy Lyapunov function [25], [21]. A different issue is discussed in [27], namely a robust MPC-concept for discrete-time TS-fuzzy systems (RFMPC) with input constraints and with persistent disturbances. The authors of [27] show that an N-step RFMPC is able to deal with a fixed terminal constraint set. The online computation of the N-step prediction control strategy involves bisection searches and solving a convex optimization problem subject to LMI constraints. A further MPC variant for discrete fuzzy systems is given in [28]. The authors of [28] compute an optimal controller with iterative quadratic programming.

In contrast to the above mentioned control schemes, a cooperative FMPC structure based on [11] is treated here. The combination of cooperative suboptimal MPC [1] and FMPC has not been presented yet. Stability proofs for each of the two utilized methods are available in literature. Therefore, in this paper a combined CFMPC structure is proposed and a stability proof is presented. Additionally, a convergence proof for the cooperative iteration loop is given.

This papers is structured as follows: The concept of an FMPC and the underlying model structure is given in Sec. II, and the principle of the suboptimal FMPC is described in Sec. III. The main part of this work, the cooperation between the FMPCs and the cooperative iteration loop, is introduced

in Sec. IV. Stability is proven in Sec. V. An example with illustrative results is given in Sec. VI, and a conclusion summarizes the main results.

II. FUZZY MODEL PREDICTIVE CONTROL (FMPC)

Linear MPC refers to a class of control algorithms that compute manipulated variables by utilizing a linear process model, [2]. Many systems are, however, inherently non-linear. This motivates the use of non-linear model predictive control. Here a non-linear and generally non-convex optimization problem has to be solved. To avoid non-convex optimization, a set of LLMs can be extracted from a TS-fuzzy model, [9], which are then used by the MPC algorithm, [8], [14], [6]. In the following, the index i of FMPCs is taken from the set $\mathbb{F} = \{1, 2, \ldots, F\}$, and the associated L_i LLMs for FMPC$_i$, $\forall i \in \mathbb{F}$, are denoted by the index $l \in \mathbb{L}_i = \{1, \ldots, L_i\}$.
The control objective in this research is given by minimizing a weighted summation of all FMPCs (so-called plant-wide cost function), for details see Eq. (26) in Sec. IV-D.

A. Takagi-Sugeno Fuzzy Model

TS-fuzzy models are suitable to approximate such non-linear systems by interpolating between local linear, time-invariant auto-regressive models with exogenous inputs (ARX), [6]. The basic element of a TS-fuzzy system is a set of fuzzy inference rules [5]. For each rule $\mathbf{R}^j$ the structure given in [5], [6] holds, $\forall j = 1, \ldots, r$. For notation, $\zeta = [\zeta_1, \ldots, \zeta_p] \in \mathbb{R}^p$ is the vector of input fuzzy variables, and $\Xi_{j,1}, \ldots, \Xi_{j,p}$ are the fuzzy sets or regions for the j-th rule $\mathbf{R}^j$ with corresponding membership functions $\mu_{j,\Xi_1}, \ldots, \mu_{j,\Xi_p}$, with $\mu_{j,\Xi_i}(\zeta_i) \mapsto [0, 1]$, for $i = 1, \ldots, p$, [4], [17], [16]. The number of rules r_i in this work is the same as the number of LLMs L_i, $\forall i \in \mathbb{F}$, [4].

The elements of the fuzzy vector are usually a subset of the past input and outputs, [6]. The overall system is approximated by a collection of coupled multiple-input multiple-output (MIMO) discrete-time TS-fuzzy models of the input-output non-linear ARX (NARX) type

$$y^{k+1} = \sum_{j=1}^{L} \Phi_j(\zeta) y_j^{k+1}, \tag{1}$$

where L denotes the global number of LLMs (rules). The degree of fulfillment of the specific j-th rule can be computed using the product operator $\mu_j(\zeta) = \prod_{i=1}^{p} \mu_{j,\Xi_i}(\zeta_i)$, furthermore, the normalized degree of fulfillment can be computed as

$$\Phi_j(\zeta) = \frac{\mu_j(\zeta)}{\sum_{l=1}^{L} \mu_l(\zeta)}, \tag{2}$$

It is obvious that there are systematic similarities between conditional parametric models and TS-fuzzy models. In this context the local neighborhood around each fitting point is determined by Gaussian kernel functions, for fuzzy models the term membership function is used for Eq.(2), [4], [6], [5], [23].

A TS-fuzzy model can be locally represented by a linear state-space model [10]

$$\begin{aligned} x^{k+1} &= A^k x^k + \tilde{B}^k \tilde{u}^k \\ y^k &= C^k x^k, \end{aligned} \tag{3}$$

with the state-vector $x^k \in \mathbb{R}^{n_x}$ at time step k. The output-vector at time step k is given by $y^k \in \mathbb{R}^{n_y}$, $u_i^k \in \mathbb{R}^{n_{u_i}}$ is the input vector at time k and $u_{\mathbb{J}_i}^k \in \mathbb{R}^{n_{u_{\mathbb{J}_i}}}$ is the vector of disturbances at time k, where $\mathbb{J}_i \subseteq \mathbb{F} \setminus i$. The combined inputs are given by $\tilde{u}^k \in \mathbb{R}^{n_{u_i}+n_{u_{\mathbb{J}_i}}}$. In addition, $\tilde{u} = [u_i, u_{\mathbb{J}_i}]'$, where u_i is the manipulated variable and $u_{\mathbb{J}_i}$ are the disturbances for FMPC$_i$, which are the manipulated variables from all other FMPCs$_{\mathbb{J}_i}$, $\forall i \in \mathbb{F}, \mathbb{J}_i \subseteq \mathbb{F} \setminus i$.

Furthermore, the matrices $A^k \in \mathbb{R}^{n_x \times n_x}$,

$$\tilde{B}^k = \begin{bmatrix} B_i & 0_{n_{x_i} \times n_{u_{\mathbb{J}_i}}} \\ 0_{n_{x_{\mathbb{J}_i}} \times n_{u_i}} & B_{\mathbb{J}_i} \end{bmatrix} \in \mathbb{R}^{(n_{x_i}+n_{x_{\mathbb{J}_i}}) \times (n_{u_i}+n_{u_{\mathbb{J}_i}})},$$

$\forall i \neq j$, $C^k \in \mathbb{R}^{n_y \times n_x}$ are considered to be non-constant (time-varying) in each time step k. Note that B_i is the input matrix for u_i, and $B_{\mathbb{J}_i}$ is the disturbance matrix for system i, depending on input $u_{\mathbb{J}_i}$ from the j-th system, $j \in \mathbb{J}_i$.
The time-variant matrices, $A^k, \tilde{B}^k$, and C^k are computed by blending parameters of all $A_{i,l}^k, \tilde{B}_{i,l}^k$, and $C_{i,l}^k$, $\forall i \in \mathbb{F}$, $l \in \mathbb{L}_i$, e.g. $A^k = \sum_{l=1}^{L_i} \Phi_{i,l} A_{i,l}^k$, $\forall l \in \mathbb{L}_i$, $i \in \mathbb{F}$. The term $\Phi_{i,l}$ denotes the fuzzy membership function in the operating point ζ for LLM$_{i,l}$, $\forall i \in \mathbb{F}$, $l \in \mathbb{L}_i$. Note that $\mathbb{L}_i$ can be different for each LLMN$_i$, $\forall i \in \mathbb{F}$.
In this work, *blended* means that more than one subsystem contributes significantly to the output.

Remark 1: In the following, all models are considered to be only input-constrained systems and the developed algorithm is derived for so-called input-coupled systems.

B. FMPC Formulation

The optimization problem for each FMPC can be formulated as:

$$J_i^\star = \min_{\Delta u_i} J_i(\tilde{u}_i) \qquad \forall i \in \mathbb{F} \tag{4a}$$

where

$$\begin{aligned} J_i(y_i^k, \tilde{u}_i^{k,k+n_p-1}) = \sum_{k=0}^{n_p-1} [&(y_{i,\text{ref}}^k - y_{i,\text{act}}^k)' \tilde{Q}_i (y_{i,\text{ref}}^k - y_{i,\text{act}}^k) \\ &+ \tilde{u}_i^{k\prime} R_i \tilde{u}_i^k] \end{aligned} \tag{4b}$$

subject to

$$u_{i,\min} \leq u_i \leq u_{i,\max}, \tag{4c}$$

$\forall i \in \mathbb{F}$, where n_p denotes the prediction horizon, and "$'$" denotes transpose. Note that the $y_{i,\text{ref}}^k$ are external reference values and are considered to be known (see Fig. 2)

It is important to note that the algorithm for FMPC$_i$ optimizes only u_i and not $\tilde{u}_i$. The values of $u_{\mathbb{J}_i}$ do not have to be calculated, they result from the known past control inputs of the other FMPCs (all FMPCs except FMPC$_i$). The formulation is valid for a general MIMO system, where

$$\tilde{U} = \begin{bmatrix} \tilde{u}_1, \tilde{u}_2, \ldots, \tilde{u}_{n_{u_i}+n_{u_{\mathbb{J}_i}}} \end{bmatrix}' \in \mathbb{R}^{n_c \times (n_{u_i}+n_{u_{\mathbb{J}_i}})}$$

denotes the control action for all manipulated variables $\tilde{u}_i \in \mathbb{R}^{n_{u_i}+n_{u_{\mathbb{J}_i}}}$ over the entire control horizon n_c. Furthermore,

$$Y^{\text{act}} = \left[\ y_{1,\text{act}}, y_{2,\text{act}}, \ldots, y_{n_y,\text{act}}\ \right]' \in \mathbb{R}^{n_p \times n_y}$$

represents the predicted output values over the prediction horizon n_p.

$$Y^{\text{ref}} = \left[\ y_{1,\text{ref}}, y_{2,\text{ref}}, \ldots, y_{n_y,\text{ref}}\ \right]' \in \mathbb{R}^{n_p \times n_y}$$

contains the values of the reference trajectory for each output, $\tilde{Q}_i \in \mathbb{R}^{n_y \times n_y}$ is a positive semi-definite weighting matrix, and $R_i \in \mathbb{R}^{(n_{u_i}+n_{u_{\mathbb{J}_i}})\times(n_{u_i}+n_{u_{\mathbb{J}_i}})}$ is a positive definite weighting matrix. The objective function of each FMPC$_i$ is also subjected to a local linear model network (LLMN) which consists of L_i LLMs, which are equivalent to r-fuzzy rules.
Note that, without loss of generality, $y^k_{i,\text{ref}}$ is assumed to be equal to zero in the following and for the stability proof. However, for any given constant non-zero $y^k_{i,\text{ref}}$ there exists a unique shift of coordinates to consider a zero-reference problem.

$$J_i(x_i^k, \tilde{u}_i^{k,k+n_p-1}) = \sum_{k=0}^{n_p-1} ({y^k_{i,\text{act}}}' \tilde{Q}_i y^k_{i,\text{act}} + \tilde{u}_i^{k\prime} R_i \tilde{u}_i^k) \quad (5a)$$

$$= \sum_{k=0}^{n_p-1} (x_i^{k\prime} \underbrace{C_i' \tilde{Q}_i C_i}_{Q_i} x_i^k + \tilde{u}_i^{k\prime} R_i \tilde{u}_i^k) \quad (5b)$$

$$= \sum_{k=0}^{n_p-1} (x_i^{k\prime} Q_i x_i^k + \tilde{u}_i^{k\prime} R_i \tilde{u}_i^k), \quad (5c)$$

$\forall i \in \mathbb{F}$, with $Q_i \in \mathbb{R}^{n_x \times n_x}$. It follows that:

$$J_i(x_i^k, \tilde{u}_i^{k,k+n_p-1}) = \sum_{k=0}^{n_p-1} (x_i^{k\prime} Q_i x_i^k + \tilde{u}_i^{k\prime} R_i \tilde{u}_i^k) \quad (6a)$$

subject to

$$u_{i,\min} \leq u_i \leq u_{i,\max}, \quad (6b)$$

$\forall i \in \mathbb{F}$ and time k.

In Eq.(4b) the input variable is denoted by $\tilde{u}_i^{k+t}, \forall t \in \{1, 2, \ldots, n_c\}$. This can be calculated by generating l sets of local linear control inputs in the first step, $\tilde{u}_{i,l}^{k+t}, \forall t \in \{1, 2, \ldots, n_c\}, \forall i \in \mathbb{F}, \forall l \in \mathbb{L}_i$. In the second step the weighted sum of the local linear control inputs give the overall blended control input:

$$\tilde{u}_i^{k+t} = \sum_{l=1}^{L_i} \Phi_{i,l} \tilde{u}_{i,l}^{k+t}, \quad (7)$$

$\forall t \in \{1, 2, \ldots, n_c\}$, $i \in \mathbb{F}$.

In the above equation, the weight of the l-th fuzzy control action $\Phi_{i,l}$ is the same as that for the l-th local linear model [6], [15], [3], [10].

C. FMPC Formulation for Unstable Plants

For controlling an unstable plant with FMPC a terminal cost has to be added to the objective function:

$$J_i(x_i^k, \tilde{u}_i^{k,k+n_p-1}) = \sum_{k=0}^{n_p-1} (x_i^{k\prime} Q_i x_i^k + \tilde{u}_i^{k\prime} R_i \tilde{u}_i^k) + {x_i^{n_p}}' \overline{P}_i x_i^{n_p} \quad (8a)$$

subject to

$$u_{i,\min} \leq u_i \leq u_{i,\max}, \quad (8b)$$

$\forall i \in \mathbb{F}$ and time k.
For Eq.(8a), $Q_i \in \mathbb{R}^{n_x \times n_x}$ is calculated as given in Eq.(5b). The computation of the terminal weight $\overline{P}_i$ is based on the theory of common quadratic Lyapunov functions (CQLF), $\forall i \in \mathbb{F}$, [29]. The weight $\overline{P}_i \in \mathbb{R}^{n_x \times n_x}$ is the CQLF for FMPC i, $\forall i \in \mathbb{F}$ and is obtained for all LLM l, $\forall l \in \mathbb{L}_i, \forall i \in \mathbb{F}$. The condition for closed-loop stabilizing unconstrained FMPCs can be constructed as given in [29]. The closed-loop fuzzy control system is globally exponentially stable if there exists a positive definite matrix $\overline{P}_i, \forall i \in \mathbb{F}$ and a set of matrices $Q_{i,l}, \forall l \in \mathbb{L}_i, \forall i \in \mathbb{F}$, such that the following LMIs are satisfied:

$$\begin{bmatrix} -\overline{P}_i^{-1} & \overline{P}_i^{-1} A_{i,l}' + Q_{i,j}' B_{i,l}' \\ A_{i,l}\overline{P}_i^{-1} + B_{i,l} Q_{i,j} & -\overline{P}_i^{-1} \end{bmatrix} < 0 \quad (9)$$

$\forall l, j \in \mathbb{L}_i, \forall i \in \mathbb{F}$. Moreover, it is assumed that the MPC controller gains of each MPC are given as state-feedback gains: $K_{i,l} = Q_{i,l}\overline{P}_i, \forall l \in \mathbb{L}_i, \forall i \in \mathbb{F}$.
Also consider a candidate Lyapunov function as: $V_i(x_i) = x_i'\overline{P}_i x_i$, and denote the closed-loop system matrix as $A_{cl,i,l} = A_{i,l} + B_{i,l}K_{i,j}, \forall l, j \in \mathbb{L}_i, \forall i \in \mathbb{F}$. The terminal constraint for each parallel local linear MPC is now given by $U_u' x^{n_p} = 0$, where U_u describes the unstable eigenmodes of the specific system matrix $A_{i,l}$, $\forall l \in \mathbb{L}_i, \forall i \in \mathbb{F}$, [2], [7], [11].

III. SUBOPTIMAL FMPC

Fuzzy MPCs (FMPC) are non-linear MPCs which achieve the global optimum for a given performance criterion (e.g. Eq.(4a)). However, for a cooperation between several FMPCs increased flexibility and a scalable control architecture can be achieved by accepting suboptimal inputs [11], [1], [17], [16]. Hence, a suboptimal FMPC analogous to suboptimal MPC presented in [1], [11] is proposed. Note that each FMPC actually acts like a parallel connection of linear MPCs with output-blending, which effectively constitutes a non-linear controller [23], [10].

In the following, definitions and stability results for a general non-linear plant are given. Furthermore, $u_{\mathbb{J}_i}^k \in \mathbb{R}^{n_{u_{\mathbb{J}_i}}}$ denotes the disturbances for FMPC$_i$ at time step k and $g : \mathbb{R}^{n_x} \to \mathbb{R}^{n_x}$ and $h^q : \mathbb{R}^{n_{u_i}+n_{u_{\mathbb{J}_i}}} \to \mathbb{R}^{n_{u_i}+n_{u_{\mathbb{J}_i}}}$ are non-linear mappings, $k \in \{0, 1, \ldots, n_p - 1\}$, $\forall i \in \mathbb{F}, \mathbb{J}_i \subseteq \mathbb{F} \setminus i$.

Then

$$x_i^{k+1} = g(x_i^k, u_i^k) \in \mathbb{R}^{n_x} \tag{10a}$$
$$u_{\mathbb{J}_i}^{k+1} \in \mathbb{R}^{n_{u_{\mathbb{J}_i}}} \tag{10b}$$
$$\tilde{u}_i^k = \begin{pmatrix} u_i^k \\ u_{\mathbb{J}_i}^k \end{pmatrix} \in \mathbb{R}^{n_{u_i}+n_{u_{\mathbb{J}_i}}} \tag{10c}$$
$$\tilde{u}_i^{k+1} = h^q(x_i^k, \tilde{u}_i^k) \in \mathbb{R}^{n_{u_i}+n_{u_{\mathbb{J}_i}}} \tag{10d}$$

holds $\forall i \in \mathbb{F}, \mathbb{J}_i \subseteq \mathbb{F} \backslash i$, where the current state for system i at time step k is denoted as x_i^k, the state update x_i^{k+1} is given by the state equation (10a). The trajectory of inputs at time step k is given by $\tilde{u}_i^k = \{\tilde{u}_i^0, \tilde{u}_i^1, \ldots, \tilde{u}_i^{n_p-1}\} \in \mathbb{R}^{n_{u_i}+n_{u_{\mathbb{J}_i}}}$. Note that disturbances are the manipulated variables of FMPCs$_{\mathbb{J}_i}$, they are included in $\tilde{u}_i^k$, see (10c). For simplification the subscript i is omitted in the following descriptions.

The function $h^q(\cdot,\cdot)$ in (10d) is the cooperative q-th iteration update, see Fig. 1, [1], [11]. Between consecutive time steps the cooperative FMPC performs q iterations of a feasible path algorithm, and $\tilde{u}$ is computed such that some cost function is minimized. A definition of $h^q(\cdot,\cdot)$ together with a proof of convergence is given in Sections IV-D. At each time step k, the first input $\tilde{u}(0) = \tilde{u}^0$ of the suboptimal trajectory is applied.

The suboptimal FMPC with initial condition $x(0) = x^0$ is initialized with the feasible input sequence $\tilde{u}^0$. For all following sampling instances, $\hat{\tilde{u}}$ is defined as the so-called warm start sequence [11], given by

$$\hat{\tilde{u}}^{k+1} = \{\tilde{u}^1, \tilde{u}^2, \ldots \tilde{u}^{n_p-1}, 0\} \in \mathbb{R}^{n_{u_i}+n_{u_{\mathbb{J}_i}}}. \tag{11}$$

The sequence $\hat{\tilde{u}}^{k+1}$ is constituted from all but the first elements of $\tilde{u}^k$ and a zero as the last input. Furthermore, $\mathcal{X}_{n_p}$ is the set of all x, for which a feasible $\tilde{u}$ exists.

The following Definition and Lemma are directly taken from [11]:

***Definition** 1 (Exponential Stability on a Set $\mathbb{X}$, [11]):* The origin is exponentially stable on the set $\mathbb{X}$ if for all $x^0 \in \mathbb{X}$, the solution $\varphi(k, x^0) \in \mathbb{X}$ and there $\exists \alpha > 0$ and $\exists \gamma \in (0,1)$ such that $\|\varphi(k,x^0)\|_2 \leq \alpha \|x^0 \gamma^k\|_2$, $\forall k \geq 0$.

***Lemma** 1 (Exponential Stability of Suboptimal MPC, [11]):* Consider a system with a steady-state solution $(0,0) = (g(0,0), h(0,0))$, where the initial values $x^0 \equiv x(0)$ and $\tilde{u}^0 \equiv \tilde{u}(0)$ are given:

$$\begin{bmatrix} x^{k+1} \\ \tilde{u}^{k+1} \end{bmatrix} = \begin{bmatrix} G(x^k, \tilde{u}^k) \\ h^q(x^k, \tilde{u}^k) \end{bmatrix} = \begin{bmatrix} g(x^k, u^i) \\ h^q(x^k, \tilde{u}^k) \end{bmatrix}, \tag{12}$$

$\forall i = \{0, 1, \ldots, n_p - 1\}$ Assume a function $V(\cdot) : \mathbb{R}^{n_x} \times \mathbb{R}^{n_u} \to \mathbb{R}_0^+ = \{x \in \mathbb{R} | x \geq 0\}$ continuous on the origin with $V(0,0) = 0$ and the input trajectory u satisfy

$$\alpha \|(x,\tilde{u})\|_2^2 \leq V(x,\tilde{u}) \leq \beta \|(x,\tilde{u})\|_2^2 \tag{13a}$$
$$V(x^{k+1}, \tilde{u}^{k+1}) - V(x^k, \tilde{u}^k) \leq -\gamma \|(x^k, \tilde{u}^0)\|_2^2 \tag{13b}$$
$$\|\tilde{u}^k\|_2 \leq \sigma \|x^k\|_2, \quad x \in \mathcal{N}_r \tag{13c}$$

with

$$\mathcal{N}_r := x \in \mathbb{R}^{n_x} : \|x\|_2 \leq r \tag{13d}$$

in which $\alpha, \beta, \gamma > 0$. If $\mathcal{X}_{n_p}$ is forward invariant for the system $x^{k+1} = g(x^k, \tilde{u}^k)$, the origin is exponentially stable for all $x^0 \in \mathcal{X}_{n_p}$.
The *proof* is given in [11].

IV. COOPERATIVE FMPC (CFMPC) CONCEPT

A. Fundamentals

In this section the CFMPC structure is introduced and in Fig. 3 the control concept for two cooperating FMPCs is illustrated. In the figure, Y^{ref} describes the reference trajectory for the closed-loop system and Y^{act} represents the actual value, for further definitions see Sec. II-B.

The global plant consists of parallel input-coupled subsystems (sub-plants), and each FMPC controls one subsystem. These subsystems are each defined by a LLMN. For each subsystem the number L_i of LLMs can be different. The matrices $A_i, B_i, \forall i \in \mathbb{F}$ for the global plant are parameter-blended matrices, see Sec. II-A and Fig. 3. The fuzzy membership functions $\Phi_{i,l}$ are given in each operating point for LLM$_{i,l}$, $\forall i \in \mathbb{F}$ and $l \in \mathbb{L}_i = \{1, 2, \ldots, L_i\}$.

In this cooperative control structure (based on Fig. 3) two FMPCs are in cooperation, the manipulated variable of one FMPC, is a disturbance to the other FMPCs and vice versa. The variables $u_i, \forall i \in \mathbb{F}$ are output-blended control inputs over

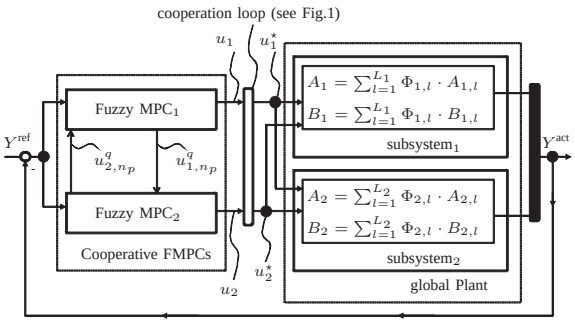

Fig. 3. Concept of Cooperative FMPCs for $\mathbb{F} = \{1, 2\}$.

the control horizon n_c in each time step k, $\mathbb{F}$ represents the set of subsystems standing in cooperation (formally defined in Sec. IV-D3). In the case of Fig. 3 u_1 and u_2 are defined as:

$$u_1^k = \sum_{l=1}^{L_1} \Phi_{1,l}^k u_{1,l}^k, \quad u_2^k = \sum_{l=1}^{L_2} \Phi_{2,l}^k u_{2,l}^k. \tag{14}$$

Furthermore, u_{1,n_p}^q and u_{2,n_p}^q denote the disturbances for the other FMPC over the prediction horizon n_p at iteration q. After the iteration loop the FMPCs get the sub-optimal solution for this time step k, namely $u_i^\star, \forall i \in \mathbb{F}$.

B. Concept for F-Subsystems

For simplify the notation the systems and proofs have been done for the case of 2 subsystems. The number of subsystems is denoted with $F < \infty$ because for each subsystem one FMPC is required and the set of FMPCs is given by $\mathbb{F} = \{1, 2, \ldots, F\}$, see Fig. 2. In general the extension to F-subsystems and resulting F-FMPCs is given in Section 6 in [11]. The extension from [11] can be adopted with one

additional assumption: It has to be assumed that the structure of all FMPCs is parallel and each set of MPC per subsystem (depending on the number of LLMs) leads to an output-blended FMPC. This assumption implies that the difference to [11] is only a linear operation (a weighted summation of signals), therefore the extension in [11] to multiple subsystems can be adopted directly.

C. Cooperative Plant-Wide Model

As mentioned in Sec. III the cooperative FMPC is a form of a suboptimal non-linear MPC. In this Section a plant-wide model is introduced for the cooperative control structure. As shown in Fig. 3, the plant consists of two parallel input-coupled subsystems, one for each FMPC. This structure is easily expandable to more FMPCs, and it is also possible to include classic MPCs in this structure or mix them with FMPCs. For the remainder of this paper it is assumed that $\mathbb{F} = \{1, 2\}$. Because the set $\mathbb{F}$ includes 2 values, the set $\mathbb{J}_i \subseteq \mathbb{F} \setminus i$ is not explicitly given by $\mathbb{J}_i$, the structure is denoted by $i, j \in \mathbb{F}, i \neq j$.

Assume that for each subsystem i a accumulation of linear models exists which describes the effects of inputs of subsystem j on the states of subsystem i, for all $(i, j) \in \mathbb{F} \times \mathbb{F}$. In Sec. II-A it was shown that TS-fuzzy models can be represented by parameter-blending which means that the non-linear structure can be seen as a local linear structure and all models, per definition, are LLMs for each subsystem. The difference equation Eq.(10a) can now be defined precisely as

$$x_{i,j}^{k+1} = A_{i,j}^k x_{i,j}^k + \tilde{B}_{i,j}^k \tilde{u}_j^k, \tag{15}$$

in which $k \in \mathbb{N}_0 = \mathbb{N} \cup 0$ represents the time step and the state-space quantities, $x_{i,j} \in \mathbb{R}^{n_{x_{i,j}}}$, $\tilde{u}_j \in \mathbb{R}^{(n_{u_j}+n_{u_i})}$, $A_{i,j} \in \mathbb{R}^{n_{x_{i,j}} \times n_{x_{i,j}}}$, and $\tilde{B}_{i,j} \in \mathbb{R}^{n_{x_{i,j}} \times (n_{u_j}+n_{u_i})}$, are defined as in Eq.(3). Note that $\tilde{u}_j$ includes also the disturbance variables u_i with dimension n_{u_i}, $\forall i \neq j$ and $i, j \in \mathbb{F}$. Following [11], the states from subsystem 1 can be accumulated as

$$\underbrace{\begin{bmatrix} x_{1,1} \\ x_{1,2} \end{bmatrix}}_{x_1}^{k+1} = \underbrace{\begin{bmatrix} A_{1,1} & \\ & A_{1,2} \end{bmatrix}}_{\Omega_1}^{k} \underbrace{\begin{bmatrix} x_{1,1} \\ x_{1,2} \end{bmatrix}}_{x_1}^{k} + \underbrace{\begin{bmatrix} B_{1,1} \\ 0 \end{bmatrix}}_{\theta_{1,1}}^{k} \underbrace{\begin{bmatrix} u_1 \\ u_2 \end{bmatrix}}_{\tilde{u}_1}^{k} + \underbrace{\begin{bmatrix} 0 \\ B_{1,2} \end{bmatrix}}_{\theta_{1,2}}^{k} \underbrace{\begin{bmatrix} u_2 \\ u_1 \end{bmatrix}}_{\tilde{u}_2}^{k}. \tag{16}$$

and for subsystem 2 in the same way as

$$\underbrace{\begin{bmatrix} x_{2,1} \\ x_{2,2} \end{bmatrix}}_{x_2}^{k+1} = \underbrace{\begin{bmatrix} A_{2,1} & \\ & A_{2,2} \end{bmatrix}}_{\Omega_2}^{k} \underbrace{\begin{bmatrix} x_{2,1} \\ x_{2,2} \end{bmatrix}}_{x_2}^{k} + \underbrace{\begin{bmatrix} B_{2,1} \\ 0 \end{bmatrix}}_{\theta_{2,1}}^{k} \underbrace{\begin{bmatrix} u_1 \\ u_2 \end{bmatrix}}_{\tilde{u}_1}^{k} + \underbrace{\begin{bmatrix} 0 \\ B_{2,2} \end{bmatrix}}_{\theta_{2,2}}^{k} \underbrace{\begin{bmatrix} u_2 \\ u_1 \end{bmatrix}}_{\tilde{u}_2}^{k}. \tag{17}$$

The models of Eq.(16) and Eq.(17) can now be written as

$$x_1^{k+1} = \Omega_1^k x_1^k + \theta_{1,1}^k \tilde{u}_1^k + \theta_{1,2}^k \tilde{u}_2^k \tag{18a}$$

and

$$x_2^{k+1} = \Omega_2^k x_2^k + \theta_{2,1}^k \tilde{u}_1^k + \theta_{2,2}^k \tilde{u}_2^k, \tag{18b}$$

with

$$\begin{aligned} \Omega_i &\in \mathbb{R}^{(n_{x_{i,i}}+n_{x_{i,j}}) \times (n_{x_{i,i}}+n_{x_{i,j}})}, \\ x_i &\in \mathbb{R}^{(n_{x_{i,i}}+n_{x_{i,j}})}, \\ \tilde{u}_i &\in \mathbb{R}^{(n_{u_i}+n_{u_j})+(n_{u_j}+n_{u_i})}, \\ \theta_{i,i} &\in \mathbb{R}^{(n_{x_{i,i}}+n_{x_{i,j}}) \times (n_{u_i}+n_{u_j})+(n_{u_j}+n_{u_i})}, \end{aligned}$$

and

$$\theta_{i,j} \in \mathbb{R}^{(n_{x_{i,i}}+n_{x_{i,j}}) \times (n_{u_i}+n_{u_j})+(n_{u_j}+n_{u_i})}$$

$\forall i \neq j \in \mathbb{F}$.

Forming a plant-wide model from subsystem 1, Eq.(18a), and subsystem 2, Eq.(18b), the model is given by

$$\underbrace{\begin{bmatrix} x_1 \\ x_2 \end{bmatrix}}_{x}^{k+1} = \underbrace{\begin{bmatrix} \Omega_1 & \\ & \Omega_2 \end{bmatrix}}_{\Omega}^{k} \underbrace{\begin{bmatrix} x_1 \\ x_2 \end{bmatrix}}_{x}^{k} + \underbrace{\begin{bmatrix} \theta_{1,1} \\ \theta_{1,2} \end{bmatrix}}_{\Theta_1}^{k} \tilde{u}_1^k + \underbrace{\begin{bmatrix} \theta_{2,1} \\ \theta_{2,2} \end{bmatrix}}_{\Theta_2}^{k} \tilde{u}_2^k \tag{19}$$

with

$$\begin{aligned} \Omega &\in \mathbb{R}^{2(n_{x_{i,i}}+n_{x_{i,j}}) \times 2(n_{x_{i,i}}+n_{x_{i,j}})}, \\ x &\in \mathbb{R}^{2(n_{x_{i,i}}+n_{x_{i,j}})}, \\ \tilde{u}_i &\in \mathbb{R}^{(n_{u_i}+n_{u_j})+(n_{u_j}+n_{u_i})}, \end{aligned}$$

and

$$\Theta_i \in \mathbb{R}^{(n_{x_{i,i}}+n_{x_{i,j}}) \times (n_{u_i}+n_{u_j})+(n_{u_j}+n_{u_i})},$$

$\forall i \neq j \in \mathbb{F}$.

For the system output

$$Y^{\text{act}} = C^k x^k = \underbrace{\begin{bmatrix} C_1 & C_2 \end{bmatrix}}_{C}^{k} \begin{bmatrix} x_1 \\ x_2 \end{bmatrix}^k \tag{20a}$$

and

$$C_1^k = \begin{bmatrix} C_{1,1} & \\ & C_{1,2} \end{bmatrix}^k, \tag{20b}$$

$$C_2^k = \begin{bmatrix} C_{2,1} & \\ & C_{2,2} \end{bmatrix}^k, \tag{20c}$$

with $C_{i,j} \in \mathbb{R}^{n_{y_{i,j}} \times n_{x_{i,j}}}$, $C_i \in \mathbb{R}^{(n_{y_{i,j}}+n_{x_{i,j}}) \times (n_{y_{i,j}}+n_{x_{i,j}})}$ and $C \in \mathbb{R}^{2(n_{y_{i,j}}+n_{x_{i,j}}) \times 2(n_{y_{i,j}}+n_{x_{i,j}})}$, $\forall i, j \in \mathbb{F}$ holds. The notation of the plant-wide model (19) and (20) can be simplified to

$$x^{k+1} = \Omega^k x^k + \Theta_1^k \tilde{u}_1^k + \Theta_2^k \tilde{u}_2^k \tag{21a}$$

$$y^k = C^k x^k \tag{21b}$$

D. Cooperative Suboptimal FMPC

In this subsection the objective function is defined (Sec. IV-D1), the constraints are established (Sec. IV-D2) and the cooperative FMPC algorithm is given in Sec. IV-D3.

1) Objective Functions: The objective functions of the individual FMPCs are given by:

$$J_i(x_i^k, \tilde{u}_i^{k,k+n_p-1}) = \sum_{k=0}^{n_p-1} (x_i^{k\prime} Q_i x_i^k + \tilde{u}_i^{k\prime} R_i \tilde{u}_i^k) + x_i^{n_p\prime} \overline{P}_i x_i^{n_p} \tag{22}$$

$\forall i \in \mathbb{F}$, $\overline{P}_i$ is formally defined in Sec. II-C, $x_i \in \mathbb{R}^{n_x}$, $\tilde{u}_i \in \mathbb{R}^{n_{u_i}+n_{u_j}}$, $Q_i \in \mathbb{R}^{n_x \times n_x}$, calculated as in Eq.(5b) and $R_i \in \mathbb{R}^{n_{u_i} \times n_{u_i}}$. The manipulated variable u_i is optimized, and the disturbance vector u_j cannot be affected by FMPC$_i$, $\forall i, j \in \mathbb{F}, i \neq j$.
The following remark is essential to motivate the stability proof in Sec.V.

***Remark** 2:* Let $\mathcal{Q}_i$ and $\mathcal{R}_i$ be diagonal time-invariant weighting matrices for FMPCs, moreover let $\overline{P}_i$ a suitable Lyapunov matrix, defined in Sec. II-C, $\forall i \in \mathbb{F}$, these weighting matrices are defined as:

$$\mathcal{Q}_i^{n_p} = \text{diag}(Q_i, Q_i, \ldots, Q_i, \overline{P}_i) \tag{23a}$$

and

$$\mathcal{R}_i^{n_p} = \text{diag}(R_i, R_i, \ldots, R_i). \tag{23b}$$

Based on the objective function Eq.(22) the objective function for subsystem 1 is given by

$$\begin{aligned} &J_1(x_1^0, \tilde{u}_1^{k,k+n_p-1}, \tilde{u}_2^{k,k+n_p-1}) \\ &= J_1(x_1^0, u_1^{k,k+n_p-1}, u_2^{k,k+n_p-1}) \\ &= \sum_{k=0}^{n_p-1} (x_1^{k\prime} Q_1 x_1^k + \tilde{u}_1^{k\prime} R_1 \tilde{u}_1^k) + x_1^{n_p\prime} \overline{P}_1 x_1^{n_p} \end{aligned} \tag{24}$$

and for subsystem 2 by

$$\begin{aligned} &J_2(x_2^0, \tilde{u}_2^{k,k+n_p-1}, \tilde{u}_1^{k,k+n_p-1}) \\ &= J_2(x_2^0, u_2^{k,k+n_p-1}, u_1^{k,k+n_p-1}) \\ &= \sum_{k=0}^{n_p-1} (x_2^{k\prime} Q_2 x_2^k + \tilde{u}_2^{k\prime} R_2 \tilde{u}_2^k) + x_2^{n_p\prime} \overline{P}_2 x_2^{n_p}, \end{aligned} \tag{25}$$

with $x_i \in \mathbb{R}^{n_{x_i}}$, $u_i \in \mathbb{R}^{n_{u_i}}$, and $\tilde{u}_i \in \mathbb{R}^{n_{u_i}+n_{u_j}}$, $\forall i \neq j$ with $i, j \in \mathbb{F}$. With Eq.(24) and Eq.(25) the plant-wide objective function is given as

$$\begin{aligned} &J(x_1^0, x_2^0, \tilde{u}_1^{k,k+n_p-1}, \tilde{u}_2^{k,k+n_p-1}) \\ &= J(x_1^0, x_2^0, u_1^{k,k+n_p-1}, u_1^{k,k+n_p-1}) \\ &= \rho_1 J_1(x_1^0, u_1^{k,k+n_p-1}, u_2^{k,k+n_p-1}) \\ &+ \rho_2 J_2(x_2^0, u_2^{k,k+n_p-1}, u_1^{k,k+n_p-1}), \end{aligned} \tag{26}$$

in which $\rho_1, \rho_2 > 0$ are relative weights, with $\rho_1 + \rho_2 = 1$.

2) Constraints: It is required that the inputs satisfy in a finite horizon

$$u_1^k \in \mathbb{U}_1^{n_p} \qquad u_2^k \in \mathbb{U}_2^{n_p} \qquad \forall k \in \mathbb{N}_0^{n_p-1}$$

where $\mathbb{U}_i$ are convex and compact sets, such that 0 is in the interior, denoted by $\mathbb{U}_i^\circ, \forall i \in \mathbb{F}$.

3) Cooperative FMPC Optimization Algorithm: Let $u^\star$ be the overall blended output, after the iteration loop, of the FMPCs with $u^0 = (u_1^0, u_2^0)$ the initial condition for the cooperative FMPC algorithm. The following optimization problem is solved at each iteration $q \geq 0$ for all subsystems $i \in \mathbb{F}$.

$$J^\star = \min_{u_i} J(x_1^0, x_2^0, u_1^{k,k+n_p-1}, u_2^{k,k+n_p-1}) \tag{27a}$$

subject to

$$x^{k+1} = \Omega^k x^k + \Theta_1^k u_1^k + \Theta_2^k u_2^k, \tag{27b}$$

$$u_i \in \mathbb{U}_i^{n_p}, \tag{27c}$$

$$\|u_i\|_2 \leq \delta_i \sum_{j \in \mathbb{F}} \|x_{i,j}^0\|_2 \quad \text{if } x_{i,j}^0 \in \mathcal{N}_r, \ \forall j \in \mathbb{F}, \tag{27d}$$

$$u_j = u_j^q \quad \forall j \in \mathbb{F} \setminus i, \tag{27e}$$

$$U_u' x^{n_p} = 0, \tag{27f}$$

where $\mathcal{N}_r$ is a neighborhood of the origin with a small radius $r > 0$, and Eq.(27f) has to be fulfilled for all LLMs$_{i,l}$, $\forall i \in \mathbb{F}, l \in \mathbb{L}_i$. Due to output-blending in the FMPCs, the blended control sequences for subsystem 1 and subsystem 2 are defined as in Eq.(14).
In this case $\Phi_{i,l}$ are the fuzzy membership functions for output-blending for LLM$_l$ of LLMN$_i$.
The (generally sub-optimal) solutions of the minimization problem (27a) subject to equations (27b)–(27e) are denoted as

$$u_1^\star(x_1^0, x_2^0, u_2^q) \tag{28a}$$

$$u_2^\star(x_1^0, x_2^0, u_1^q) \tag{28b}$$

Given the prior feasible iteration (u_1^q, u_2^q), then the next iteration is defined to be

$$\begin{aligned} u^{q+1} &= (u_1^{q+1}, u_2^{q+1}) \\ &= \Psi_1 \cdot (u_1^\star(u_2^q), u_2^q) + \Psi_2 \cdot (u_1^q, u_2^\star(u_1^q)) \\ &= \Psi_1 \left(\sum_{l=1}^{L_1} \Phi_{1,l} u_{1,l}^\star \left(\sum_{l=1}^{L_2} \Phi_{2,l} u_{2,l}^q \right), \sum_{l=1}^{L_2} \Phi_{2,l} u_{2,l}^q \right) \\ &+ \Psi_2 \left(\sum_{l=1}^{L_1} \Phi_{1,l} u_{1,l}^q, \sum_{l=1}^{L_2} \Phi_{2,l} u_{2,l}^\star \left(\sum_{l=1}^{L_1} \Phi_{1,l} u_{1,l}^q \right) \right) \end{aligned} \tag{29}$$

$$\sum_{i \in \mathbb{F}} \Psi_i = 1 \qquad \forall \Psi_i > 0, i \in \mathbb{F}. \tag{30}$$

Here, Ψ_i are arbitrary scalar weighting factors.

The iteration loop is computed between consecutive time steps. Furthermore, the matrices $\Omega^k, \Theta_1^k, \Theta_2^k$ are constant during the iteration loop, only u_i for FMPC$_j$ and u_j for FMPC$_i$, $\forall i, j \in \mathbb{F}, i \neq j$, are iteratively updated. Hence, the index k is not included in the notation of the iteration loop. To simplify notation the state dependence of u_i has not been explicitly written, $\forall i \in \mathbb{F}$. The following Lemma is specifically defined for 2 subsystems, for its extension to more subsystems see Sec. IV-B.

***Lemma** 2:* (*Feasibility*) see [11].
Given a feasible initial input sequence, the iterates satisfy

$$(u_1^q, u_2^q) \in \mathbb{U}_1^{n_p} \times \mathbb{U}_2^{n_p}, \forall q \geq 1.$$

For *proof* see [11], page 9. The arguments from [11] can be adopted because of the linear output-blending in the FMPCs. The structure is equivalent to parallel MPCs and becomes a fuzzy system structure in the output-blending. It is also important to mention that the non-linear fuzzy output is a

linear combination (summation) of local outputs, therefore, the proof of [11] can be adopted. As mentioned before in Lemma 2, also in the next Lemma the extension to more subsystems is discussed in Sec. IV-B.

***Lemma** 3:* (*Convergence of suboptimal $J(.,.)$ subject to the cooperative iteration loop, Eq.(26)*)
The cost $J(x^0, u^q)$ is not increasing for each iteration q and converges as $q \to \infty$.

Proof: For every $q \geq 0$, the cost function satisfies the following relation:

$$\begin{aligned}
J(x^0, u^{q+1}) &= J(x^0, \Psi_1(u_1^\star, u_2^q) + \Psi_2(u_1^q, u_2^\star)) \\
&= J\Bigg(x^0, \Psi_1\left(\sum\nolimits_{l=1}^{L_1} \Phi_{1,l} u_{1,l}^\star, \sum\nolimits_{l=1}^{L_2} \Phi_{2,l} u_{2,l}^q\right) \\
&+\Psi_2\left(\sum\nolimits_{l=1}^{L_1} \Phi_{1,l} u_{1,l}^q, \sum\nolimits_{l=1}^{L_2} \Phi_{2,l} u_{2,l}^\star\right)\Bigg) \\
&\leq \Psi_1 J\left(x^0, \left(\sum\nolimits_{l=1}^{L_1} \Phi_{1,l} u_{1,l}^\star, \sum\nolimits_{l=1}^{L_2} \Phi_{2,l} u_{2,l}^q\right)\right) \\
&+\Psi_2 J\left(x^0, \left(\sum\nolimits_{l=1}^{L_1} \Phi_{1,l} u_{1,l}^q, \sum\nolimits_{l=1}^{L_2} \Phi_{2,l} u_{2,l}^\star\right)\right) \quad (31a) \\
&\leq \Psi_1 J\left(x^0, \left(\sum\nolimits_{l=1}^{L_1} \Phi_{1,l} u_{1,l}^q, \sum\nolimits_{l=1}^{L_2} \Phi_{2,l} u_{2,l}^q\right)\right) \\
&+\Psi_2 J\left(x^0, \left(\sum\nolimits_{l=1}^{L_1} \Phi_{1,l} u_{1,l}^q, \sum\nolimits_{l=1}^{L_2} \Phi_{2,l} u_{2,l}^q\right)\right) \quad (31b) \\
&= J\left(x^0, \left(\sum\nolimits_{l=1}^{L_1} \Phi_{1,l} u_{1,l}^q, \sum\nolimits_{l=1}^{L_2} \Phi_{2,l} u_{2,l}^q\right)\right) \quad (31c) \\
&= J(x^0, u^q)
\end{aligned}$$

The inequality (31a) follows from convexity of $J(.)$. Inequality (31b) follows from optimality of $u_i^\star, \forall i \in \mathbb{F}$, and the last equality (31c) comes from the fact that $\sum_{i\in\mathbb{F}} \Psi_i = 1$. Because of output-blending for the FMPCs, u is a sum of weighted scalar inputs. As the sum operator is a linear operator, the reasoning of inequality conversion is adapted from [11]. Because of the fact that the cost is bounded below ($J(\cdot) \geq 0$), it converges. ■

V. STABILITY OF COOPERATIVE FMPC

Stability for FMPC can be shown in different ways, see [25], [30], [23], [24], [26], [20]. For the proof $\mathbb{F} = \{1, 2\}$ is assumed, for an extension to $\mathbb{F} = \{1, 2, \ldots, F\}$ see Sec. IV-B. To prepare for the stability proof of the cooperative FMPC structure the following two assumptions are necessary:

***Assumption** 1:* For all $i \in \mathbb{F}$ the following properties are assumed to hold:

1) The systems (Ω_i, Θ_i) are stabilizable.
2) The systems (Ω_i, Q_i) are detectable.
3) The input weights are positive definite: $R_i > 0$.
4) The state weights are positive semi-definite: $Q_i \geq 0$.
5) $n_c \geq \max(n^u)$, in which n^u is the number of unstable eigenvalues of $A_{i,l}$, $\forall i \in \mathbb{F}, l \in L_i$.
6) The FMPCs have to operate as parallel linear MPCs for each LLM and the output has to be blended for each FMPC.

***Assumption** 2:* Let $r > 0$ be given, $\forall i \in \mathbb{F}$, $\delta_i \in \mathbb{R}^+$ be chosen large enough such that there exists a $\tilde{u}_i \in \mathbb{U}^{n_p}$ satisfying $\|\tilde{u}_i\|_2 \leq \delta_i \sum_{j\in\mathbb{F}} \|x_{i,j}^0\|_2$, $\forall x_{i,j} \in \mathcal{N}_r$, $\forall j \in \mathbb{F}$.

Because of Assumption 2 the set $\mathcal{X}_{n_p}$ is invariant.
Now the stability for the closed-loop system with cooperative FMPCs is introduced, based on [11], [12]. Define the following as the warm start sequence of each subsystem i:

$$\hat{\tilde{u}}_i^{k+1} = \{\tilde{u}_i^1, \tilde{u}_i^2, \ldots, \tilde{u}_i^{n_p-1}, 0\}, \quad (32)$$

$\forall i \in \mathbb{F}$.
The warm start sequence in Eq.(32) is used as the initial condition for the cooperative FMPC problem in each subsystem i. Let the output of the cooperative FMPC control iteration, see Eq.(29), be defined as functions h_1^q and h_2^q:

$$\tilde{u}_1^{k+1} = h_1^q(x_1, x_2, \tilde{u}_1, \tilde{u}_2), \quad (33a)$$
$$\tilde{u}_2^{k+1} = h_2^q(x_1, x_2, \tilde{u}_1, \tilde{u}_2). \quad (33b)$$

The closed-loop system then is given by

$$\begin{bmatrix} x_1^{k+1} \\ x_2^{k+1} \\ \tilde{u}_1^{k+1} \\ \tilde{u}_2^{k+1} \end{bmatrix} = \begin{bmatrix} \Omega_1^k x_1^k + \theta_{1,1}^k \tilde{u}_1^k + \theta_{1,2}^k \tilde{u}_2^k \\ \Omega_2^k x_2^k + \theta_{2,1}^k \tilde{u}_1^k + \theta_{2,2}^k \tilde{u}_2^k \\ h_1^q(x_1, x_2, \tilde{u}_1, \tilde{u}_2) \\ h_2^q(x_1, x_2, \tilde{u}_1, \tilde{u}_2) \end{bmatrix}. \quad (34)$$

The system Eq.(34) can be simplified to

$$\begin{bmatrix} X^{k+1} \\ \tilde{u}^{k+1} \end{bmatrix} = \begin{bmatrix} \Omega^k X^k + \Theta_1 \tilde{u}_1^k + \Theta_2 \tilde{u}_2^k \\ h^q(X, \tilde{u}) \end{bmatrix}. \quad (35)$$

Based on Lemma 1, the next lemma can be introduced.

***Lemma** 4 (Exponential Stability, [11]):* Given Assumption 1 and Assumption 2, the origin $x = 0$ of the closed-loop system $x^{k+1} = \Omega^k X^k + \Theta_1 \tilde{u}_1^k + \Theta_2 \tilde{u}_2^k$ is exponentially stable on the set $\mathcal{X}_{n_p}$.

Proof: Equation (35) is of the same type as given in [11]. Because of Assumption 1, item 6), the summation for blending is a linear operation. In addition, Assumption 1 and Assumption 2 are fulfilled for Eq. (35), therefore it is possible to directly adopt the proof from [11]. ■

***Corollary** 1:* For suboptimal FMPC the stability proof holds if Eq. (31b) is fulfilled and Eq. (32) is given. If these two relations are fulfilled the stability proof above holds, even if no convergence in the iterative cooperation loop occurs.

***Remark** 3:* The extension from unconstrained guaranteed stable FMPCs (see Sec. II-C) to input-constrained stable FMPC has to be carried out as shown in [29] (Sec.10.3.1, pp.205–213).

VI. SIMULATION EXAMPLE

A simulation study of the CFMPC concept is shown in the following, where two FMPCs are in cooperation (see Fig. 3). LLMN_1 is given by 3 LLMs each with oscillatory dynamics. The second LLMN_2 is described by 3 unstable LLMs. Hence, $\mathbb{F} = \{1, 2\}$ and $\mathbb{L}_i = \{1, 2, 3\}$, $\forall i \in \mathbb{F}$ holds. In Fig.4 the poles of the second-order LLMs for both subsystems and the unit circle (dashed dotted line) are shown. The diamonds represent the poles of the oscillatory $\text{LLM}_{1,l}$, and the circles represent the poles of unstable $\text{LLM}_{2,l}$, $\forall l \in \mathbb{L}_i$. In all simulations the reference steps Y^{ref} are given by a black dashed-dotted line (Figs. 5, 6, and 9). During the simulations the first reference step occurs at $k = 100$ from 2 to 40, at $k = 250$ the reference

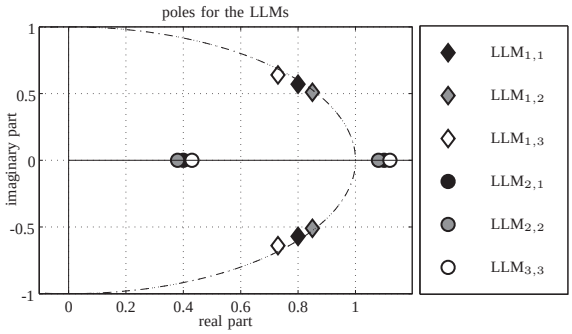

Fig. 4. Poles of oscillatory and unstable LLMs.

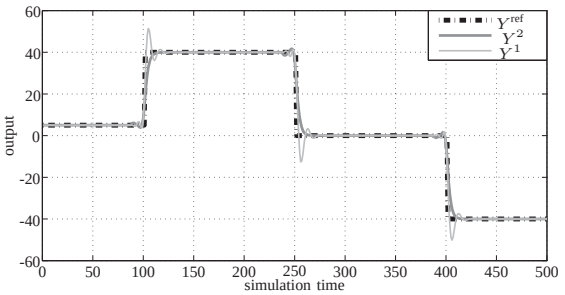

Fig. 6. Outputs of subsystems 1 and 2 with cooperation

step goes to 0 and the last reference step goes to -40 at $k = 400$.

The fuzzy partition space is given as a two-dimensional space spanned by the manipulated variables $[u_1, u_2]$ (the splits are shown in black dashed lines, see Fig. 11). Therefore, the blending zones (areas of overlap) are very small and the borders are sharp, which makes control design more difficult. The reference FMPC is a non-cooperative FMPC, which means that the structure and parameters of the used controller are the same as utilized for the CFMPC. The sole exception is the cooperative iteration loop which is not active in the non-cooperative FMPC. In Fig. 5 non-cooperative FMPC are shown, Y^1 (light-gray solid line) indicates the output of the oscillating LLMN_1, and Y^2 (gray solid line) is the output of the unstable LLMN_2. Fig. 6 shows the CFMPC with 10 iteration steps (q = $\text{it}_{\max} = 10$) in between each time step. It illustrates that the CFMPC is able to stabilize the interacting FMPCs. Note that fast cooperation is not guaranteed in general, but in this simulation example the convergence of the inner iteration loop works well and fast. In both cases the FMPCs are affecting each other as disturbances, but in the non-cooperative case the FMPCs cannot compensate spurious interactions and generate a limit circle. In the case of CFMPC the cooperative optimization guarantees the desired closed-loop performance. Fig. 7 and Fig. 8 show the manipulated

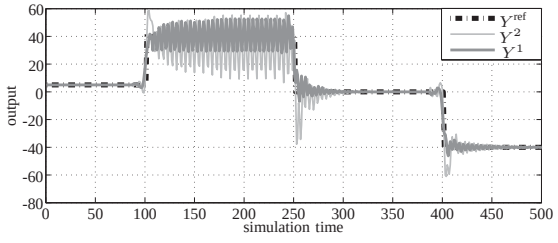

Fig. 5. Outputs of subsystems 1 and 2 without cooperation.

variables $u_{i,l}$ and $u^\star_{i,l}$ for each single $\text{LLM}_{i,l}$ vs. the global manipulated variables u_i or rather $u^\star_i$, $\forall i \in \mathbb{F}, \forall l \in \mathbb{L}_i$. In the next simulation on Fig. 9 the case of a constrained CFMPC is presented, see Sec.IV-D2. Note that the manipulated variable

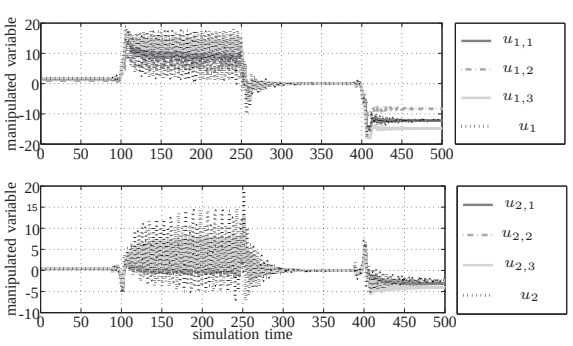

Fig. 7. The plot on the top shows the global fuzzy manipulated variable of the oscillating $\text{LLM}_{1,l}$ vs. the single control from each $\text{LLM}_{1,l}$, $\forall l \in \mathbb{L}_i$, $\forall i \in \mathbb{F}$, without cooperation in between each time step. The plot on the bottom shows the same for the unstable $\text{LLMs}_{2,l}$.

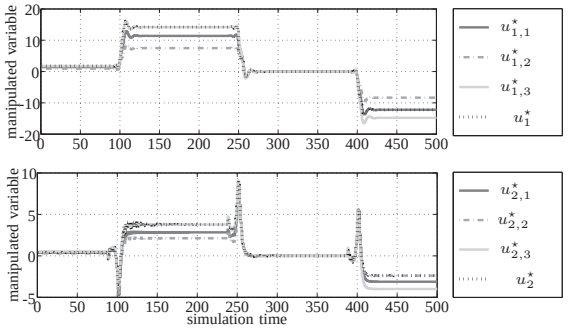

Fig. 8. Both plots shows the results of controlling with CFMPC. The plot on the top shows the global fuzzy manipulated variable of the oscillating $\text{LLMs}_{1,l}$ vs. the cooperative single control from each $\text{LLM}_{1,l}$, $\forall i \in \mathbb{F}, \forall l \in \mathbb{L}_i$. The plot on the bottom shows the same for the unstable $\text{LLMs}_{2,l}$.

for controlling without cooperative iteration loop is denoted by $u_i, \forall i \in \mathbb{F}$, and after running through the cooperative iteration loop by $u_i^\star, \forall i \in \mathbb{F}$. Fig. 9 shows that FMPC$_1$ (solid

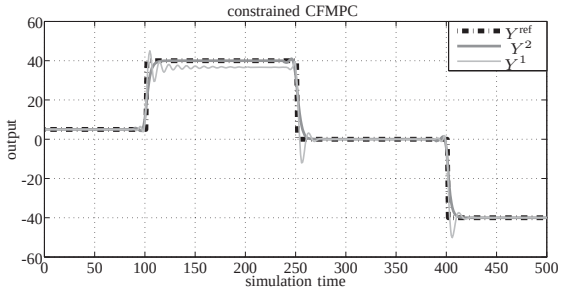

Fig. 9. Outputs of subsystems 1 and 2 with cooperation and active constraints in $u_1^\star$ and $u_2^\star$.

line) is not able to reach its reference after the first step ($k = 100$ to $k = 250$) because of the hard constraints in $u_{i,l}^\star, \forall i \in \mathbb{F}, \forall l \in \mathbb{L}_i$. In Fig.10 it is shown that the manipulated variables are saturated by the constraints (dashed lines) after the first step. It is also important to mention that after the last reference step $u_{1,3}^\star$, $u_{2,1}^\star$,and $u_{2,3}^\star$ remain entirely in the lower constraints. Note that the constraints for LLM$_{i,l}$ are the same $\forall l \in \mathbb{L}_i$, but are different for $\forall i \in \mathbb{F}$.

In Fig. 11 the global fuzzy trajectories in the partition

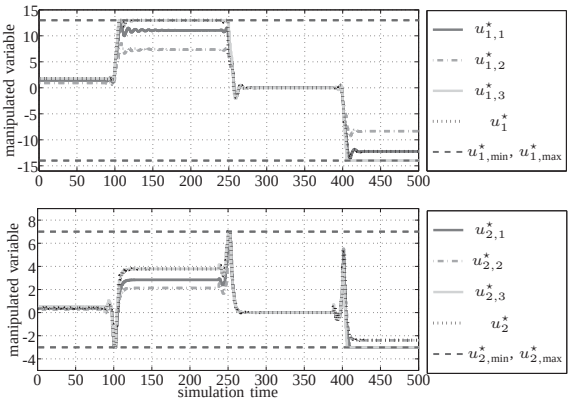

Fig. 10. Manipulated variables of CFMPC with active constrained set in $u_1^\star$ and $u_2^\star$

space are given. The gray rectangle in this figure shows the active constrained intersection set in the partition space. The trajectories of $u_1^\star$ and $u_2^\star$ hit each constraint at least once during the simulation.

VII. CONCLUSION

The CFMPC algorithm is introduced and the cooperative model structure is defined. It is important to notice that the single FMPCs have to be output-blended and the global plant has to be parameter-blended in this approach. The stability

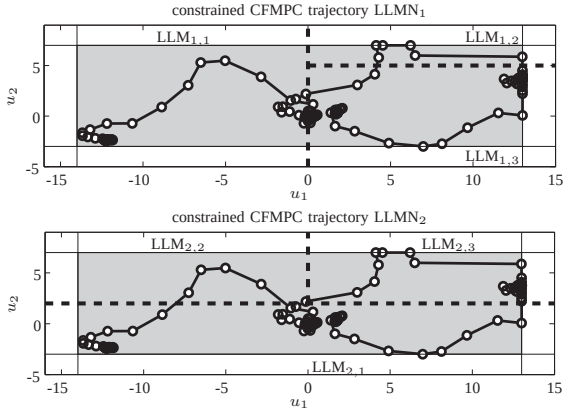

Fig. 11. This plot shows the constrained CFMPC trajectories in the corresponding partition space. The gray box shows the active set of constraints.

problem for CFMPCs has been studied in this paper and a proof for the closed-loop stability of the CFMPC system is given. Moreover, a convergence proof for the cooperative iteration loop is presented. This work shows also theoretically that the CFMPC algorithm is able to handle hard constraints as well as unstable LLMs. In the first simulation example a non-cooperative FMPC is compared to a CFMPC. In the second simulation it is shown that the CFMPC is able to satisfy hard constraints in u_1 and u_2. These simulation examples verify the advantages and effectiveness of the proposed approach.

APPENDIX

The system matrices of the simulation are given as:

$$A_{1,1} = \begin{bmatrix} 0.8 & 0.57 \\ -0.57 & 0.8 \end{bmatrix}; B_{1,1} = \begin{bmatrix} -0.2525 \\ 1.4289 \end{bmatrix}; E_{1,1} = \begin{bmatrix} 0.5260 \\ 1.2344 \end{bmatrix};$$
$$A_{1,2} = \begin{bmatrix} 0.85 & 0.51 \\ -0.51 & 0.85 \end{bmatrix}; B_{1,2} = \begin{bmatrix} -0.2429 \\ 1.7826 \end{bmatrix}; E_{1,2} = \begin{bmatrix} 0.6064 \\ 1.1856 \end{bmatrix};$$
$$A_{1,3} = \begin{bmatrix} 0.73 & 0.64 \\ -0.64 & 0.73 \end{bmatrix}; B_{1,3} = \begin{bmatrix} -0.3424 \\ 1.7354 9 \end{bmatrix}; E_{1,3} = \begin{bmatrix} 0.5658 \\ 0.9511 \end{bmatrix};$$
$$A_{2,1} = \begin{bmatrix} 0.4 & 0 \\ 0 & 1.7 \end{bmatrix}; B_{2,1} = \begin{bmatrix} -0.7586 \\ -0.4142 \end{bmatrix}; E_{2,1} = \begin{bmatrix} -0.9482 \\ -0.2209 \end{bmatrix};$$
$$A_{2,2} = \begin{bmatrix} 0.35 & 0 \\ 0 & 1.4 \end{bmatrix}; B_{2,2} = \begin{bmatrix} -1.6385 \\ -1.0090 \end{bmatrix}; E_{2,2} = \begin{bmatrix} -1.5020 \\ -0.5381 \end{bmatrix};$$
$$A_{2,3} = \begin{bmatrix} 0.45 & 0 \\ 0 & 1.75 \end{bmatrix}; B_{2,3} = \begin{bmatrix} -1.5504 \\ -0.8435 \end{bmatrix}; E_{2,3} = \begin{bmatrix} -1.3954 \\ -0.3749 \end{bmatrix}.$$

Note that, because of the fact that the output is the summation of the states $C_{i,i} = [1 \quad 1]$, $\forall i \in \mathbb{F}$ holds.
The constraints are chosen as follows:

$$-14 \leq u_{1,l}^\star \leq 13,$$
$$-3 \leq u_{2,l}^\star \leq 7,$$

$\forall l = \{1, 2, 3\}$.

References

[1] P. O. M. Scokaert, D. Mayne, and J. Rawlings, "Suboptimal model predictive control (feasibility implies stability)," *Automatic Control, IEEE Transactions on*, vol. 44, no. 3, pp. 648–654, Mar 1999.

[2] E. Camacho and C. Bordons, *Model Predictive Control*, ser. Advanced Textbooks in Control and Signal Processing. Springer London, 2004.

[3] Y. L. Huang, H. Lou, J. P. Gong, and T. Edgar, "Fuzzy model predictive control," *Fuzzy Systems, IEEE Transactions on*, vol. 8, no. 6, pp. 665–678, Dec 2000.

[4] O. Nelles, *Nonlinear System Identification: From Classical Approaches to Neural Networks and Fuzzy Models*, ser. Engineering online library. Springer, 2001.

[5] T. Takagi and M. Sugeno, "Fuzzy identification of systems and its applications to modeling and control," *Systems, Man and Cybernetics, IEEE Transactions on*, vol. SMC-15, no. 1, pp. 116–132, Jan 1985.

[6] J. Abonyi, *Fuzzy Model Identification for Control*. Birkhauser Boston, 2002.

[7] J. Rawlings and D. Mayne, *Model Predictive Control: Theory and Design*. Nob Hill Publishing, 2009.

[8] R. Babuska, *Fuzzy Modeling for Control*, 1st ed. Norwell, MA, USA: Kluwer Academic Publishers, 1998.

[9] S. Mollov, P. V. D. Veen, R. Babuska, J. Abonyi, J. A. Roubos, and H. Verbruggen, "Extraction of local linear models from takagi-sugeno fuzzy model with application to model-based predictive control," in *In Proceedings Seventh European Congress on Intelligent Techniques and Soft Computing EUFIT99*, 1999, pp. 147–154.

[10] S. Mollov, R. Babuska, J. Abonyi, and H. Verbruggen, "Effective optimization for fuzzy model predictive control," *Fuzzy Systems, IEEE Transactions on*, vol. 12, no. 5, pp. 661–675, Oct 2004.

[11] B. T. Stewart, A. N. Venkat, J. B. Rawlings, S. J. Wright, and G. Pannocchia, "Cooperative distributed model predictive control," *Systems & Control Letters*, vol. 59, no. 8, pp. 460 – 469, 2010.

[12] B. T. Stewart, S. J. Wright, and J. B. Rawlings, "Cooperative distributed model predictive control for nonlinear systems," *Journal of Process Control*, vol. 21, no. 5, pp. 698 – 704, 2011, special Issue on Hierarchical and Distributed Model Predictive Control.

[13] B. Ding, "Dynamic output feedback predictive control for nonlinear systems represented by a takagi-sugeno model," *Fuzzy Systems, IEEE Transactions on*, vol. 19, no. 5, pp. 831–843, Oct 2011.

[14] J. Roubos, S. Mollov, R. Babuska, and H. Verbruggen, "Fuzzy model-based predictive control using takagi-sugeno models," *International Journal of Approximate Reasoning*, vol. 22, no. 12, pp. 3 – 30, 1999.

[15] M. V. Sy and P. Xuan, "Fuzzy model predictive control using takagi-sugeno model," in *Control, Automation and Systems, 2008. ICCAS 2008. International Conference on*, Oct 2008, pp. 632–637.

[16] M. Killian, B. Mayer, and M. Kozek, "Hierarchical Fuzzy MPC Concept for Building Heating Control," in *Proceedings of the 19th World Congress of the International Federation of Automatic Control (IFAC'14)*, August 2014.

[17] B. Mayer, M. Killian, and M. Kozek, "Cooperative and Hierarchical Fuzzy MPC for Building Heating Control," in *Proceedings of the 2014 IEEE International Conference on Fuzzy Systems (FUZZ-IEEE 2014)*, July 2014.

[18] L. Wang, *Model Predictive Control System Design and Implementation Using MATLAB*, 1st ed. Springer Publishing Company, Incorporated, 2009.

[19] M. Killian, S. Grosswindhager, M. Kozek, and B. Mayer, "Preprocessing of partition data for enhancement of lolimot," in *Proceedings of the 2013 8th EUROSIM Congress on Modelling and Simulation*, ser. EUROSIM '13. Washington, DC, USA: IEEE Computer Society, 2013, pp. 271–275.

[20] S. Mollov, T. Van den Boom, F. Cuesta, A. Ollero, and R. Babuska, "Robust stability constraints for fuzzy model predictive control," *Fuzzy Systems, IEEE Transactions on*, vol. 10, no. 1, pp. 50–64, Feb 2002.

[21] T. Zhang, G. Feng, and J. Lu, "Fuzzy constrained min-max model predictive control based on piecewise lyapunov functions," *Fuzzy Systems, IEEE Transactions on*, vol. 15, no. 4, pp. 686–698, Aug 2007.

[22] X. Zhao, L. Zhang, P. Shi, and H. Karimi, "Novel stability criteria for t–s fuzzy systems," *Fuzzy Systems, IEEE Transactions on*, vol. 22, no. 2, pp. 313–323, April 2014.

[23] K. Tanaka and H. Wang, *Fuzzy Control Systems Design and Analysis: A Linear Matrix Inequality Approach*. Wiley, 2004.

[24] K. Tanaka, T. Hori, and H. Wang, "A fuzzy lyapunov approach to fuzzy control system design," in *American Control Conference, 2001. Proceedings of the 2001*, vol. 6, 2001, pp. 4790–4795 vol.6.

[25] ——, "A multiple lyapunov function approach to stabilization of fuzzy control systems," *Fuzzy Systems, IEEE Transactions on*, vol. 11, no. 4, pp. 582–589, Aug 2003.

[26] H. Wang, K. Tanaka, and M. Griffin, "An approach to fuzzy control of nonlinear systems: stability and design issues," *Fuzzy Systems, IEEE Transactions on*, vol. 4, no. 1, pp. 14–23, Feb 1996.

[27] W. Yang, G. Feng, and T. Zhang, "Robust model predictive control for discrete-time takagi-sugeno fuzzy systems with structured uncertainties and persistent disturbances," *Fuzzy Systems, IEEE Transactions on*, vol. 22, no. 5, pp. 1213–1228, Oct 2014.

[28] C. Arino, E. Perez, A. Querol, and A. Sala, "Model predictive control for discrete fuzzy systems via iterative quadratic programming," in *Fuzzy Systems (FUZZ-IEEE), 2014 IEEE International Conference on*, July 2014, pp. 2288–2293.

[29] G. Feng, *Analysis and Synthesis of Fuzzy Control Systems: A Model-Based Approach*, 1st ed. Boca Raton, FL, USA: CRC Press, Inc., 2010.

[30] D. Mayne, J. Rawlings, C. Rao, and P. Scokaert, "Constrained model predictive control: Stability and optimality," *Automatica*, vol. 36, no. 6, pp. 789 – 814, 2000.

Michaela Killian received the M.Sc. degree in technical mathematics from Vienna University of Technology, Vienna, Austria, in 2012. Since 2012, she is Ph.D. student at the Institute of Mechanics and Mechatronics, Devision of Control and Process-Automation, University of Technology, Vienna, Austria. Her research interests include fuzzy model predictive control, fuzzy systems, fuzzy control and non-linear dynamic system identification.

Barbara Mayer received her M.S. degree in technical mathematics from University of Technology, Graz, Austria, in 2004. Since 2009 she is lecturer at the FH Joanneum GmbH, Graz, Austria, and since 2011 external Ph.D. student at the Institute of Mechanics and Mechatronics, Vienna University of Technology, Vienna, Austria. Her research interests include mixed-integer model predictive control, non-linear system identification and hybrid systems.

Alexander Schirrer received his M.S. degree in mechanical engineering in 2007, the Ph.D. degree in 2011. Since 2011 he is a postdoctoral researcher and teacher of graduate-level lectures on the Institute for Mechanics and Mechatronics at Vienna University of Technology. His research interests include modeling, simulation, optimization algorithm, and optimization of distributed-parameter systems.

Martin Kozek received the M.S. degree in mechanical engineering in 1994, the Ph.D. in 2000 and the Habilitation in 2009. He is currently Professor at the Institute of Mechanics and Mechatronics, Vienna University of Technology. His theoretical areas of research interests are non-linear systems modeling and identification, model predictive process control, and active control of structural vibrations.

2.3 Publication C

Michaela Killian, Barbara Mayer, and Martin Kozek.
Cooperative fuzzy model predictive control for heating and cooling of buildings.
Energy and Buildings, Volume 112, 2016, pages 130–140, ISSN: 0378-7788.
DOI: 10.1016/j.enbuild.2015.12.017

Own contribution
Problem analysis, advancement of methods, execution of the solution, development and programming of algorithms, consideration of implementation aspects, performing simulation studies, and structuring, writing and editing of the manuscript was done by the applicant. Discussion of methodology, and editing of the manuscript was done by the second author. Problem statement, discussion and editing was done by the third author.

Energy and Buildings 112 (2016) 130–140

Contents lists available at ScienceDirect

Energy and Buildings

journal homepage: www.elsevier.com/locate/enbuild

Cooperative fuzzy model predictive control for heating and cooling of buildings

M. Killian [a,*], B. Mayer [b], M. Kozek [a]

[a] Vienna University of Technology, Institute of Mechanics and Mechatronics, Getreidemarkt 9, 1060 Vienna, Austria
[b] FH Joanneum, Werk-VI-Strasse 46, 8605 Kapfenberg, Austria

ARTICLE INFO

Article history:
Received 10 July 2015
Received in revised form
10 December 2015
Accepted 11 December 2015
Available online 14 December 2015

Keywords:
Grey-box modelling
Fuzzy MPC
Cooperative FMPC
Building control

ABSTRACT

This paper presents a cooperative fuzzy model predictive control (CFMPC) for heating and cooling of buildings. Because of different supply zones, the large time constants and the non-linear building dynamics with respect to the different seasons, a CFMPC concept is proposed. The overall non-linear building is split into different zones, which are consisting of input-coupled Takagi-Sugeno (TS)-fuzzy models. Each such TS-fuzzy model is constituted by a local linear model network (LLMN). The LLMN consists of local linear models (LLM), which are representing the different seasons: winter, transition season (fall and spring), and summer. The control of each LLM is realized by model predictive control (MPC). For each building zone the associated MPCs are output-blended by the fuzzy membership functions, which leads to fuzzy model predictive control (FMPC). In addition to the FMPCs a global MPC is controlling the thermally activated building systems, which affect all other zones. To coordinate the different controllers a cooperative iteration-loop is assumed, which leads to cooperative fuzzy model predictive control (CFMPC). The concept is developed for a specific demonstration building and can be easily adapted for other complex buildings. A simulation example demonstrates that the proposed CFMPC achieves a performance increase with less energy consumption, as compared to FMPC controllers and historical measured data of the demonstration building.

1. Introduction

1.1. Motivation and contribution

Energy efficient climate control is an important current task, hence there has been a growing rethinking in energy savings. The building sector accounts for about 40% of the total energy consumption [1]. In order to guarantee user comfort in complex office-buildings an intelligent automation system has to be implemented. Such controversial optimization problems, as minimizing energy cost while maximizing user comfort, are suitable for model predictive control (MPC). Furthermore, external disturbances for buildings as weather (ambient temperature and radiance) can be explicitly handled by MPCs. Also internal disturbances caused by occupancy, large time-delays caused by the building's heat capacity, strong couplings between different supply zones, and constraints in all variables can be incorporated in the MPC optimization. This complete coverage of the control problem together with the possibility to directly balance the trade-off between comfort and energy saving makes a strong point for MPC in building automation. Since one of the most time-consuming parts for the design of model-based controllers is the model design [2], it is essential to choose the best fitting model structure. Therefore, this work presents a grey-box modelling method for buildings, which approximates the non-linear building behaviour with local linear models (LLM). This non-linear behaviour is mainly caused by the seasonal changes in building dynamics, which is especially important when designing indoor-room temperature control for both heating and cooling. Conventional non-predictive control concepts can robustly compensate these non-linearities only by accepting performance losses. The standard in building control is currently rule-based control utilizing expert knowledge combined with PID-control for manipulated variables [3]. In order to avoid this disadvantage non-linear concepts such as fuzzy predictive control have to be employed. Because of the aforementioned large time constants the combination with MPC is favourable. The use of LLMs lead to a special type of non-linear MPC (NMPC),

* Corresponding author.
E-mail addresses: michaela.killian@tuwien.ac.at (M. Killian), barbara.mayer@fh-joanneum.at (B. Mayer), martin.kozek@tuwien.ac.at (M. Kozek).

http://dx.doi.org/10.1016/j.enbuild.2015.12.017
0378-7788/

Nomenclature

ARX	auto-regressive model with exogenous input
CFMPC	cooperative FMPC
FC	fan coil
FMPC	fuzzy MPC
$h^q_{F_i}$	cooperative iteration-update of zone i
h^q_T	cooperative iteration-update of coupling zone
k_σ	steepness of the membership function
LLM	local linear model
LLMN	local linear model network
LoLiMoT	local linear model tree
$\dot{m}$	mass flow in kg· s^{-1}
MISO	multi-input single-output
MPC	model predictive control
NARX	non-linear ARX
NE	north-east
NMPC	non-linear MPC
NW	north-west
occ_i	occupancy of zone i in %
$\dot{Q}_{F_i}$	heat flow of zone i in kW
$\dot{Q}_T$	heat flow of coupling zone in kW
$\dot{Q}_{\sum}$	sum of all heat flows in kW
rad_i	radiance of zone i in W/m^2
SE	south-east
SW	south-west
TABS	thermally activated building system
TS	Takagi-Sugeno
ϑ_{amb}	ambient temperature in K
Y_i^{act}	actual indoor room temperature of zone i in K
Y_i^{ref}	reference indoor room temperature of zone i in K
$\bar{Y}^{\text{act}}$	actual mean indoor room temperature in K
$\bar{Y}^{\text{ref}}$	reference mean indoor room temperature of coupling zone in K
$\Delta\vartheta_j$	difference between heat flow and heat return for supply source j

the so-called fuzzy MPC (FMPC) [4]. If several zones of a building are controlled by dedicated FMPCs a coordinated controller scheme provides additional advantages. In order to coordinate different buildings zones, including coupling zones, a cooperative FMPC (CFMPC) is introduced. In addition, the proposed models for the CFMPC cover all seasons, hence, heating as well as cooling are shown for a specific demonstration building. Building climate control in general includes several systems as heating, ventilation and air conditioning (HVAC) systems, lighting systems, and many more.

In this work the focus is put on the control of indoor-room temperature, which is controlled by both fan coils (FC) and thermally activated building system (TABS). The proposed concept is applicable to other control configurations; especially if ventilation and air conditioning (VAC) significantly contributes to indoor-room temperature it must be included in the control concept as an additional manipulated variable.

The main contributions of this work are for one thing non-linear grey-box models, which are valid for all seasons (heating and cooling). In addition, the second main part of the work is the cooperative FMPC structure. This CFMPC provides a novel, more flexible and intelligent opportunity for temperature control of the office rooms of a complex multi-zone building. The scope of the control design is to provide separate FMPC controllers independently designed for each building zone, and to incorporate the strong coupling of the activated concrete core by a cooperative scheme. A comparison between a rule-based PID-controller [3] and two predictive controllers (linear MPC and fuzzy MPC) is performed in this work.

1.2. State-of-the-art system identification

Classical system identification algorithms are useful in the case of MPC [5]. Black-box models are known as purely data-driven models. Such a data-driven algorithm is the local linear model tree (LoLiMoT) algorithm, which has been introduced in [6,7]. LoLiMoT approximates non-linear systems with LLMs, which leads to an overall fuzzy model. Another black-box method for building models are subspace identification methods, like n4SID, which provides a model in state-space form [2], this is purely linear. Furthermore, other methods as the prediction error method or a deterministic semi-physical modelling method are introduced in [2].

The next category is grey-box models. These model types are hybrid models that use simplified physical descriptions to simulate the behaviour. Model coefficients are identified based on the operating data of the building. Therefore, the combination of black-box and white-box model is called grey-box [8].

In [9], a comparison is given between black-box and grey-box models for HVAC systems. It was found that artificial neural networks perform best followed by the auto-regressive model with exogenous input (ARX) and the grey-box model. In this work, the grey-box model is based on an ARX-algorithm, but one of the most important tasks is done by expert knowledge, the choice of the so-called partition space [6]. This fact leads to a grey-box model in this work.

The last general group of models is white-box models, which are purely physical. A lot of mature white-box software tools such as EnergyPlus and TRNSYS have been widely used [8]. The choice of the model type is depending on three main factors: effort, complexity and accuracy. The cost for parameterizing of white-box models is very high, but the resulting accuracy is high as well. In the case of MPC design the order and complexity of white-box models implies an enormous effort, because of the necessary model reduction and possible problems such as underlying switching control loops. Therefore, black-box and grey-box models are more suitable for the design of MPC. In this work the grey-box approach is chosen, based on a black-box model as the incorporation of expert knowledge additionally reduces the dimension of the partition space in the LoLiMoT method [7].

The use of Takagi-Sugeno (TS)-fuzzy models is widespread for fuzzy identification [10]. These models can be extracted from LLMs and can be directly fed into the FMPC design [11]. Fuzzy identification for control in general is illustrated in [12]. FMPC using TS-fuzzy models is a smart way to use general linear MPC optimization formulations, while afterward blending the different controller outputs with a non-linear validity function [13]. In case of buildings a fuzzy modelling approach is given in [14]. Skrjanc et al. [14] have introduced two different types of modelling: theoretical and experimental. The theoretical approach is based on energy balances, which is described by differential equations.

The grey-box model, in this application, is based on TS-fuzzy models, and the controller is based on non-linear output-blending.

1.3. State-of-the-art MPC

Classical MPC approaches are presented in [15]. However, thermal behaviour of buildings is typically non-linear especially when considering both heating and cooling. As already mentioned, this work illustrates a cooperative concept including more than one FMPC (CFMPC) [16]. The authors of [17] present an energy efficient MPC for temperature control, based on a model from a simulation package. The authors of [18] use fuzzy logic-based advanced on-off control for thermal control in residential buildings. They achieved a

reduction of energy consumption while improving the control performance. The focus in [17] is on controlling the vapor compression cycle in an air-condition system, which is used for cooling. An MPC only for a building heating system is introduced in [19], in contrast to [20], where only building cooling systems are taken into account. In opposition to [17,19,20], in this work the building is controlled for heating and cooling.

In this work, not only a straight-forward FMPC for buildings is shown. A more intelligent algorithm for more than one FMPC is given, a coordinated FMPC (CFMPC) [16]. This problem formulation is similar to distributed MPCs [21], both leading to a suboptimal solution. The authors of [21] present a distributed MPC structure for thermal regulation in buildings with an inner cooperation-loop. In [21], a simulated building with 3 rooms (one room is one zone) is presented. Moreover, only heating is proposed. In contrast to [21], in this work a real demonstration building with 4 zones, each zone includes approximately 61 rooms per floor, is shown. Therefore, the complexity in the recent work is much higher and the optimization problem for all seasons is more challenging. Furthermore, in [21], only output-coupling is taken into account, which is irrelevant in sense of building temperature control where the room/zone differences are very small. It is much more complex to consider input-coupled systems, as it is presented in the recent work.

Furthermore [22], illustrates the concept of suboptimal MPCs. Scokeart et al. [22] establish conditions under which suboptimal MPCs are stabilizing. The theoretical background of cooperative MPCs is given in [23], where the theoretical assumptions are discussed and proved. In addition [24,25], introduce a hierarchical concept for MPCs, respectively FMPCs. Also in this work, such a hierarchical scheme is assumed to exist, but it is assumed that a suitable energy management system (EMS) as introduced in [26] is existing.

Added flexibility of CFMPC is given by the possibility to either add or omit specific zones of the building with minimum effort, depending on the building's current usage. Furthermore, CFMPC achieves higher control performance with slightly less energy consumption. Both stability and convergence are secured by theoretic results [16]. While many state-of-the-art MPCs in buildings just control heating or cooling systems, the presented CFMPC is able to provide control for all seasons, both in terms of heating and cooling.

The remainder of this work is structured as follows: in Section 2, a general formulation of the grey-box modelling is given and the most important tasks are introduced. A general description of the demonstration building and the final building model are given in Section 3. The methodology of cooperative fuzzy model predictive control (CFMPC) for the specific building is outlined in Section 4. Simulation and validation results are presented in Section 5, and Section 6 summaries the results.

2. Grey-box model

It is common for modelling a process to use one of the introduced methods: white-box models, black-box models or grey-box models [9]. White-box models require the understanding of the system physics and use physical parameters for modelling the system dynamics. But these models are usually not suitable for model predictive control of buildings because of their high order and complexity. Black-box models are purely data-driven models [7].

In the recent work, grey-box models were used for modelling the building. A balance between good generalization and high accuracy is given by grey-box models. In addition, this approach validly presents a grey-box model for building control, both for heating as well as for cooling.

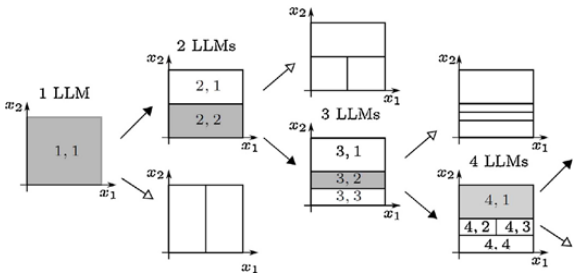

Fig. 1. First four iterations of LoLiMoT algorithm for a two-dimensional input space ($m=2$).

2.1. Grey-box model as local lineal model network

In this work, a local linear model network (LLMN) approach is chosen for modelling the different building zones. The so-called local linear model tree (LoLiMoT) algorithm combines a heuristic strategy for partition space decomposition with weighted least squares optimization or output error optimization [6]. It therefore provides a local linear model (LLM) approximation of globally nonlinear dynamic systems.

The main part of the algorithm are Gaussian Kernel functions, which are fitted to a rectangular partitioning of the m-dimensional input or *partition space* performed by a decision tree with axis-orthogonal splits at the internal nodes (Fig. 1). Each local model belongs to one hyper-rectangle in the center of which the fitting point is placed. New hyper-rectangles are found by testing the possible splits in all dimensions and taking the one with the highest performance improvement. The choice of the partition space is the key point of this LoLiMoT algorithm; it should describe the strongest non-linearities in the process to reach the best results. The algorithm is described in detail in [6,7].

For the global non-linearities in the building, the LLMs are blended with mentioned Gaussian Kernel functions, which leads to fuzzy modelling, see Section 2.2 and subsequently to fuzzy model predictive control (FMPC).

It is known that buildings are complex non-linear dynamic processes. Therefore, the behaviour of the specific building is approximated by LLMs, where the partitioning variable ϑ_{amb} is chosen by expert knowledge. This fact turns the modelling into a grey-box model.

Both analysis of historical data and expert knowledge (building operators) indicate the choice of the different LLMs, which are given by the seasons: winter, transition season (fall and spring), summer. Thus, the partition space for the specific building is 1-dimensional. Therefore, ϑ_{amb} is the only variable for the validity of the different local models. Furthermore, each split of the partition space is equivalent to fuzzy inference rules and can be mathematically formulated as Takagi-Sugeno (TS)-fuzzy models, see Section 2.2 [11].

The parameters of each input to output transfer function are estimated from historical data. The model validation of each zone is given in Section 5.2.

2.2. Takagi-Sugeno (TS)-fuzzy model

TS-fuzzy models are suitable for approximating systems by interpolating between local linear, time-invariant auto-regressive models with exogenous inputs (ARX) [12]. The resulting output of the LoLiMoT algorithm, see Section 2.1, are parameters for an ARX-model. Therefore, the equivalence to a TS-fuzzy model is obtained.

The basic element of a TS-fuzzy system is a set of fuzzy inference rules. In general, each inference rule consists of two elements: the IF-part (antecedent) and the THEN-part (consequent) [10], the set of rules is given by $\mathcal{R}$ in this work.

Here $\zeta = [\zeta_1, \zeta_2, \ldots, \zeta_p] \in \mathbb{R}^p$ is the vector of input fuzzy variables. The elements of the fuzzy vector are usually a subset of the past input and outputs [12]. This vector is defined as:

$$\zeta \in \{y^k, \ldots, y^{k-n_a+1}, u_s^{k-\tau}, \ldots, u_s^{k-n_b-\tau+1}\} \in \mathbb{R}^p, \quad (1)$$

where y is the output, u_s is the input s where s denotes the specific input parameter or number of input, n_a is the maximum lag considered for the output and n_b is the maximum lag considered for the input terms. Furthermore, τ is the discrete dead time.

The overall system is approximated by a collection of coupled multiple-input single-output (MISO) discrete-time TS-fuzzy models of the input-output non-linear ARX (NARX) type

$$y^{k+1} = \sum_{j=1}^{r} \Phi_j(\zeta) y_j^{k+1}, \quad (2)$$

where r denotes the global number of rules. The degree of fulfillment of the specific jth rule can be computed using the product operator $\mu_j(\zeta) = \prod_{i=1}^{p} \mu_{j,\Xi_i}(\zeta_i)$, where Ξ_i are the antecedent fuzzy set or regions for the jth rule $\mathcal{R}^j$. Furthermore, the normalized degree of fulfillment can be computed as

$$\Phi_j(\zeta) = \frac{\mu_j(\zeta)}{\sum_{i=1}^{r} \mu_i(\zeta)}. \quad (3)$$

The membership function is parameterized properly by the centers, the spreads and the steepness value k_σ [6,12,10].

Note, $\Phi_{i,l}$ denotes the fuzzy membership function for LLM_l of LLMN_i, which is expressed by $\text{LLM}_{i,l}$, $i \in \mathbb{F}, l = \{1, \ldots, L_i\} = \mathbb{L}$. In the remainder of this work $\mathbb{F}$ denotes the number of FMPCs, which is equivalent to the number of LLMNs, and is set to the number of buildings zones, which are considered to be 4 zones, thus, $\mathbb{F} = \{1, 2, 3, 4\}$. Note, the number of LLMs L_i is the same as the number of rules r, therefore $L_i \equiv r$ holds, here $L_i \equiv r$ is assumed to be equal to 3 for all $i \in \mathbb{F}$. In this work, *blended* describes the mixture between LLMs, where $\sum_{l=1}^{L_i} \Phi_{i,l} = 1$ holds $\forall i \in \mathbb{F}$. Blended zones are the areas in the partition space where the LLMs are overlapping each other.

Note, the manipulated variables of the FMPC_i, $\forall i \in \mathbb{F}$ are given by output blending, not by parameter blending, see Section 4.3.

3. Building model

The building presented in this work is a 27,000 m^2 university building in the center of Salzburg, Austria. It has five floors above ground containing several large and numerous smaller meeting rooms, offices and lecture rooms. The facade of this special building has a glass ratio of about 70% and outside blinds over 2 floors, see

Fig. 2. Photo of the University building in Salzburg, Austria. © Luigi Caputo.

Fig. 2. On each floor. The building contains 250 office rooms, the footprint of these floors is identical and each has an effective area of about 6500 m^2. The building contains four shafts, which connect the piping for the cooling and heating supply and return with the supply level in the basement. The modelling of this specific building is based on these four main shafts, because each of these shafts supplies one building zone. These zones are distributed according to the building's orientation, which is equal to the cardinal direction. This fact makes the modelling more difficult, since the radiance input is given as a mixture from North-East (NE – zone_1), South-East (SE – zone_2), South-West (SW – zone_3) and North-West (NW – zone_4). For control purposes, the building model is split into these four independent zones and one coupling zone, see Fig. 3. Energy supply in this specific building is provided by a concrete activated floor distributing supply water in a second circuit, which means that this building has a thermally activated buildings system (TABS – coupling zone). Another supply into the building is based on Fan Coils (FC), which are required for the fast dynamics. The time constant of TABS is given by approximately 48h, in contrast to which the time constant for FC is assumed to be 4 h.

The energy demand of each zone i, respectively the coupling zone TABS, is denoted by $\dot{Q}_{F_i}$, $i \in \mathbb{F}$, and $\dot{Q}_T$. Note, it is assumed that a suitable energy management system (EMS) exists, which is able to provide the requested energy demand of the cooperative fuzzy model predictive control (CFMPC) scheme. An appropriate energy management system is presented in [26,24].

The coupling zone is controlled by TABS, which spans over all 4 zones and feeds the energy into the building through the concrete floor. TABS has a slow dynamic, but a very high thermal coefficient. Hence, it is beneficial to provide the building with a base level of energy. Each individual zone is managed by FC, which are able to control fast and react to short-term disturbances.

In the recent approach for the specific building, 13 models were made for control purposes depending on historical data and expert knowledge, see Section 2.1. For each FMPC_i, $i \in \mathbb{F}$, 3 models ($L_i \equiv 3$)

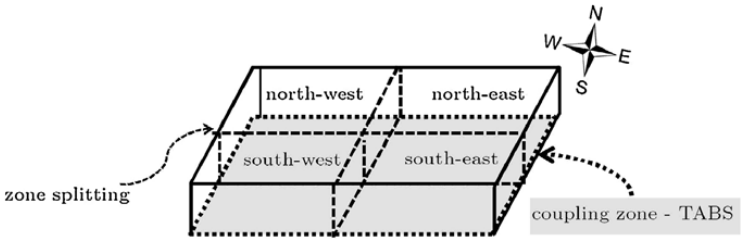

Fig. 3. Zone splitting for modelling the university building in Salzburg, Austria.

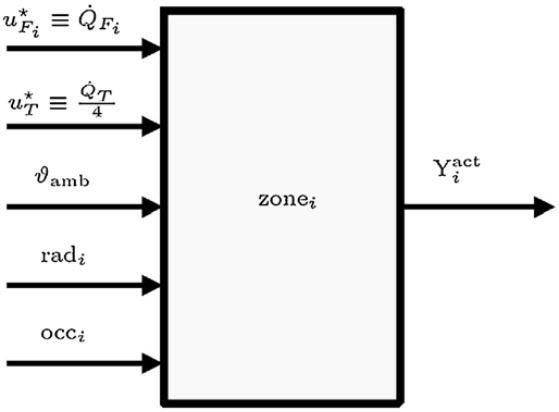

Fig. 4. Scheme of input-output relation for each MISO zone_i model, $\forall i \in \mathbb{F}$. The manipulated variables after the cooperation loop are denoted by $u^\star_{F_i}$ for FC of zone_i and $u^\star_T$ for TABS. The heat supply $\dot{Q}_T$ is divided by 4, because each zone comprises one quarter of the floor. Furthermore, ϑ_{amb} denotes the ambient temperature in K, rad_i the radiance input in the ith zone in W/m^2, occ_i the occupancy in zone_i in %, and Y_i^{act} represents the actual average indoor room temperature in zone_i in K, $\forall i \in \mathbb{F}$.

are in use, constituting the LLMs. In addition, one global model for the whole floor (TABS) is designed for the global MPC (MPC_T).

The 3 LLMs of each FMPC are dedicated to the relevant seasons: winter, transition season (spring and fall), and summer. Therefore, for the zone-FMPCs, 12 LLMs are needed and 1 additional model for MPC_T, which is also valid for all seasons. The CFMPC is able to control the building over the whole year, because the fuzzy rules are switching between the three different seasons.

Note, for heat flow $\dot{Q}_j, j = \{T, F_i\}, i \in \mathbb{F}$ of TABS and FC the following relation holds:

$$\dot{Q}_j = \underbrace{\dot{m}_j}_{const.} \cdot \Delta\vartheta_j \cdot \underbrace{c_p}_{const.}, \tag{4}$$

where c_p, the specific heat capacity of water, is assumed to be constant and has no sub fix j, $\Delta\vartheta_j$ denotes the temperature difference between the supply and the return auf the jth control input, $j = \{T, F_i\}, i \in \mathbb{F}$. Also, the mass flows $\dot{m}_j$ are assumed to be constant, further $j = \{T, F_i\}, \forall i \in \mathbb{F}$. The heat supplies are given in kW (heating – positive; cooling – negative) in the remainder of this work. The summation of the manipulated variables

$$\dot{Q}_{\sum} = \sum_{i \in \mathbb{F}} |\dot{Q}_{F_i}| + |\dot{Q}_T|, \tag{5}$$

is sent to the suitable EMS [26], where the energy supply is optimized and delivered to the building. All zones_i of the plant are MISO-models, the input-output relation is demonstrated in Fig. 4.

Note that the effect of existing HVAC systems on indoor-room temperature must be included in the model. The best approach would be to include the dynamic response of the HVAC together with other heating and cooling systems in the grey-box model. It would then constitute just another manipulated variable. An alternative is given by considering the HVAC as an disturbance to the indoor-room temperature control; this known disturbance could consequently be included in the CFMPC concept.

4. Cooperative fuzzy model predictive control

Linear MPC refers to a class of control algorithms that compute manipulated variables by utilizing a linear process model [15]. However, many systems are inherently non-linear. This motivates the use of non-linear MPCs (NMPC). Here a non-linear and generally non-convex optimization problem has to be solved. To avoid non-convex optimization, a set of LLMs can be extracted from a TS-fuzzy model [11], which is then used by the MPC algorithm [27,13,12]. The overall control structure in this specific problem leads to FMPCs and subsequently to CFMPC – because of the different building zones and one coupling zone, see Section 3. The concept of the CFMPC in general is presented in [16].

In the following, the index i of FMPCs is taken from the set $\mathbb{F} = \{1, 2, 3, 4\}$, and the associated $L_i \in \mathbb{L}$ LLMs for FMPC_i, $\forall i \in \mathbb{F}$, are denoted by the index $l \in \mathbb{L} = \{1, 2, 3\}$.

4.1. CFMPC for specific building

In this section, the CFMPC structure for the specific building is introduced. The CFMPC controls the average indoor-room temperature in the office rooms by manipulating supply temperatures of both FCs and TABS, while considering main disturbances given by ambient temperature, radiance, and occupancy. In Fig. 5 the control concept for 4 FMPCs ($\text{FMPC}_i, \forall i \in \mathbb{F}$) cooperating with 1 global coupling MPC (MPC_T) is illustrated.

The controlled variable is the average indoor room temperature of each zone denoted by $Y_i^{\text{act}}, \forall i \in \mathbb{F}$. In Fig. 5, Y_i^{ref} describes the reference trajectory for the ith FMPC of the closed-loop system, and Y_i^{act} represents the actual value. For the coupling zone, the mean $\bar{Y}^{\text{ref}}$ of the other 4 reference values is taken, and the actual mean indoor room temperature is given as $\bar{Y}^{\text{act}}$.

The manipulated variables before the cooperative iteration-loop are denoted by $u_j, j = \{T, F_i\}, \forall i \in \mathbb{F}$. The "T" denotes "TABS" and "F_i" denotes the control by FC for zone_i. After the cooperation, the manipulated variables are star-variables $u_j^\star$. Furthermore, three main disturbances to the building are considered:

- ambient temperature denoted by "ϑ_{amb}" in K,
- radiance denoted by "rad" in W/m^2,
- occupancy denoted by "occ" in %, adapted from [28].

The cooperative iteration-loop is introduced in Section 4.2. Note that the manipulated variables u_j (and consequently $u_j^\star$) are equal to the energy demand $\dot{Q}_j$, see Section 3 Eqs. (4) and (5). Furthermore, the disturbances "rad" and "occ" are split into rad_i and occ_i depending on the zones, $\forall i \in \mathbb{F}$.

The global plant (see Fig. 5 "building") consists of 4 parallel input-coupled zones, and each FMPC controls one zone. The manipulated coupling variable $u_T^\star$ influences all 4 zones. These zones are each defined by one LLMN, split into the cardinal directions, see Section 3. As introduced in Section 2.2, ARX transfer functions can be transformed state-space matrices. Therefore, the overall non-linear building plant, consisting of 4 input-coupled zones (by TABS), is possible to be presented in time-variant state-space matrices. These matrices are given as: A_i^k, $\tilde{B}_i^k$, C_i^k, $\forall i \in \mathbb{F}$. Note in contrast to the output-blended controller, for the global plant parameter-blended matrices are assumed. This means that the system matrix at time k is calculated as: $A_i^k = \sum_{l \in \mathbb{L}} A_{i,l}^k \Phi_{i,l}, \forall i \in \mathbb{F}$.

Note $\tilde{B}_i^k = [B_i^k; E_i^k]$ is a stacked matrix for the input-matrix and the disturbance-matrix, for details see Section 4.3. In contrast to parameter-blending, the manipulated variable for each FMPC is computed by output-blending:

$$u_i^k = \sum_{l \in \mathbb{L}} u_{i,l}^k \Phi_{i,l}. \tag{6}$$

The fuzzy membership functions $\Phi_{i,l}$ are given for the fuzzy input vector depending on all $\text{LLMs}_{i,l}$, $\forall i \in \mathbb{F}$ and $l \in \mathbb{L}$.

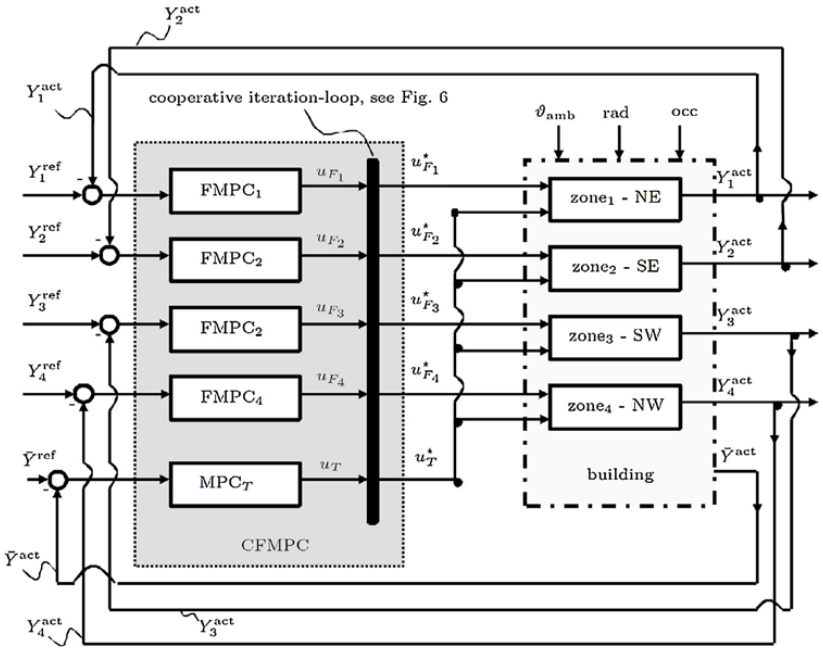

Fig. 5. CFMPC scheme for the specific building. The scheme shows the structure of a CFMPC, which is used for the demonstration building, with 4 different zones.

In this cooperative control structure (based on Fig. 5), four FMPCs are in cooperation with one global MPC. Each manipulated variable of the ith FMPC is a disturbance to the global MPC, and the manipulated variable of MPC$_T$ is an additional disturbance to each FMPC$_i$, $\forall i \in \mathbb{F}$.

4.2. Cooperative iteration-loop

The cooperative iteration-loop is computed between consecutive time steps. Furthermore, only u_i for FMPC$_i$ and u_T for MPC$_T$, $\forall i \in \mathbb{F}$, are iteratively updated, all other variables are assumed to be constant during the iteration-loop (e.g. external disturbances). The functions

$$u_{F_i}^q = h_{F_i}^q(\cdot|u_T^q), \tag{7}$$

$$u_T^q = h_T^q(\cdot|u_{F_1}^q, \ldots, u_{F_4}^q), \tag{8}$$

$\forall i \in \mathbb{F}$ are the cooperative qth iteration-updates, see Fig. 6 [22,23].

Between consecutive time steps, the cooperative MPCs perform q iterations of a feasible path algorithm. Let $u^\star$ be the overall blended output after the iteration loop, see Fig. 6. $u^\star$ is computed such that some cost function, see Eq. (9), is minimized and acceptable for each zone. The cooperation update $u_{F_i}^q = h_{FC,i}^q(\cdot|u_T^q)$ denotes the iteration-update for each FMPC$_i$, dependent on the additional disturbance u_T^q. Furthermore, $u_T^q = h_T^q(\cdot|u_{F_1}^q, \ldots, u_{F_4}^q)$ is the cooperative iteration-update for the manipulated variable of the coupling zone, dependent on the other 4 manipulated variables from each FMPC within the qth iteration. Note that all other disturbances (ϑ_{amb}, rad, occ) are held constant during the iteration-loop.

The cooperative iteration-updates are calculated in a loop until a maximal number of iteration-steps is reached or if the increment between the $(q-1)$th and qth manipulated variable (for all five variables) is smaller then a given threshold ε. If one of these criteria is fulfilled, the algorithm is advancing to time step $k = k+1$, see Fig. 6.

4.3. CFMPC optimization problem

FMPC are non-linear MPCs, which achieve the global optimum for a given performance criterion. However, for a cooperation between a global MPC with several FMPCs, increased flexibility and a scalable control architecture can be achieved by accepting suboptimal inputs [23,22,25,24]. Hence, a suboptimal FMPC analogous to suboptimal MPC presented in [22,23] is proposed. Note that each FMPC actually acts like a parallel connection of linear MPCs with output-blending, which effectively constitutes a non-linear controller [29,30]. The cost functions for all, the FMPCs and the MPC$_T$, are equal. For the FMPCs $\#\mathbb{L} = 3$ parallel MPCs (for the defined seasons, see Section 3) of each zone are output blended as defined in Section 4.1, Eq. (6), to the overall blended output. In this section, the derivation to the CFMPC optimization problem definition is given and explained. In the following, the variable $\tilde{u} = [u; z]$ describes the stacked variable of manipulated variable and disturbances.

The optimization problem for each MPC can be formulated as:

$$J_j^\star = \min_{\Delta u_j} J_j(\tilde{u}_j) \forall j = T, F_i, \forall i \in \mathbb{F} \tag{9}$$

where

$$J_j(\tilde{u}_j^{k,k+n_p-1}) = \sum_{k=0}^{n_p-1} [(Y_j^{\mathrm{ref},k} - Y_j^{\mathrm{act},k})' \tilde{Q}_j (Y_j^{\mathrm{ref},k} - Y_j^{\mathrm{act},k}) + \tilde{u}_j^{k\prime} R_j \tilde{u}_j^k] \tag{10}$$

subject to

$$u_{j,\min} \le u_j \le u_{j,\max}, \tag{11}$$

$$Y_{j,\min}^{\mathrm{act}} \le \quad Y_j^{\mathrm{act}} \le Y_{j,\max}^{\mathrm{act}}, \tag{12}$$

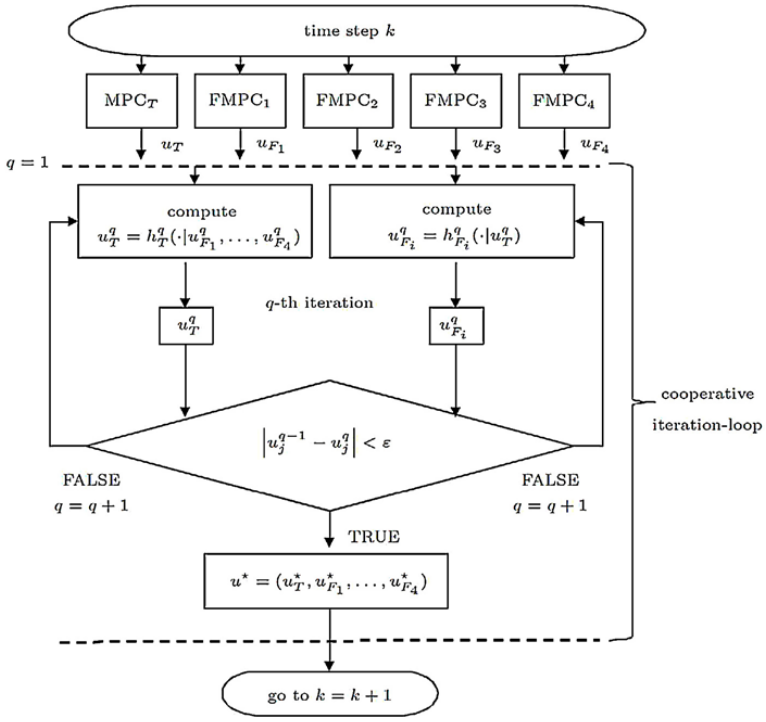

Fig. 6. Schematic flow-chart of cooperative iteration loop of CFMPC. Between consecutive time steps k and $k+1$, the qth cooperative iteration update $h_j^q(\cdot|\cdot)$ is computed in a loop, $\forall j \in \{T, F_i\}, \forall i \in \mathbb{F} = \{1, 2, 3, 4\}$. The resulting cooperative solution for the manipulated variable is given by $u^\star$. The abort criterion has to be fulfilled for all, the MPC$_T$ and the i FMPCs, in the same iteration-step q to advance to $k = k+1$, or the maximal number of iterations-steps has to be reached.

$j = \{T, F_i\}, \forall i \in \mathbb{F}$, where n_p denotes the prediction horizon and "′" denotes transpose. Note that the $Y_i^{\mathrm{ref},k}$ are external reference values and are considered to be known (see Fig. 5). Furthermore, $Y_T^{\mathrm{act}} \equiv \tilde{Y}^{\mathrm{act}}$ and $Y_T^{\mathrm{ref}} \equiv \tilde{Y}^{\mathrm{ref}}$. Note that the optimization (9)–(12) applies only the u_j, the first part of $\tilde{u}_j = [u_j, z_j]$, $\forall j = T, F_i, \forall i \in \mathbb{F}$. Hence, $\tilde{Q}_j \in \mathbb{R}^{n_{y_j} \times n_{y_j}}$ is a positive semi-definite weighting matrix with dimension n_{y_j}, and $R_j \in \mathbb{R}^{n_{\tilde{u}_j} \times n_{\tilde{u}_j}}$ is a positive definite weighting matrix, with $j = \{T, F_i\}, \forall i \in \mathbb{F}$. Note that $n_{\tilde{u}_j}$ is the dimension of the manipulated variable of u_j including the number of disturbances for the jth MPC, $j = \{T, F_i\}, \forall i \in \mathbb{F}$. The objective function of each FMPC$_i$ is also subjected to a LLMN, which consists of L_i LLMs, which are equivalent to r-fuzzy rules.

Now only the i FMPCs are considered. These manipulated variables u_i^{k+t} can be calculated by generating l sets of local linear control inputs in the first step, $u_{i,l}^{k+t}, \forall t \in \{1, 2, \ldots, n_c\}, \forall i \in \mathbb{F}, \forall l \in \mathbb{L}$, where n_c denotes the control horizon. In the second step, the weighted sum of the local linear control inputs give the overall output-blended control input as defined in Eq. (6), see Section 4.1. The weight of the lth fuzzy control action $\Phi_{i,l}$ is the same as that for the lth local linear model [12,4,30].

Let $u^\star$ be the overall blended output, after the iteration loop, see Section 4.2 Fig. 6, with arbitrary chosen initial condition for the CFMPC algorithm. Then the suboptimal optimization problem is formulated as given in [23] and solved at each iteration $q \geq 0$ for all zones $i \in \mathbb{F}$.

In following equations $\Phi_{i,l}$ are the fuzzy membership functions for output blending for LLM$_l$ of LLMN$_i$.

Given the prior feasible iteration $(u_T^q, u_{F_i}^q)$, then the next iteration for the cooperative iteration-loop (for the iteration-update $u_{F_i}^q = h_{F_i}^q(\cdot|u_T^q)$), see Fig. 6, is defined to be

$$\begin{aligned} u^{q+1} &= (u_{F_i}^{q+1}, u_T^{q+1}) \\ &= \Psi_{F_i} \cdot (u_{F_i}^\star(u_T^q), u_T^q) + \Psi_T \cdot (u_{F_i}^q, u_T^\star(u_{F_i}^q)) \\ &= \Psi_{F_i} \cdot \left(\sum_{l \in \mathbb{L}} \Phi_{F_i,l} u_{F_i,l}^\star \left(u_T^q\right), u_T^q \right) \\ &\quad + \Psi_T \cdot \left(\sum_{l \in \mathbb{L}} \Phi_{F_i,l} u_{F_i,l}^q, u_T^\star \left(\sum_{l \in \mathbb{L}} \Phi_{F_i,l} u_{F_i,l}^q \right) \right) \end{aligned} \tag{13}$$

$$\sum_{j=\{T,F_i\}} \Psi_j = 1 \forall \Psi_j > 0, i \in \mathbb{F}. \tag{14}$$

Here, Ψ_j are arbitrary scalar weighting factors. For $u_T^q = h_T^q(\cdot|u_{F_1}^q, \ldots, u_{F_4}^q)$, the calculation is equivalent to Eq. (13) with Eq. (14) with the four FC input as disturbance vector. Stability of the CFMPC concept is proven and discussed in [16].

5. Simulation and validation results

In the following Sections 5.1–5.3, the main simulation results are given and discussed. The CFMPC concept is compared to the FMPC concept, see Fig. 5, without the cooperative iteration-loop, see Fig. 6, is denoted by FMPC$_{\mathrm{wo,c}}$. Furthermore, the CFMPC compared to a global linear MPC concept, denoted as MPC$_{\mathrm{lin}}$, and to the actual implemented rule-based PID-controller strategy from measured data is given.

Unfortunately, a direct comparison between the simulated CFMPC and the historical measured data is not completely fair.

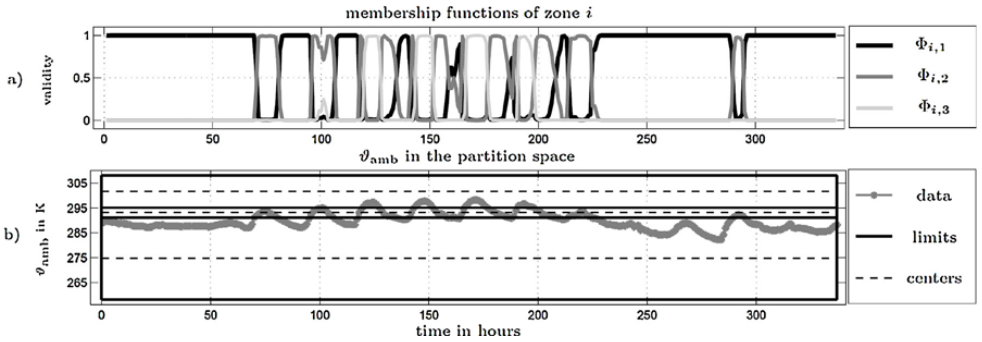

Fig. 7. In (a) the validity of the membership functions is shown during the chosen period. In this sub-figure a, $\Phi_{i,1}$ denotes the winter model, $\Phi_{i,2}$ the transition season model, and $\Phi_{i,3}$ the summer model. Because of the fact that the partition variable is an external input, the validity of the different LLMs is equal for all zones$_i$, $\forall i \in \mathbb{F}$. In (b), the corresponding partition space is given with the partition variable ϑ_{amb}. Furthermore, the limits of the individual models are illustrated with their center points.

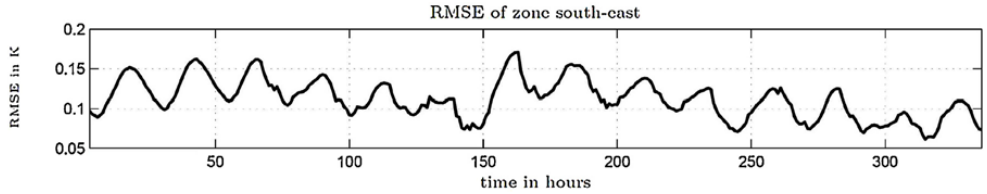

Fig. 8. This figure shows the worst 24-h ahead prediction RMSE of the four zone models in K. The 24 h ahead prediction RMSE values for all zones are given in Table 1.

The actual implemented rule-based PID-controller in the demonstration building is not controlled to one set-point. It is a range [294.15K; 296.15K] where the indoor room temperature is acceptable during working hours. In addition, this range is widened on weekends and during the night. However, for comparison the measured outputs and manipulated variables are shown in the following sections.

5.1. Simulation setup

The setup of four controller schemes is shown for 2 weeks in September 2014. For the CFMPC, the FMPC$_{wo,c}$ and a linear global MPC acting on the office level as a whole, all disturbances are measured from the introduced period. The actual implemented controller is a state-of-the-art rule-based PID-controller, where expert rules in if-then form are combined with PID control for continuous variables. The zoning for the CFMPC is based on the actual supply shafts (which coincide with the cardinal directions) in the demonstration building. Note that the designation of an individual zone is only meaningful if an individual supply (manipulated variable) is available for that zone. If a zone is overlapping with others (as is the case for the TABS), a weighted average of temperature measurements is assigned to that zone, but otherwise the FMPC design is done separately. The cooperative iteration loop then takes care of the proper interaction of the individual FMPC controllers. All results for the rule-based PID-controller are denoted with the subfix "meas", which stands for "measured" and the linear global MPC is given by MPC$_{lin}$. Furthermore, for the rule-based PID-controller, the reference value is illustrated by the mean of the comfort range [294.15K; 296.15K]. Thus, Y^{ref}_{meas} is equal to 295.15K. For the MPC$_{lin}$ one global model for all four zones is considered. Therefore the reference value $Y^{ref}_{MPC_{lin}}$ has been defined as the mean of the four zone reference values.

The period of these 2 weeks in September 2014 is chosen, because all possible cases for the fuzzy membership functions are included: full validity of one LLM, part-validity of 2 LLMs, part-validity of all 3 LLMs, and fast transition between the LLMs. The validation of the zone models is given in Section 5.2, and the comparison of the different controller schemes is described in Section 5.3.

5.2. Model validation

In Fig. 7b, the ambient temperature ϑ_{amb} in the partition space is given for 2 weeks in September 2014. Moreover, the validity of the membership functions is illustrated above in Fig. 7a. It is obvious which function $\Phi_{i,l}$ is valid $\forall i \in \mathbb{F}, \forall l \in \mathbb{L}$, because in Fig. 7b it is well illustrated in the partition space. The steepness k_σ of all LLMs is chosen by $k_\sigma = 1/3$. Therefore, more than 1 LLM is valid in the transitional regions. For instance, 3 LLMs are part-valid at time step $k = 100h$ or 2 LLMs are part-valid at $k = 165h$ ($\Phi_{i,1}$ and $\Phi_{i,2}$).

The model validation is based on a 24-h ahead prediction. The root-mean-square error (RMSE) is computed over 24 values in each time step k for model performance. This statistical value is computed as:

$$\mathrm{RMSE}_j \equiv \sqrt{\frac{\sum_{k=1}^{N} \| \hat{Y}^k - Y^k_{meas} \|_2^2}{N}}, \tag{15}$$

where $\hat{Y}^k$ is value of the 24-h ahead prediction at time step k, Y^k_{meas} gives the output measured from historical data, and N is the number of measurements for Y, $j = \{T, F_i\}$, $\forall i \in \mathbb{F}$.

The RMSE value is directly interpretable in Kelvin K. In Fig. 8, the RMSE is plotted over the time in hours (226 h = 2 weeks) for the worst model fit.

The model performance shown in the RMSE values in K for all zones i, $i \in \mathbb{F}$, is given in Table 1.

As shown in Table 1, the fit of all models is in the same range, which is in an error rate of about 10% only. Note that a model error of 0.18 K (see Fig. 8) is smaller than the accuracy of measurement. The comparison of these models is presented at the zone

Table 1
RMSE values (model performance) of 24-h ahead prediction of all zones.

$Zone_1$-NE	$Zone_2$-SE	$Zone_3$-SW	$Zone_4$-NW
0.111	0.112	0.106	0.091

level only. The building's system level is discussed separately in [7]. One advantage of the proposed concept is the decoupled controller structure between the comfort and the supply level [24]. Hence, in our manuscript the comfort maximization in the different zones is the optimization goal. Realistic fluctuations in the occupancy profile do not significantly influence the model performance for a 24-h ahead prediction. This is mainly due to the averaging effect of more than 500 users.

5.3. Closed-loop controller simulation

In this Section, the performance of the four introduced controller schemes is compared. Furthermore, the energy consumption of the manipulated variables, calculated in an adapted form (Eq. (16)) as given in Eq. (5), is compared. Occupant thermal comfort is defined as minimal deviation from the indoor-room temperature set-point. Other factors such as radiance, lighting, and humidity [31] are not considered, as they are neither measured nor included in the existing automation system. Therefore, in the comparison before and after the implementation of CFPMC only room temperature deviations are considered. Since all other influencing factors are not significantly changed by the different control schemes, this comparison should be fair. Note that for the measured historical data only an indoor mean room temperature Y^{act}_{meas} is given, because the zone splitting is not implemented in the demonstration building yet. In addition, Y^{ref}_{meas} is assumed to be equal to 295.15 K. Note that the coupling zone TABS is included in the CFMPC and the MPC_{lin} concepts, in contrast to the FMPC without cooperation, $FMPC_{wo,c}$, where the information about TABS is not included. In Fig. 9a–c, the outputs for each zone and their reference values are illustrated. The disturbances are given in Fig. 9d–f. The disturbances are taken from measured historical data. Therefore, the energy consumption of the CFMPC is compared to the energy demand depending on historical measured data, the $FMPC_{wo,c}$, and the MPC_{lin}. Energy consumption is proportional to the measured temperature difference between feed and return, as the circulation pumps are operating with fixed speed. The heat flow is therefore calculated using this constant mass flow (has been measured during commissioning) and the temperature difference. It is obvious in Fig. 9a–c that the model predictive controllers, which are including the coupling zone TABS, perform better than the state-of-the-art rule-based PID-controller. As the building's rule-based PID-control has been optimized for minimal energy consumption over the last two years, all other control schemes are tuned to the same consumption. The control performance can therefore be seen as main criterion in the comparison. The deviation in the measured data from its assumed set-point is up to 1 K in some regions. Furthermore, a strong time-delayed correlation between the measured indoor room temperature data Y^{act}_{meas} and ϑ_{amb} is illustrated in Fig. 9c–d.

With the assumed set-point for the measured indoor temperature, the CFMPC concept is better in performance by 21.86% as compared to the $FMPC_{wo,c}$. Performance of the presented CFMPC concept provides an improvement of 19.67% over the rule-based PID-controller in the specific demonstration building and 16.17% against the MPC_{lin}.

The corresponding manipulated variables are shown in Figs. 10 and 11. Fig. 10 shows the manipulated variables $u^{\star}_{T,CFMPC}$ and $u_{T,p}$ for the different controllers in kW, and "p" stands for $FMPC_{wo,c}$, MPC_{lin} or meas. Note that the star-variable results from the cooperative iteration-loop. It demonstrates the different behaviour in this manipulated variable due to different controller schemes. However, the energy cost of TABS is not as high as the cost for FC. Therefore, the different strategies in TABS see Fig. 10, and the higher cost of the fuzzy predictive controllers in TABS, are

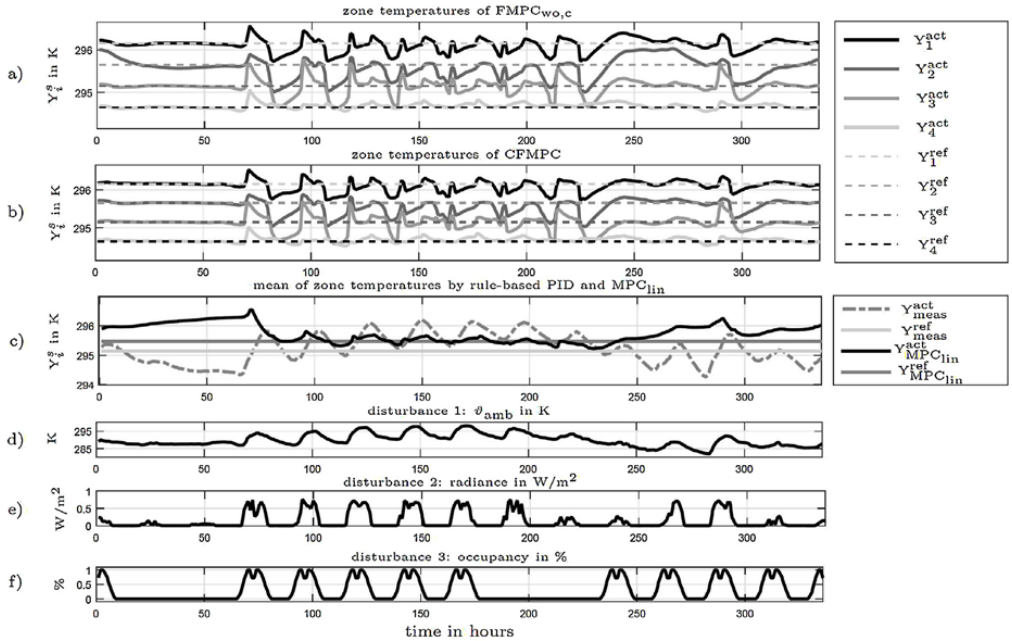

Fig. 9. In subplot (a), the indoor zone temperatures of the $FMPC_{wo,c}$ are given. The same is given for the CFMPC in subplot (b), and the measured output as well as the output of MPC_{lin} is shown in (c). The disturbances are pictured in the subplots (d–f). Note that "s" stands for $s = \{act, ref\}$ and $\forall i \in \mathbb{F} \cap \{meas, MPC_{lin}\}$.

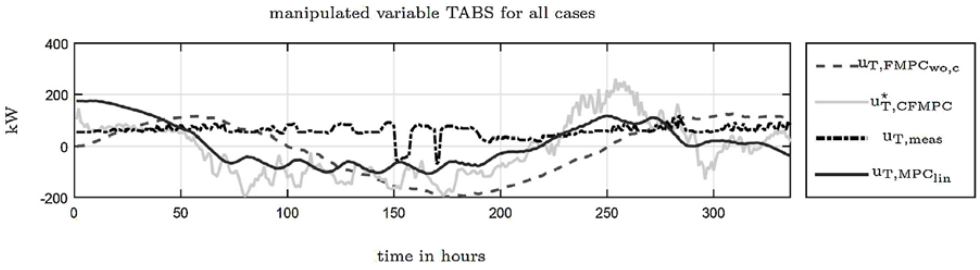

Fig. 10. Manipulated variables $u^{\star}_{T,CFMPC}$ and $u_{T,p}$ for TABS, where "p" stands for $FMPC_{wo,c}$, MPC_{lin} or meas.

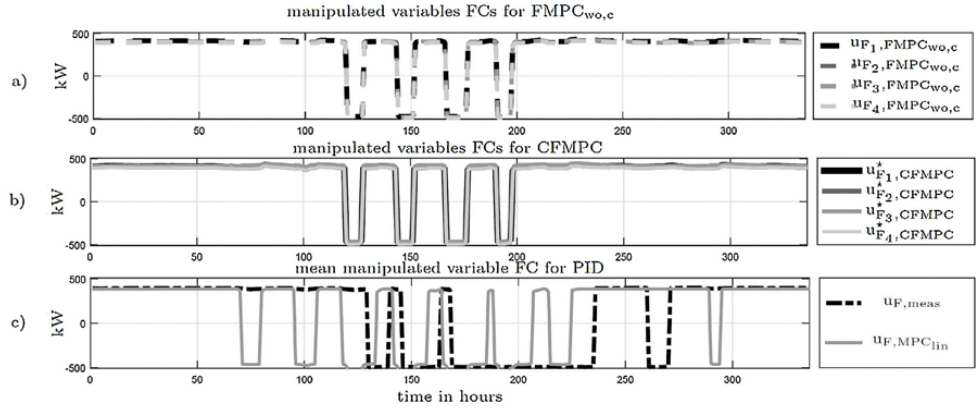

Fig. 11. Manipulated variables $u^{\star}_{F_i,CFMPC}$ and $u_{F_i,p}$ for FC, where "p" stands for the different controllers $FMPC_{wo,c}$, MPC_{lin} or meas and $i \in \mathbb{F}$, in kW.

Table 2
Comparison of performance and energy supply of four different controller schemes.

Concept	Performance	Energy supply
CFMPC	100%	100%
$FMPC_{wo,c}$	78.14%	100.21%
MPC_{lin}	83.83%	100.55%
Rule-based PID	80.33%	100.43%

compensated by the predictive use of the FCs, see Fig. 11. The strategies for $FMPC_{wo,c}$ are given in Fig. 11a. They are similar to the FC strategies of the CFMPC, see Fig. 11b. The subplot in the bottom Fig. 11c shows the measured strategy of the manipulated PID variable FC and of the MPC_{lin} during the chosen 2 weeks. It is illustrated that the FCs with PID are in the cooling mode for a longer period of time. Furthermore, it is obvious that the predictive controllers, Fig. 11a and b, are able to cool and heat predictively.

For a comparison of energy costs, Eq. (5) is adapted for each controller concept:

$$\dot{Q}_{\sum,\nu} = \sum_{i \in \mathbb{F}} |\dot{Q}_{F_i,\nu}| + |\dot{Q}_{T,\nu}|, \tag{16}$$

$\nu = \{FMPC_{wo,c}, CFMPC, meas, MPC_{lin}\}$. The results of the four mentioned controller schemes in performance and energy demand are summarised in Table 2. Note that all controllers are compared to the CFMPC, for which the reference values in performance as well as in energy supply are assumed to be 100%.

It follows that the energy costs of all controllers is nearly in the same range, see Table 2. Thus, it is noteworthy that the presented CFMPC concept is able to achieve a great performance increase with less energy consumption as compared to all other controllers. It is to mention that the $FMPC_{wo,c}$ has no information about the coupling zone TABS, and the rule-based PID-controller in the demonstration building has been optimized over the last 2 years.

6. Conclusion

A cooperative FMPC has been proposed for heating and cooling of buildings. It is important to notice that the FMPCs for each zone are designed by input-coupled LLMNs. One coupling variable exists, which influences each building zone. One great advantage of the underlying MPC models is the validity over all seasons – winter, transition season (spring and fall) and summer. Thus, the presented CFMPC concept is able to control both modes, heating and cooling, in contrast to most of the state-of-the-art MPCs in buildings, where just heating or cooling systems are controlled. Another benefit of the CFMPC is the independence of the building and system type. The CFMPC is useful and implementable for all building types with multiple heat/cooling supplies. The data-based model has to be identified for each for specific building, which is standard in process industry. Hence, for each zone a model (suitable for MPC) has to be created which requires availability of suitable input (heat supply and disturbances) and output (temperatures) data. For the demonstration building a model validation of all zones is given, where the fuzzy grey-box model approach is underlined with excellent results.

A cooperative FMPC (CFMPC) is presented to coordinate the different input-coupled manipulated variables. The outstanding performance results are given with a closed-loop simulation. The CFMPC achieves significantly higher control performance with slightly less energy consumption in contrast to two predictive controllers and the rule-based PID-controller which is implemented

in the demonstration building. The simulation examples verify the advantages and effectiveness of the CFMPC for heating and cooling in the field of building control.

Acknowledgements

This work was supported by the project “SMART MSR” (FFG, No. 832103) in cooperation with evon GmbH and Unipark Nonntal, University of Salzburg.

References

[1] L. Pérez-Lombard, J. Ortiz, C. Pout, A review on buildings energy consumption information, Energy Build. 40 (3) (2008) 394–398, http://dx.doi.org/10.1016/j.enbuild.2007.03.007.
[2] S. Prívara, J. Cigler, Z. Váňa, F. Oldewurtel, C. Sagerschnig, E. Žáčeková, Building modeling as a crucial part for building predictive control, Energy Build. 56 (0) (2013) 8–22, http://dx.doi.org/10.1016/j.enbuild.2012.10.024.
[3] M. Gwerder, S. Bötschi, D. Gyalistras, C. Sagerschnig, D. Sturzenegger, R. Smith, B. Illi, Integrated predictive rule-based control of a Swiss office building, in: Clima – RHEVA World Congress, Prague, Czech Republic, 2013, pp. 1723–1732.
[4] Y.L. Huang, H. Lou, J.P. Gong, T. Edgar, Fuzzy model predictive control, IEEE Trans. Fuzzy Syst. 8 (6) (2000) 665–678, http://dx.doi.org/10.1109/91.890326.
[5] L. Ljung, System Identification: Theory for the User, Prentice-Hall Information and System Sciences Series, Prentice Hall PTR, 1999.
[6] O. Nelles, Nonlinear System Identification: From Classical Approaches to Neural Networks and Fuzzy Models, Engineering Online Library, Springer, 2001.
[7] M. Killian, B. Mayer, M. Kozek, Effective fuzzy black-box modeling for building heating dynamics, Energy Build. 96 (0) (2015) 175–186, http://dx.doi.org/10.1016/j.enbuild.2015.02.057.
[8] X. Li, J. Wen, Review of building energy modeling for control and operation, Renew. Sustain. Energy Rev. 37 (2014) 517–537, http://dx.doi.org/10.1016/j.rser.2014.05.056.
[9] A. Afram, F. Janabi-Sharifi, Black-box modeling of residential {HVAC} system and comparison of gray-box and black-box modeling methods, Energy Build. 94 (2015) 121–149, http://dx.doi.org/10.1016/j.enbuild.2015.02.045.
[10] T. Takagi, M. Sugeno, Fuzzy identification of systems and its applications to modeling and control, IEEE Trans. Syst. Man Cyber. SMC-15 (1) (1985) 116–132, http://dx.doi.org/10.1109/TSMC.1985.6313399.
[11] S. Mollov, P.V.D. Veen, R. Babuška, J. Abonyi, J.A. Roubos, H. Verbruggen, Extraction of local linear models from Takagi-Sugeno fuzzy model with application to model-based predictive control, in: Proceedings Seventh European Congress on Intelligent Techniques and Soft Computing EUFIT'99, 1999, pp. 147–154.
[12] J. Abonyi, Fuzzy Model Identification for Control, Birkhauser, Boston, 2002.
[13] J. Roubos, S. Mollov, R. Babuska, H. Verbruggen, Fuzzy model-based predictive control using Takagi-Sugeno models, Int. J. Approx. Reason. 22 (12) (1999) 3–30, http://dx.doi.org/10.1016/S0888-613X(99)00020-1.
[14] I. Škrjanc, B. Zupančič, B. Furlan, A. Krainer, Theoretical and experimental fuzzy modelling of building thermal dynamic response, Build. Environ. 36 (9) (2001) 1023–1038, http://dx.doi.org/10.1016/S0360-1323(00)00053-6.
[15] E. Camacho, C. Bordons, Model Predictive Control, Advanced Textbooks in Control and Signal Processing, Springer, London, 2004.
[16] M. Killian, B. Mayer, A. Schirrer, M. Kozek, Cooperative fuzzy model predictive control, IEEE Trans. Fuzzy Syst. (2015), http://dx.doi.org/10.1109/TFUZZ.2015.2463674 (in press).
[17] M. Wallace, R. McBride, S. Aumi, P. Mhaskar, J. House, T. Salsbury, Energy efficient model predictive building temperature control, Chem. Eng. Sci. 69 (1) (2012) 45–58, http://dx.doi.org/10.1016/j.ces.2011.07.023.
[18] C.-S. Kang, C.-H. Hyun, M. Park, Fuzzy logic-based advanced on-off control for thermal comfort in residential buildings, Appl. Energy 155 (2015) 270–283, http://dx.doi.org/10.1016/j.apenergy.2015.05.119.
[19] S. Prívara, J. Široký, L. Ferkl, J. Cigler, Model predictive control of a building heating system: the first experience, Energy Build. 43 (2–3) (2011) 564–572, http://dx.doi.org/10.1016/j.enbuild.2010.10.022.
[20] Y. Ma, F. Borrelli, B. Hencey, B. Coffey, S. Bengea, P. Haves, Model predictive control for the operation of building cooling systems, IEEE Trans. Control Syst. Technol. 20 (3) (2012) 796–803, http://dx.doi.org/10.1109/TCST.2011.2124461.
[21] P.-D. Moroşan, R. Bourdais, D. Dumur, J. Buisson, Building temperature regulation using a distributed model predictive control, Energy Build. 42 (9) (2010) 1445–1452, http://dx.doi.org/10.1016/j.enbuild.2010.03.014.
[22] P.O.M. Scokaert, D. Mayne, J. Rawlings, Suboptimal model predictive control (feasibility implies stability), IEEE Trans. Autom. Control 44 (3) (1999) 648–654, http://dx.doi.org/10.1109/9.751369.
[23] B.T. Stewart, A.N. Venkat, J.B. Rawlings, S.J. Wright, G. Pannocchia, Cooperative distributed model predictive control, Syst. Control Lett. 59 (8) (2010) 460–469, http://dx.doi.org/10.1016/j.sysconle.2010.06.005.
[24] M. Killian, B. Mayer, M. Kozek, Hierachical Fuzzy MPC Concept for Building Heating Control, in: Proceedings of the 19th World Congress of the International Federation of Automatic Control (IFAC'14), 2014, pp. 12048–12055, http://dx.doi.org/10.3182/20140824-6-ZA-1003.00772.
[25] B. Mayer, M. Killian, M. Kozek, Cooperative and hierarchical fuzzy MPC for building heating control, in: IEEE International Conference on Fuzzy Systems (FUZZ-IEEE), 2014, pp. 1054–1059, http://dx.doi.org/10.1109/FUZZ-IEEE.2014.6891573.
[26] B. Mayer, M. Killian, M. Kozek, Management of hybrid energy supply systems in buildings using mixed-integer model predictive control, Energy Convers. Manag. 98 (2015) 470–483, http://dx.doi.org/10.1016/j.enconman.2015.02.076.
[27] R. Babuška, Fuzzy Modeling for Control, 1st ed., Kluwer Academic Publishers, Norwell, MA, USA, 1998.
[28] W.-K. Chang, T. Hong, Statistical analysis and modeling of occupancy patterns in open-plan offices using measured lighting-switch data, Build. Simul. 6 (1) (2013) 23–32, http://dx.doi.org/10.1007/s12273-013-0106-y.
[29] K. Tanaka, H. Wang, Fuzzy Control Systems Design and Analysis: A Linear Matrix Inequality Approach, Wiley, 2004.
[30] S. Mollov, R. Babuska, J. Abonyi, H. Verbruggen, Effective optimization for fuzzy model predictive control, IEEE Trans. Fuzzy Syst. 12 (5) (2004) 661–675, http://dx.doi.org/10.1109/TFUZZ.2004.834812.
[31] F.R. d'Ambrosio Alfano, B.W. Olesen, B.I. Palella, G. Riccio, Thermal comfort: design and assessment for energy saving, Energy Build. 81 (2014) 326–336, http://dx.doi.org/10.1016/j.enbuild.2014.06.033.

2.4 Publication D

Barbara Mayer, Michaela Killian, and Martin Kozek.
Management of hybrid energy supply systems in buildings using mixed-integer model predictive control.
Energy Conversion and Management, Volume 98, 2015, pages 470–483, ISSN: 0196-8904.
DOI: 10.1016/j.enconman.2015.02.076

Own contribution
Problem analysis, selection of methods, execution of the solution, development and programming of algorithms, consideration of implementation aspects, performing simulation studies, and structuring, writing and editing of the manuscript was done by the first author. Providing reference trajectories, discussion of methodology, and editing of the manuscript was done by the applicant. Problem statement, discussion and editing was done by the third author.

Energy Conversion and Management 98 (2015) 470–483

Contents lists available at ScienceDirect

Energy Conversion and Management

journal homepage: www.elsevier.com/locate/enconman

Management of hybrid energy supply systems in buildings using mixed-integer model predictive control

Barbara Mayer [a,*], Michaela Killian [b], Martin Kozek [b]

[a] FH Joanneum, Institute of Industrial Management, Werk-VI-Strasse 46, 8605 Kapfenberg, Austria
[b] Vienna University of Technology, Institute of Mechanics and Mechatronics, Getreidemarkt 9, 1060 Vienna, Austria

ARTICLE INFO

Article history:
Received 3 December 2014
Accepted 25 February 2015
Available online 18 April 2015

Keywords:
Mixed-integer model predictive control (MI-MPC)
Hybrid energy supply system
Building control
Unit commitment
Stratified storage tank management

ABSTRACT

In this paper a mixed-integer model predictive controller for hybrid energy supply systems in buildings is presented. This approach is based on a hierarchical building control concept where the energy supply level is coupled to the energy consumption level only by the heat load. The supply level is characterized by non-linear dynamics due to a stratified water storage tank and a switched heat pump with minimum on/off times. The mixed-integer model predictive controller optimizes the unit commitment problem at minimum costs while satisfying the consumption level's predicted heat load. The hybrid system is formulated as a piecewise affine model comprising continuous and discrete system inputs. Moreover, the proposed controller is able to manage the stratified storage tank including switching sequences of the heat pump with respect to energy price forecasts. The effectiveness of this approach is shown by a comparison to a model predictive controller with an a priori fixed operation mode profile, where the heat pump is only operating at night, and discussing the effect of the variation of the stratified storage tank size. The proposed concept is able to flexibly manage all sizes of stratified storage tanks with better performance than the reference control strategy, which is only effective for larger tanks. Additionally, a robustness analyses demonstrates that the mixed-integer model predictive controller can handle errors in the heat load prediction from the consumption level. Both analyses show promising results for the practical use of the proposed controller within the hierarchical control concept or as a control module in a similar but more general application.

1. Introduction

According to the statistics of the International Energy Agency the building sector consumes up to 40% of the total final energy consumption, [1]. In order to achieve significant reductions in primary energy consumption passive measures like improved insulation are taken, but also renewable energy sources are being considered, which are highly dependent on weather conditions. Therefore, the periods of efficient energy production do usually not coincide with the energy demand of buildings. That is why appropriate thermal energy storages become necessary, [2]. They are realized either by thermally activated building systems (TABS), where massive concrete structures are thermally activated, or by dedicated thermal storage such as stratified tanks. The usage of an increasing number of energy sources, the combination of continuous and switching heat sources, together with the management of storage requires new control strategies. Regarding management of the energy production level, the points of view differ considerably and range from peak load shifting approaches, [3], to integrated storage management with building automation systems, [4].

Model-based predictive control (MPC) has been proven as a promising technology for building control, [5]. Most of the presented approaches of recent years focus on the control of the entire building comprising the buildings' zone control as well as the energy supply optimization within one model and controller. In [6] building modeling approaches are discussed, whereas [7] presents how to include forecasts into the MPC strategy. However, a building can be seen as a two-layer structure, the High Level (HiLe) energy-consuming layer and the Low Level (LoLe) energy providing layer, [8]. This paper is based on the fundamental concept presented in [8]: (i) A HiLe-MPC optimizes the heat load for maximum comfort and minimum energy consumption, (ii) the LoLe-MPC provides the requested heat load with minimum monetary costs. As the two layers exhibit different non-linear system dynamics and optimization targets an hierarchical

* Corresponding author. Tel.: +43 386233600 6347.
E-mail addresses: barbara.mayer@fh-joanneum.at (B. Mayer), michaela.killian@tuwien.ac.at (M. Killian), martin.kozek@tuwien.ac.at (M. Kozek).

http://dx.doi.org/10.1016/j.enconman.2015.02.076
0196-8904/

approach is reasonable, splitting one modeling and control problem into two optimization tasks. The resulting modularity in implementation and operation is an important advantage for industrial implementation.

Focusing on the LoLe, the presence of possibly numerous switching aggregates such as heat pumps requires the management of on/off times which consequently influences the operation modes of the stratified storage tanks at each time step. Furthermore, this unit commitment problem involves constraints on the minimum on/off times, which are considered due to constraints on the aggregates' actuators and the aim to reduce maintenance costs over the whole lifecycle. The resulting system is a hybrid system, [9], where each operation mode requires a dedicated, generally non-linear, model. The combination of continuous and discrete decision variables leads to a mixed-integer non-linear optimization problem (MINP), for which there is no exact solution technique. However, by approximating the dedicated models by piecewise linear models, mixed-integer linear programming (MILP) can be used to solve the optimization problem, yielding suboptimal solutions.

Summarizing, the main challenges for the LoLe control are (i) the hybrid energy supply system including continuous as well as discrete control variables for switching aggregates with minimum on/off times, (ii) the mixed-integer MPC formulation (with time variant cost structure) and (iii) the coupling to the HiLe controller with uncertain load prediction.

Using MPC requires accurate but rather simple models. Therefore, appropriate assumptions on the system have to be made. Refs. [10,11] have presented hybrid system formulations for cooling systems including different operation modes. In [10] a two-layered stratified storage tank was considered with constant tank temperatures as well as fixed return temperatures from the building. Ref. [11] generalizes the stratified storage tank management for an arbitrary number of stratification layers, energy sources and consumers. Nevertheless, both [10,11] assume two tank operation modes, charging and discharging, specified by an a priori fixed operation plan. Subsequently, chillers are only switched on at night, in order to charge the stratified storage tank, and switched off during day, when the tank is discharged. In contrast to the aforementioned building control references, this paper focuses on the model-based predictive control of the buildings' heating supply (LoLe) covering the unit commitment problem and introduces the hybrid mixed-integer MPC (MI-MPC) approach; a method which has not yet been applied to building heating control. The energy supply system includes a geothermal heat pump, a stratified two-layered water storage tank, and a TABS system. District heat supply is considered as an additional heating circuit providing energy for the Fan Coils (FC) in the indoor rooms. While [12] shows first experimental results on MPC for building heating control, in [7] focus is put on the comparison of different MPC concepts. However, both use bi-linear models to describe the overall system, whereas this paper introduces a hybrid mixed-integer formulation including discrete decision variables for aggregate switching times as well as constraints on minimum on/off times. The resulting unit commitment and MILP problem has also been theoretically introduced in the field of microgrid operation optimization, [13]. The feasibility and effectiveness of this approach has been experimentally proven in [14], where the method was applied to a microgrid in Athens, Greece. Although the fundamental problem formulation is similar, the model depth for the microgrid is lower than needed for building energy supply, where pumps must be controlled individually. In contrast to [13,14], the modeling approach utilized here is based on analytically derived first order non-linear differential equations, approximated by piecewise linear models. The hybrid mixed-integer problem formulation is carried out as introduced in [9] resulting in a piecewise affine (PWA) system.

The simulation results of the proposed decoupled LoLe mixed-integer MPC are compared to those with an a priori fixed tank operation mode profile in terms of mean error, (monetary) costs and coefficient of performance (COP) of the energy supply of the TABS system. Additionally, the effect of varying the tank size on the controller's decision and the resulting costs are discussed. Since recent work show that the impact of forecasting accuracy on the predictive control strategy is high, [15], an analysis of the MI-MPCs robustness is given with respect to the uncertainty of the heat load prediction from the HiLe. For simulating this error the deterministic reference trajectory is disturbed with a fixed bias and a randomly generated white noise over the entire simulation period.

The paper is structured as follows: The problem is formulated in Section 2, followed by introduction of the model of the energy supply hybrid system, Section 3. The mixed-integer MPC formulation is given in Section 4 and the simulation results discussed in Section 5. Finally, conclusions are drawn in Section 6.

2. Building control

In this Section the fundamental approach, the concept of hierarchical building control, the energy supply system, and the problem formulation are given.

2.1. Fundamental approach

Large building heating control necessarily includes the whole building, the High Level (HiLe), where the building indoor rooms are conditioned, as well as the Low Level (LoLe), where heating is provided. In recent years, most of the MPC approaches have focused on the control of both layers in one controller, [7,6]. Therefore, one model including both systems' dynamics has to be taken into account. The complexity for modeling and control is high as both systems are inherently non-linear and the time constants and optimization targets are completely different. The approach presented in [8] splits this optimization problem by defining a dedicated MPC for each of the two levels, which interact via the predicted heat load from the HiLe $\dot{Q}_i^{\mathrm{ref}}$ and the actual delivered heat from the LoLe $\dot{Q}_i$, where i denotes different heating supply circuits. The maximization of the users' comfort is the central objective for the HiLe-MPC, considering stochastic disturbances ambient temperature, radiance and occupancy. In contrast, the LoLe controller optimizes the operation of the switching aggregate and consequently the number of available energy sources used to meet the HiLe requirement by minimizing the costs. This is a classical unit commitment problem (when to optimally switch an aggregate on/off), but additionally the stratified storage tank's operation and the usage of electric energy with time-varying pricing is optimized. Note that the relevant dynamics in the higher level is comparatively slow (from hours to several days), whereas in the lower level it is faster (from minutes to several hours). In [8], this hierarchically decoupled approach was presented, which is briefly explained in Section 2.2 since it defines the requirement for control of the energy supply system Section 2.3 and in [16] the HiLe-MPC was further developed.

2.2. Hierarchic building control

Fig. 1 shows a schematic diagram of the two building layers and the single coupling point between the controllers. The HiLe optimizes the user comfort by minimizing the deviation of the indoor temperature from the consumer preference. $\dot{Q}_i^{\mathrm{ref}}$, for $i = \{\mathrm{TABS}, \mathrm{FC}\}$, depicts the energy demand of the HiLe to fulfill the optimization target, which constitutes the control variables

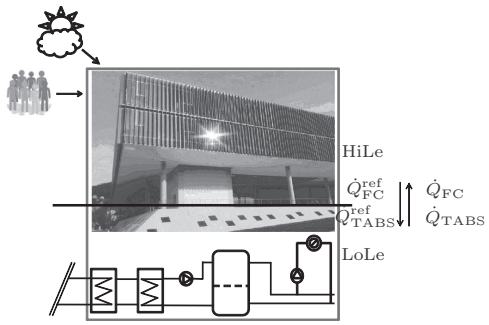

Fig. 1. Concept of hierarchic building control.

of the HiLe-MPC at the same time. As each building zone j can be controlled individually by a separate MPC, the sum of these control variables $\sum_j \dot{Q}^{\mathrm{ref}}_{i,j}$ is the reference value for the energy supply of the LoLe-MPC. However, the important fact is the decoupling of the optimization problems. Stochastic disturbances such as weather and occupancy information only affect the HiLe-MPC, [7], Fig. 1. Decoupling is useful due to the fact that (i) the dynamic behavior is significantly different in HiLe-MPC and LoLe-MPC, (ii) the modeling and optimization problem is split into two tasks, and (iii) the possibility of modular application is given. Minimum up- and down-times and operation modes of the stratified storage tank are the reason for the dynamics in LoLe, whereas the dynamics in the HiLe differ not least due to large time constants. Global optimal solutions may not be reached with a decoupled method, but two local optimal solutions are more likely to be feasible and easier in operation due to the resulting real time capability. Industrially motivated, system identification of the HiLe may be data-driven, [17], while LoLe can be modeled by an analytical approach. Additionally, the optimization targets of the two layers differ fundamentally, so that large benefits arise with an hierarchically decoupled approach that allows modular application in industry.

2.3. Energy supply system

In the following the variables, parameters and subscriptions given in Tables 1 and 2, respectively, will be used.

Due to the different temperature levels, the heating supply system consists of two separated supply circuits, see Fig. 2, one responsible for the Fan Coil (FC) system in the indoor rooms and the other one for the TABS system implemented as activated concrete in two office floors.

District heating is the source of the first circuit, directly fed through to the distributor for the office floors, whereas the TABS system is provided by a geothermal-based heat pump and a subsequent stratified water storage tank. The water-glycol mixture fed by the geothermal pipes varies between 12 °C and 16 °C depending on the season and ambient temperature. The TABS system has a minimum supply temperature constraint which depends on the insulation of the pipe system. Therefore, it is reasonable to operate a stratified storage tank in order to compensate the temperature gap. This also enables an energy saving management since the heat pump can be switched off regularly. As in [11,10], the assumption is that the warm water enters the storage tank at the top and is also drawn from there, whereas the cold return water from the building is supplied to the bottom. The storage tank can operate in two basic operation modes: charging and discharging. These operation modes depend on the status of the heat pump (on/off) and on the difference of the mass flows to, $\dot{m}_{\mathrm{HP}}$, and from, $\dot{m}_{\mathrm{TABS}}$ the storage tank. As the supply systems are located in the basement of the building, the ambient temperature T_{amb} is assumed to be constant with 20 °C. The water return temperatures $T_{\mathrm{TABS},r}$ and $T_{\mathrm{FC},r}$ are also assumed to have a constant level of 22 °C and 30 °C. This assumption is plausible, because the HiLe-MPC optimizes the energy amount needed to guarantee user comfort. Since the LoLe controller is designed to meet these requirements, the resulting return temperatures are almost constant.

Table 1
Definition of variables and parameters.

Variables	Description
z	Height of stratified water storage tank [m]
T	Temperature of the water [°C]
$\dot{m}$	Mass flow rate [kg/s]
$\dot{Q}$	Heat flow from LoLe to HiLe [W]
cp	Specific heat capacity of water [J/kg K]
ρ	Density of water [g/cm^3]
r	Radius of tank [m]
k	Coefficient of thermal conductivity of the storage tank [W/m °C]
v	Volume of the stratified water storage tank [m^3]
δ	Discrete variable

Table 2
Definition of subscripts.

Subscripts	Description
'h'	Hot water above thermocline
'c'	Cold water below thermocline
's'	Supply water to the building
'r'	Return water from the building
'TABS'	TABS system
'FC'	Fan Coils system
'HP'	Heat pump
'DH'	District heat
'amb'	Ambient
'in'	Indoor

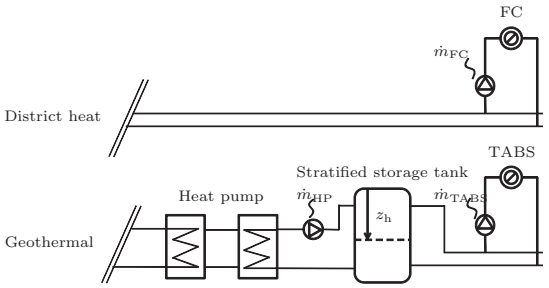

Fig. 2. Heating circuits for FC and TABS.

2.4. Control problem statement

For the energy supply system outlined in Section 2.3 a control design should be performed which guarantees that the actual heat supply $\dot{Q}_i$ tracks the desired heat load $\dot{Q}^{\mathrm{ref}}_i$ with optimal performance (meaning both minimum error and minimum costs). Available variables for that task are heat pump, supply pumps, and supply temperature. Moreover, the management of the stratified storage tank should utilize the storage capacity as effectively as possible. As a model based control scheme is to be used, the following Section focuses on the modeling of the energy supply system.

3. Energy supply system model

In this Section the models for both heating circuits are derived analytically. The non-linear equations are given and the linearization is outlined.

3.1. FC supply model

The FC supply model is determined as a static first order non-linear differential equation with the control output $\dot{Q}_{FC}$ and the manipulated variables $\dot{m}_{FC}$ and $T_{FC,s}$:

$$\dot{Q}_{FC} = \dot{m}_{FC} \cdot (T_{FC,s} - T_{FC,r}) \cdot cp, \tag{1}$$

with $T_{FC,s} = T_{DH}$ and $\dot{m}_{FC}$ as the system's inputs. Linearizing the model at the operating point $O = \left\{T^o_{FC,s},\ \dot{m}^o_{FC}\right\}$, results in:

$$\Delta\dot{Q}_{FC} = c_1 \cdot cp \cdot \Delta T_{FC,s} + c_2 \cdot cp \cdot \Delta\dot{m}_{FC}, \tag{2}$$

with $\Delta T_{FC,s} = T_{FC,s} - T^o_{FC,s}$ and $\Delta\dot{m}_{FC} = \dot{m}_{FC} - \dot{m}^o_{FC}$. The coefficients c_1 and c_2 are provided in Appendix A.

3.2. TABS supply model

For the TABS supply model, the water storage tank is modeled as a two-layer stratified storage tank with one perfectly separating thermocline as in [10]. As the tank is within a closed hydraulic system, the water level in the storage tank is assumed to be constant with $z = z_h + z_c$ at each time. Nevertheless, as the focus of this work is placed on heating control, only the height and volume of water above the thermocline z_h and v_h, respectively, are of importance in the following. On the hot generation side, the tank is supplied by the mass inflow $\dot{m}_{HP}$ with water from the heat pump, whereas on the consumption side, the mass outflow $\dot{m}_{TABS}$ determines the amount of hot water provided for the TABS system, see Fig. 2. Consequently, the status of the heat pump determines the mass flow rate $\dot{m}_{HP}$. In order to make the controller decide whether the heat pump is switched on or off, the discrete variable $\delta_{HP} \in \{0, 1\}$ is introduced, which affects the mass flow rate $\dot{m}_{HP}$ and its constraints, see Section 4.2. If the heat pump is switched on, it operates between 30% and 70% of its nominal power, whereas there is no mass flow at all if the pump is switched off. Therefore, the stratified storage tank's operation mode depends on the controller's decision, on the difference of the two mass flows, and on the status of the heat pump, see Fig. 3.

The water supply temperature $T_{TABS,s}$ depends on the active operation mode. Each mode is represented by one dedicated model. The hybrid system's dynamics are given by the change in z_h and the temperature of the hot water in the stratified storage tank T_h over time. Thus, these two variables form the states of the system. The manipulated variables are given by the mass flows $\dot{m}_{HP}$ and $\dot{m}_{TABS}$ and by the temperature of the water supply from the heat pump T_{HP} to the stratified storage tank. The control outputs $\dot{Q}_{TABS}$ and T_{TABS} are expressed by the two states and the manipulated variables in each case.

3.2.1. Continuous non-linear model

The TABS supply model is determined as a set of non-stationary first order non-linear differential equations based on heat and mass flow balances:

$$\frac{dQ_h(m_h, T_h)}{dt} = \dot{Q}^{in}_h - \dot{Q}^{out}_h, \tag{3}$$

$$\dot{m}_h = \dot{m}^{in}_h - \dot{m}^{out}_h = \dot{m}_{HP} - \dot{m}_{TABS}. \tag{4}$$

For all operation modes, m_h is the mass of hot water in the stratified storage tank above the thermocline, r denotes the radius of the tank and ρ the density of the hot water:

$$m_h = z_h \cdot r^2\pi\rho. \tag{5}$$

Hence, the derivative of the height of stratified water storage tank above the thermocline $\dot{z}_h$ can be derived from Eqs. (4) and (5) independently from the operation mode:

$$\frac{dz_h}{dt} = g(\dot{m}_{HP}, \dot{m}_{TABS}) = \frac{\dot{m}_{HP} - \dot{m}_{TABS}}{r^2\pi\rho}. \tag{6}$$

The heat flow based on the heat balance Eq. (3) is expressed by the following total differential, where the derivative of the temperature $\dot{T}_h$ is denoted by the losses to the ambiance:

$$\frac{dQ_h}{dt}(m_h, T_h) = \dot{m}_h \cdot T_h \cdot cp + m_h \cdot \dot{T}_h \cdot cp = (\dot{m}_{HP} - \dot{m}_{TABS}) \cdot T_h \cdot cp - 2r\pi \cdot k \cdot z_h \cdot (T_h - T_{amb}). \tag{7}$$

Charging: $\dot{m}_{HP} > \dot{m}_{TABS}$ and $\delta_{HP} = 1$

The mass flow rate of the heat pump is higher than the mass flow needed for the TABS system. Therefore, the energy content rises and z_h increases as the thermocline lowers, see Fig. 3(a). This operation mode is only feasible if the heat pump is active. In this case the temperature T_h can approximated by T_{HP} and Eq. (7) can be written as:

$$\dot{m}_h \cdot T_h \cdot cp + m_h \cdot \dot{T}_h \cdot cp = (\dot{m}_{HP} - \dot{m}_{TABS}) \cdot T_{HP} \cdot cp - 2r\pi \cdot k \cdot z_h \cdot (T_h - T_{amb}) \tag{8}$$

The time derivative of the temperature of the hot water in the stratified storage tank $\dot{T}_h$ can therefore be expressed by utilizing Eq. (8) where m_h is substituted by Eq. (5) and $\dot{m}_h$ is substituted by Eq. (4):

$$\dot{T}_h = \frac{(\dot{m}_{HP} - \dot{m}_{TABS}) \cdot (T_{HP} - T_h) \cdot cp - 2r\pi \cdot k \cdot z_h \cdot (T_h - T_{amb})}{z_h \cdot r^2\pi\rho \cdot cp}. \tag{9}$$

As the mass flow to the storage tank is higher than the mass flow to the TABS system, the temperature of the water supply for the TABS system, $T_{TABS,s}$, is assumed to be the temperature of the water supply from the heat pump (direct feed through). Hence, the heat flow to the TABS system is derived from this assumption and the non-stationary heat balance (3):

$$T_{TABS,s} = T_{HP}, \tag{10a}$$

$$\dot{Q}_{TABS} = \dot{m}_{TABS} \cdot (T_{HP} - T_{TABS,r}) \cdot cp. \tag{10b}$$

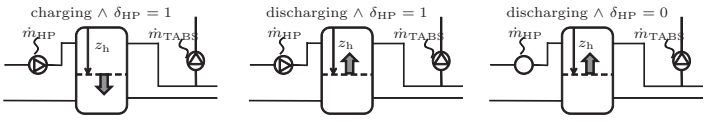

(a) $\dot{m}_{HP} > \dot{m}_{TABS},\ \dot{z}_h > 0$ (b) $\dot{m}_{HP} \leq \dot{m}_{TABS},\ \dot{z}_h \leq 0$ (c) $0 \leq \dot{m}_{TABS},\ \dot{z}_h \leq 0$

Fig. 3. The three operation modes of the stratified storage tank.

Discharging: $\dot{m}_{\mathbf{HP}} \leqslant \dot{m}_{\mathbf{TABS}}$ **and** $\delta_{\mathbf{HP}} = 1$

If the mass flow rate produced by the heat pump is lower than the mass flow needed for the TABS system, the stratified storage tank is discharged, see Fig. 3(b). The time derivative of the temperature of the hot water in the stratified storage tank $\dot{T}_h$ can be directly expressed from Eq. (7):

$$\frac{\mathrm{d}T_h}{\mathrm{d}t} = \frac{-2r\pi \cdot k \cdot z_h \cdot (T_h - T_{\mathrm{amb}})}{z_h \cdot r^2\pi\rho \cdot cp}. \tag{11}$$

If the heat pump is active the water supply temperature to the TABS system, $T_{\mathrm{TABS},s}$, is a mixture of the water supply temperature from the heat pump and temperature of the hot water in the stratified storage tank weighted by the corresponding mass flows. This also causes a different formulation of the heat flow to the TABS system than in the charging mode:

$$T_{\mathrm{TABS},s} = \frac{\dot{m}_{\mathrm{HP}} \cdot T_{\mathrm{HP}} - (\dot{m}_{\mathrm{HP}} - \dot{m}_{\mathrm{TABS}}) \cdot T_h}{\dot{m}_{\mathrm{TABS}}}, \tag{12a}$$

$$\dot{Q}_{\mathrm{TABS}} = \dot{m}_{\mathrm{HP}} \cdot (T_{\mathrm{HP}} - T_h) \cdot cp + \dot{m}_{\mathrm{TABS}} \cdot (T_h - T_{\mathrm{TABS},r}) \cdot cp. \tag{12b}$$

Discharging: $0 \leqslant \dot{m}_{\mathbf{TABS}}$ **and** $\delta_{\mathbf{HP}} = 0$

If the mass flow rate produced by the heat pump is zero the stratified storage tank is discharged, see Fig. 3(c). The deviation of the temperature of the hot water in the stratified storage tank $\dot{T}_h$ is equal to the corresponding formulation for charging while the heat pump is on. The water supply temperature to the TABS system $T_{\mathrm{TABS},s}$ is then equal to the temperature of the hot water in the stratified storage tank:

$$T_{\mathrm{TABS},s} = T_h, \tag{13a}$$

$$\dot{Q}_{\mathrm{TABS}} = \dot{m}_{\mathrm{TABS}} \cdot (T_h - T_{\mathrm{TABS},r}) \cdot cp. \tag{13b}$$

3.2.2. Continuous linearized model

In order to use the MI-MPC a piecewise linear model is required to formally describe the hybrid system. For the linear approximation, operating points for both states and all manipulated variables are fixed, $O = \{z_h^o,\ T_h^o,\ T_{\mathrm{HP}}^o,\ \dot{m}_{\mathrm{HP}}^o,\ \dot{m}_{\mathrm{TABS}}^o\}$. The linearized, continuous system is given by the three sets of linear Eqs. (17)–(19) derived from the respective non-linear part of the model (9)–(13). The coefficients $c_3 - c_{19}$ are provided in Appendix A.

The method to derive the following linearized equations for each operation mode is exemplarily demonstrated for one specific model equation. For all operation modes $\dot{z}_h$ is given by Eq. (6).

The following Δ-variables define the deviation from the operating point: $\dot{z}_h = \Delta\dot{z}_h, \dot{m}_{\mathrm{HP}} = \dot{m}_{\mathrm{HP}}^o + \Delta\dot{m}_{\mathrm{HP}}$ and $\dot{m}_{\mathrm{TABS}} = \dot{m}_{\mathrm{TABS}}^o + \Delta\dot{m}_{\mathrm{TABS}}$. Consequently, Eq. (6) can be rewritten:

$$\Delta\dot{z}_h = g(\dot{m}_{\mathrm{HP}}^o + \Delta\dot{m}_{\mathrm{HP}}, \dot{m}_{\mathrm{TABS}}^o + \Delta\dot{m}_{\mathrm{TABS}}). \tag{14}$$

Developing Eq. (14) in a first-order Taylor series at the operating point results in:

$$\Delta\dot{z}_h = g(\dot{m}_{\mathrm{HP}}^o, \dot{m}_{\mathrm{TABS}}^o) + \frac{\partial g(\dot{m}_{\mathrm{HP}}, \dot{m}_{\mathrm{TABS}})}{\partial \dot{m}_{\mathrm{HP}}}|_o \Delta\dot{m}_{\mathrm{HP}} + \frac{\partial g(\dot{m}_{\mathrm{HP}}, \dot{m}_{\mathrm{TABS}})}{\partial \dot{m}_{\mathrm{TABS}}}|_o \Delta\dot{m}_{\mathrm{TABS}}. \tag{15}$$

With $g(\dot{m}_{\mathrm{HP}}^o, \dot{m}_{\mathrm{TABS}}^o) = 0$ the linearized equation for $\Delta\dot{z}_h$ is given by:

$$\Delta\dot{z}_h = \frac{1}{r^2\pi\rho}\Delta\dot{m}_{\mathrm{HP}} - \frac{1}{r^2\pi\rho}\Delta\dot{m}_{\mathrm{TABS}}. \tag{16}$$

Charging: $\dot{m}_{\mathbf{HP}} > \dot{m}_{\mathbf{TABS}}$ **and** $\delta_{\mathbf{HP}} = 1$

$$\Delta\dot{T}_h = c_3 \cdot \Delta T_{HP} + c_4 \cdot \Delta\dot{m}_{HP} + c_5 \cdot \Delta\dot{m}_{\mathrm{TABS}} + c_6 \cdot \Delta z_h + c_7 \cdot \Delta T_h$$

$$\Delta T_{\mathrm{TABS},s} = \Delta T_{\mathrm{HP}}$$

$$\Delta\dot{Q}_{\mathrm{TABS}} = c_8 \cdot cp \cdot \Delta T_{\mathrm{HP}} + c_9 \cdot cp \cdot \Delta\dot{m}_{\mathrm{TABS}} \tag{17}$$

Discharging: $\dot{m}_{\mathbf{HP}} \leqslant \dot{m}_{\mathbf{TABS}}$ **and** $\delta_{\mathbf{HP}} = 1$

$$\Delta\dot{T}_h = \frac{-2k}{r\rho \cdot cp}\Delta T_h$$

$$\Delta T_{\mathrm{TABS},s} = c_{10} \cdot \Delta T_{\mathrm{HP}} + c_{11} \cdot \Delta\dot{m}_{\mathrm{HP}} + c_{12} \cdot \Delta\dot{m}_{\mathrm{TABS}} + c_{13} \cdot \Delta T_h$$

$$\Delta\dot{Q}_{\mathrm{TABS}} = c_{14} \cdot cp \cdot \Delta T_{\mathrm{HP}} + c_{15} \cdot cp \cdot \Delta\dot{m}_{\mathrm{HP}} + c_{16} \cdot cp \cdot \Delta\dot{m}_{\mathrm{TABS}} + c_{17} \cdot cp \cdot \Delta T_h \tag{18}$$

Discharging: $0 \leqslant \dot{m}_{\mathbf{TABS}}$ **and** $\delta_{\mathbf{HP}} = 0$

$$\Delta\dot{T}_h = \frac{-2k}{r\rho \cdot cp}\Delta T_h$$

$$\Delta T_{\mathrm{TABS},s} = \Delta T_h$$

$$\Delta\dot{Q}_{\mathrm{TABS}} = c_{18} \cdot cp \cdot \Delta T_h + c_{19} \cdot cp \cdot \Delta\dot{m}_{\mathrm{TABS}} \tag{19}$$

Summarized, the system manipulated Δ-variables, the state Δ-variables, and the system output Δ-variables are given by:

$$\Delta u = [\Delta T_{\mathrm{HP}}, \Delta\dot{m}_{\mathrm{HP}}, \Delta\dot{m}_{\mathrm{TABS}}, \Delta T_{\mathrm{FC}}, \Delta\dot{m}_{\mathrm{FC}}]^T,$$

$$\Delta x = [\Delta z_h, \Delta T_h]^T,$$

$$\Delta y = [\Delta\dot{Q}_{\mathrm{TABS}}, \Delta T_{\mathrm{TABS},s}, \Delta\dot{Q}_{\mathrm{FC}}]^T. \tag{20}$$

3.3. Piecewise affine (PWA) model

The MI-MPC requires a model formulation in a linear state space form. Therefore, the overall hybrid system introduced in Sections 3.1 and 3.2 is transformed into a piecewise affine (PWA) model. As motivated in Section 3 the hybrid system consists of two continuous states, $X = X_c = \{z_h,\ T_h\} \in \mathbb{R}^2$, five continuous manipulated variables, $U_c = \{T_{\mathrm{HP}}, \dot{m}_{\mathrm{HP}},\ \dot{m}_{\mathrm{TABS}},\ T_{\mathrm{FC}},\ \dot{m}_{\mathrm{FC}}\} \in \mathbb{R}^5$, one discrete input $U_d = \delta_{\mathrm{HP}}$ with $U = \begin{Bmatrix} U_c \\ U_d \end{Bmatrix} \in \mathbb{R}^5 \times \{0,1\}$ and three continuous outputs, $Y = Y_c = \left\{\dot{Q}_{\mathrm{TABS}}, T_{\mathrm{TABS},s}, \dot{Q}_{\mathrm{FC}}\right\} \in \mathbb{R}^3$.

The auxiliary logical variables $\delta_m(t) \in \{0,1\}, \forall m = 1,..,3$ are introduced to denote the operation mode of the stratified storage tank. As the system can only be in one mode at each time they are satisfying

$$\sum_{m=1}^{3} \delta_m(t) = 1 \tag{21}$$

as an additional constraint. In the following, the overall discrete-time PWA system is considered, which is derived from (2), (17)–(19) with a sampling time of $t_s = 1$ h:

$$x(t+1) = \begin{cases} A_1 x(t) + B_1 u(t), & \text{if } \delta_1(t) = 1 \\ A_2 x(t) + B_2 u(t), & \text{if } \delta_2(t) = 1 \\ A_3 x(t) + B_3 u(t), & \text{if } \delta_3(t) = 1, \end{cases}$$
$$y(t) = \begin{cases} C_1 x(t) + D_1 u(t), & \text{if } \delta_1(t) = 1 \\ C_2 x(t) + D_2 u(t), & \text{if } \delta_2(t) = 1 \\ C_3 x(t) + D_3 u(t), & \text{if } \delta_3(t) = 1, \end{cases} \tag{22}$$

where the matrices $A_m \in \mathbb{R}^{2\times2}$, $B_m \in \mathbb{R}^{2\times5}$, $C_m \in \mathbb{R}^{3\times2}$ and $D_m \in \mathbb{R}^{3\times5}$ are given in the Appendix. The auxiliary variables δ_m for m = 1,2,3 can be expressed by:

$$\delta_1(t) = \delta_{\mathrm{charge}}(t)\delta_{\mathrm{HP}}(t)$$
$$\delta_2(t) = (1 - \delta_{\mathrm{charge}}(t))\delta_{\mathrm{HP}}(t)$$
$$\delta_3(t) = (1 - \delta_{\mathrm{charge}}(t))(1 - \delta_{\mathrm{HP}}(t)), \tag{23}$$

with

$$\delta_{\mathrm{charge}} = \begin{cases} 1 & \text{if } \dot{m}_{\mathrm{HP}} - \dot{m}_{\mathrm{TABS}} > 0 \\ 0 & \text{if } \dot{m}_{\mathrm{HP}} - \dot{m}_{\mathrm{TABS}} \leqslant 0. \end{cases}$$

The non-linear model (22) and the logical expressions in (23) can be transformed to a set of mixed integer linear inequalities as presented in [9].

4. Mixed-integer MPC formulation

The MI-MPC formulation consists of its objective function and a set of constraints. In this section both parts are motivated and formally described. The objective of the MI-MPC is to minimize both the deviation to the head load prediction from the HiLe and the costs while respecting constraints on control inputs, states and minimum on/off times of the heat pump. The optimization procedure is carried out as a moving horizon control strategy [18], at time t an optimal solution for the manipulated variables $U^\star = \left\{u^\star_{t|t}, \cdots, u^\star_{t+Np-1|t}\right\}$ is calculated for the complete horizon. Only the first element $u^\star_{t|t}$ is actually applied to the plant (22), then the optimization problem is repeated at time $t+1$ with the updated states x_{t+1}.

4.1. Objective function

For the LoLe optimization problem, minimum deviation to the head load prediction from the HiLe, the minimum costs, and sustainable management of the stratified tank are relevant.

Note that each Δ-variable in (24) denotes the respective deviation from the fixed operating point: $v = v^o + \Delta v$. The corresponding Δ-vectors used are given in (20). The MI-MPC optimization function is formulated over the prediction horizon Np as follows:

$$J^\star = \min_{\Delta u \in U} \sum_{k=0}^{Np-1} [(1-\alpha)\cdot(|Q(\Delta y_{\mathrm{ref}}(t+k) - \Delta y_{\mathrm{act}}(t+k))| + |S(\Delta x_{\mathrm{ref}} - \Delta x_{\mathrm{act}}(t+k))|) + \alpha\cdot(R(t+k)(\Delta u(t+k)+u^o) + |T(\Delta u(t+k) - \Delta u(t+k-1))|)], \quad (24)$$

where Δy_{ref} denotes the shifted reference output vector and Δx_{ref} the shifted reference state vector. The objective function (24) consists of four additive terms covering the four objectives. The first addresses the three continuous outputs, whereas the second term refers to the continuous states of the stratified storage tank. The third covers the costs occurring due to the manipulated variables and the fourth is limiting the change in control increments. Each of these terms is penalized individually. The weights on the output deviation to the reference heat load Q, the weights on the state deviation S and the weights on control increments T are time-invariant. The weight on control inputs $R(t+k)$ depends on the fluctuating, possibly predicted energy prices and is therefore time-variant. Since the linearized model is formulated in Δ-values (see (2), (17)–(19)), all variables in the objective function (24) are deviations to the operating point, e.g. $\Delta u_{\mathrm{act}} = u_{\mathrm{act}} - u^o$. However, in order to penalize the absolute costs, in the third term the manipulated variables $\Delta u(t+k)$ are re-shifted by their operating points u^o.

Apart from the primary weights Q, S, T and $R(t+k), \alpha \in \{0,1\}$ is an additional weight of the minimization criterion, which allows a global balance between performance and cost variables, respectively.

4.2. Constraints

The MI-MPC has to cope with several types of constraints, for the overall optimization problem defined in Section 4.3. Firstly, constraints on operation and capacities for control inputs and states:

$$x_{i,\min} \leqslant x_i \leqslant x_{i,\max}, \quad (25a)$$

$$u_{i,\min} \leqslant u_i \leqslant u_{i,\max}. \quad (25b)$$

As the heat pump is a switching aggregate operating either between 30% and 70% of its nominal power or at zero level if it is switched off, the constraint set for $\dot{m}_{\mathrm{HP}}$ is disconnected. Therefore, the corresponding constraint (25b) is modified:

$$\dot{m}_{\mathrm{HP},\min}\delta_{\mathrm{HP}} \leqslant \dot{m}_{\mathrm{HP}} \leqslant \dot{m}_{\mathrm{HP},\max}\delta_{\mathrm{HP}}. \quad (26)$$

Constraints for minimum on/off times in each sampling time $t+k$ for which the heat pump has to be kept on/off can be expressed by the following mixed integer linear inequalities, as demonstrated in [13]:

$$\delta_{\mathrm{HP}}(t+k) - \delta_{\mathrm{HP}}(t+k-1) \leqslant \delta_{\mathrm{HP}}(\omega_{\mathrm{up}}), \quad (27a)$$

$$\delta_{\mathrm{HP}}(t+k-1) - \delta_{\mathrm{HP}}(t+k) \leqslant 1 - \delta_{\mathrm{HP}}(\omega_{\mathrm{down}}), \quad (27b)$$

with $\omega_{\mathrm{up}} = t+k, t+k+1, \ldots, \min(t+Np, t+k+T^{\mathrm{up}}_{\mathrm{HP}}-1)$ and $\omega_{\mathrm{down}} = t+k, t+k+1, \ldots, \min(t+Np, t+k+T^{\mathrm{down}}_{\mathrm{HP}}-1)$.

4.3. MPC optimization target by MILP

According to the predictive control theory with moving horizon strategy, [18], the MPC is solving an MILP at each time step $t+k$, given initial storage states z_h and T_h and a prediction horizon Np, but only the first sample of the input sequence is implemented. The MPC solves an optimal finite-horizon control problem given in (24).

subject to

- The PWA model (21) and (22) in terms of linear inequalities,
- the input and state constraints on operation and capacity (25) and (26) with (30),
- the constraints for minimum on- and off times (27).

The controller for the comparison analysis is set up with the same structure, substituting the discrete manipulative variable δ_{HP} by the predefined operation mode profile.

5. Simulation results

In this Section the simulation results for the comparison of the MI-MPC and the MPC with fixed operation mode profile are given. Therefore the comparison metrics will be defined. For this analysis, the volume of the stratified tank v_h is varied in the simulation, see Section 5.3. Hence, its maximum ranges from 30 m^3 to 50 m^3. In a second analysis, the robustness of the MI-MPC with respect to uncertain heat load predictions and depending on the length of the prediction horizon is shown in Section 5.4 based on an approximated Pareto front.

5.1. Comparison metrics

The mean error (ME) is a critical value as the LoLe MI-MPC has to provide the energy demanded by the HiLe. The costs are caused by the electric costs to generate the mass flow rates and temperatures and by the penalties on control increments:

$$\mathrm{ME} = \frac{1}{Np}\sum_{i=1}^{Np}(|Q(y_{\mathrm{ref}}(i) - y_{\mathrm{act}}(i))| + |S(x_{\mathrm{ref}} - x_{\mathrm{act}}(i))|), \quad (28)$$

$$\mathrm{costs} = \sum_{i=1}^{Np}(R(i)(u(i)+u_o) + |T(u(i) - u(i-1))|). \quad (29)$$

For the comparison analysis of the two controllers the coefficient of performance (COP) of the TABS system is additionally defined as the

ratio of the thermally generated energy $E_{t.g.}$ (for the usage in the building) and the amount of electrical energy consumed $E_{e.c.}$ by the energy supply systems, [10]:

$$\mathrm{COP} = E_{t.g.}/E_{e.c.},$$

with

$$E_{t.g.} = \sum_{i=0}^{Np-1} \dot{m}^i_{\mathrm{TABS}} \cdot \left(T^i_{\mathrm{TABS},s} - T_{\mathrm{TABS},r}\right) \cdot \Delta t,$$

$$E_{e.c.} = \sum_{i=0}^{Np-1} k1 \cdot \dot{m}^i_{\mathrm{HP}} + k2 \cdot \dot{m}^i_{\mathrm{TABS},s} + \frac{\dot{m}^i_{\mathrm{HP}} \cdot \left(T^i_{\mathrm{HP},s} - T_{c,s}\right) \cdot cp}{\mathrm{COP}_{\mathrm{HP}}}.$$

The $\mathrm{COP}_{\mathrm{HP}}$ is approximated by a linear equation, as discussed in [19]:

$$\mathrm{COP}_{\mathrm{HP}} = c_0 + c_1 \cdot T_{c,s} + c_2 \cdot T_{h,s}$$

with $c_0 = 5.593$, $c_1 = 0.0569\ \mathrm{K}^{-1}$ and $c_2 = -0.0661\ \mathrm{K}^{-1}$ constant. $T_{h,s}$ denotes the temperature of the heat pump on the hot side which is $T^o_{\mathrm{HP},s} = 35$, and the cold supply to the heat pump $T_{c,s}$ is assumed to be constant with 16 °C as the water is taken from the geothermal pipes. The comparison of the ME, the costs, and the COP for the two different control strategies is shown in SubSection 5.3.

5.2. Simulation setup

The MI-MPC is implemented in the Matlab framework using Yalmip, [20]. For the MILP task the Gurobi solver, [21], was added. The hybrid system is formulated as a PWA system. The MPC for comparison analysis is run with the same Yalmip implementation exchanging the discrete manipulated variable δ_{HP} with the a priori fixed storage tank operation mode profile.

The University of Salzburg, representing the demonstration building, contains the energy heat supply circuits such as shown in Fig. 2.

The only important coupling point between the HiLe and the LoLe is the heat demand of the HiLe and the effectively realized amount of energy provided by the LoLe, as depicted in Fig. 1. The corresponding picture of the building shows the modern 27.000 m² building in the center of Salzburg, Austria. It has five floors above ground containing several large and numerous smaller meeting rooms, offices and lecture rooms. There are six atrium within the modern building complex. For this study, the second and third floor of the building is considered, comprised of about 500 rooms, almost all used as offices, and about 13.000 m². The corresponding characteristics of the heat supply circuit as admissible ranges, see (30), for pumps and the heat pump are derived from the characteristic curves and technical data sheets. The operation constraints and admissible ranges for this work are therefore given by:

$$\begin{aligned}
&T_{\mathrm{HP}} \in [20, 60][^\circ\mathrm{C}]\\
&\dot{m}_{\mathrm{HP}} \in \{0\} \cup [6, 15][kg/s]\\
&\dot{m}_{\mathrm{TABS}} \in [6, 15][\mathrm{kg/s}]\\
&T_{\mathrm{FC}} \in [20, 70][^\circ\mathrm{C}]\\
&\dot{m}_{\mathrm{FC}} \in [7, 18][\mathrm{kg/s}]\\
&T_h \in [0, 60][^\circ\mathrm{C}]\\
&z_h \in [0.1, 2][\mathrm{m}].
\end{aligned} \tag{30}$$

The operating points are chosen as given in Table 3 for linearizing the non-linear models:

Table 3
Operating points of input and state variables.

Variables	Operating point	Unit
z^o_h	1	[m]
T^o_h	30	[°C]
T^o_{HP}	35	[°C]
$\dot{m}^o_{\mathrm{HP}}$	9	[kg/s]
$\dot{m}^o_{\mathrm{TABS}}$	7	[kg/s]
T^o_{FC}	70	[°C]
$\dot{m}^o_{\mathrm{FC}}$	12	[kg/s]

The radius of the stratified storage tank r is varied from 2.03 m to 2.8 m in order to study the effects on an increase in volume v_h. The coefficient of thermal conductivity k amounts 0.01 W/m² °C and the ambient temperature in the basement, T_{amb}, is assumed to be constant with 20 °C. The minimum on/off-times for the heat pump for this work are given by $T^{\mathrm{up}}_{\mathrm{HP}} = T^{\mathrm{down}}_{\mathrm{HP}} = 1$ h.

The energy costs used for the simulation runs are given in Table 4. The assumption comprises a low night rate and a high day rate in the morning for electric energy. In the afternoon, the costs change every two hours between the low night and the high day tariff. The costs for the district heat are assumed to be constant.

The prediction horizon is 24 h, and the simulation is presented for three days, the sampling time is one hour. The desired energy from the HiLe for the TABS as well as for the FC system, $\dot{Q}^{\mathrm{ref}}_i$, is a snapshot of historic data from the demonstration building. This output reference is firstly interpreted deterministically. In a further simulation study, robustness is shown. The desired heat demand trajectory is overlaid by a low pass filtered sinus as a bias and a random white noise in order to simulate error of the heat load prediction from the HiLe.

5.3. Analysis of simulation results

For the comparison analysis, the weighting parameter α is kept constant with 0.1 and the initial states $v_h(0)$ and $T_h(0)$ are chosen at their operating points, such that the stratified storage tank is half full with hot water. The stratified storage tank is assumed to have a volume of 30 m³ for the first comparison analysis. Figs. 4 and 5 show the simulation results of the MI-MPC and the MPC with fixed operation mode profile, respectively. The first subplots (a) show the output and the reference trajectories for both circuits. In subplot (b) one can see the manipulated temperatures from the heat pump, the district heat and the temperature of the hot water in the stratified storage tank. The third subplot (c) depicts the manipulated mass flows to and from the tank to the building for the TABS system as well as the mass flow to the fan coil system, whereas subplot (d) shows the trajectories of the states v_h and T_h. The last subplot (e) in Fig. 4 shows the decision on δ_{HP}, whereas in Fig. 5 the corresponding line represents the fixed operating mode

Table 4
Energy costs [€/kW h].

Time slots	Electric energy	District heat
08:00–12:00	€0.12	€0.09
12:00–14:00	€0.06	€0.09
14:00–16:00	€0.12	€0.09
16:00–18:00	€0.06	€0.09
18:00–20:00	€0.12	€0.09
20:00–08:00	€0.06	€0.09

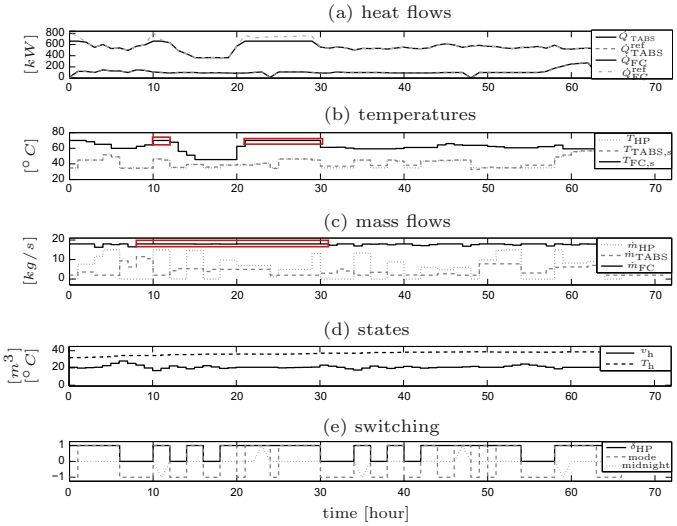

Fig. 4. MI-MPC with optimized operation mode. Bold rectangles mark sections where manipulated variables are limited by constraints and control errors result. (For interpretation of the references to colour in this figure legend, the reader is referred to the web version of this article.)

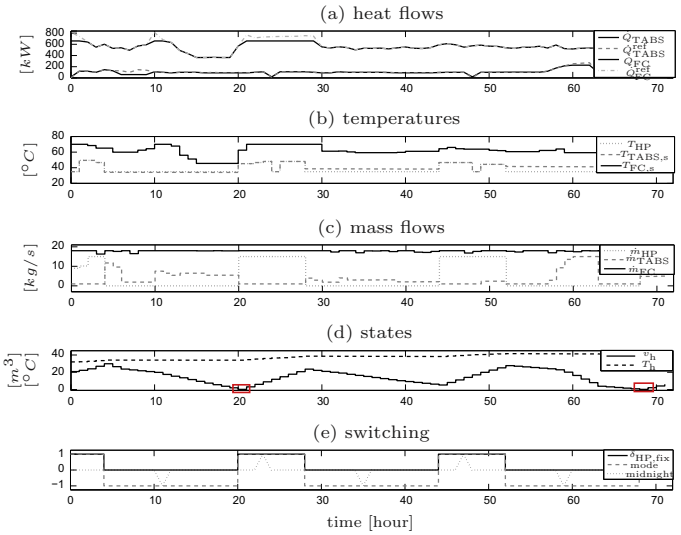

Fig. 5. MPC with fixed operation mode profile. Bold rectangles mark sections where the output of hot water volume in the tank remains in its lower constraint. (For interpretation of the references to colour in this figure legend, the reader is referred to the web version of this article.)

profile. It should be noted, that both controllers are not able to provide the heat load demanded for the FC at all times, because both manipulated variables $\dot{m}_{FC}$ and $T_{FC,s}$ are at their upper bounds and the saturation level is reached, see Figs. 4 and 5 at simulation time 10–12 h and 22–30 h, respectively. In Fig. 5 (d) the volume reaches the lower constraint at the end of the first and third discharging period, whereas the MI-MPC is able to operate the stratified storage tank more efficiently. The actual storage tank volume used by the two controllers differs considerably. The MI-MPC uses an actual volume of 11.22 m^3 for its optimal management strategy, whereas the MPC with fixed operation mode profile needs an actual volume of 27.22 m^3.

The comparison according to the metrics introduced in Section 5.1 is given in Table 5. For this analysis the radius of the stratified storage tank r is increased from 2.03 m to 2.8 m, so that the maximum volume is increased from 26 m^3 up to 49.4 m^3. The simulation results show that for a stratified storage tank volume below 32.5 m^3 there is no feasible solution for the MPC with fixed operation mode profile, as long as the stratified storage tank is supposed to be half full with hot water at the start of the simulation.

Table 5
Performance comparison for different levels of the storage tank volume $v_h^{\max}$.

	$v_h^{\max} = 26\ \mathrm{m}^3$		$v_h^{\max} = 36.4\ \mathrm{m}^3$		$v_h^{\max} = 49.4\ \mathrm{m}^3$	
Metrics	MI-MPC	MPC	MI-MPC	MPC	MI-MPC	MPC
ME	60.93	–	55.64	82.71	55.78	84.95
Costs [10^4]	0.01	–	2.90	2.88	2.90	2.88
Costs on elec. energy [€]	611.36	–	598.41	413.99	640.27	414.46
Energy therm. gen. [10^4 kW h]	3.95	–	3.76	3.28	3.98	3.29
Energy elec. cons. [10^3 kW h]	8.53	–	7.81	6.90	8.36	6.91
COP	4.63	–	4.81	4.75	4.76	4.76
Volume spread [m^3]	24.57	–	14.2	33.72	16.03	46.72

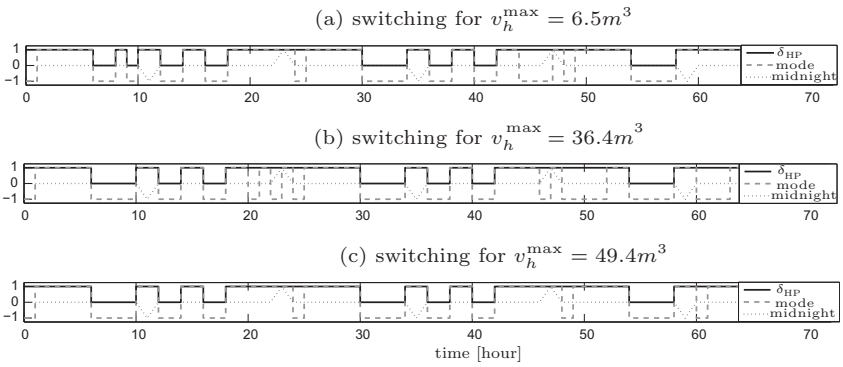

Fig. 6. Comparison of operation mode profile for MI-MPC and different storage tank volume levels.

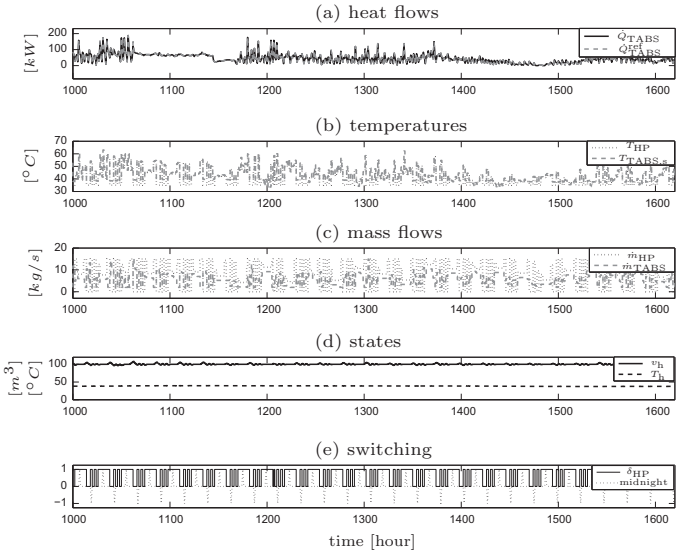

Fig. 7. MI-MPC with optimized operation mode.

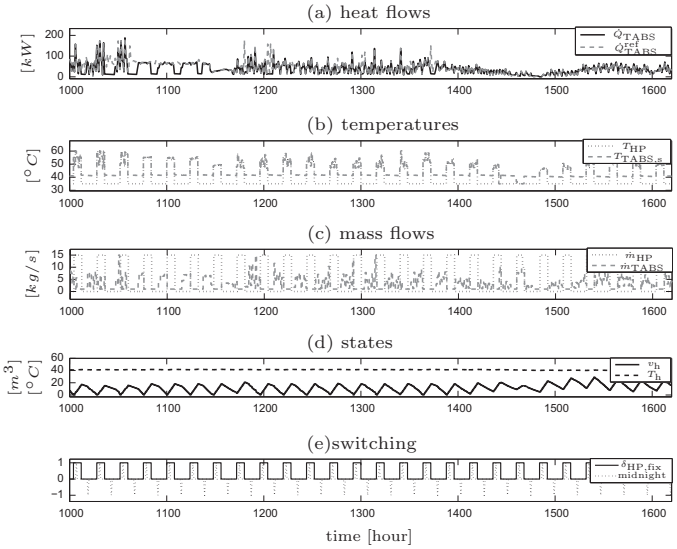

Fig. 8. MPC with fixed operation mode profile.

For a stratified storage tank full with hot water, the minimum volume for achieving a feasible solution is 20.8 m³. The MI-MPC yields better results in terms of the mean error which is an essential requirement with regard to the user comfort because the HiLe-MPC already makes use of the temperature tolerance band at minimal energy demand. Therefore, deviations to the requested energy amount result most likely in a user comfort band violation.

Variation of the stratified storage tank volume results in two major outcomes: Firstly, only the MI-MPC achieves feasible solutions for small tank volumes and secondly, the change in the strategy for the stratified storage tank management differs for small to middle size in different decisions for δ_{HP}, whereas for middle to big volume only the decision for the operation mode changes, see Fig. 6(a)–(c).

Figs. 7 and 8 show a cutout of a simulation for the heating period from December 2013 until March 2014 for the TABS system. The heat demand has characteristics from strongly variant to almost stationary, so that the difference of the controllers' strategies becomes apparent. The controller with the fixed operation mode profile runs a cyclically recurring strategy, which is successful in terms of ME if the reference trajectory is quite stationary. When the heat demand becomes higher in frequency the MI-MPC benefits from its flexibility in operation. The difference of the controllers strategies lie as well in the management of the storage tank as well as in the usage of different temperature levels. Important to mention is, that with the given set of constraints for operation and capacities for control inputs, the MPC with the fixed operation mode profile only yields feasible optimization results for very large storage tanks, whereas the MI-MPC is implementable also for small sizes. Table 6 show the results for the whole period regarding the comparison metrics. The effects on the gap between the ME as well as the costs and the volume spread of the short run analysis are intensified over the long period, meaning that the more weight is put on the comfort the more beneficial is the implementation of the MI-MPC.

Table 6
Performance comparison for long term simulation for $v_h^{\max} = 260\ \mathrm{m}^3$.

Metrics	MI-MPC	MPC
ME	18.37	59.95
Costs [10^4]	116.56	115.79
Costs on elec. energy [10^4 €]	3.05	1.97
Energy therm. gen. [10^4 kW h]	190.41	162.90
Energy elec. cons. [10^3 kW h]	406.56	328.39
COP	4.69	4.96
Volume spread [m³]	11.89	106.68

5.4. Robustness analysis

In order to prove robustness of the MI-MPC with respect to disturbances of the heat load prediction (which has been assumed deterministic in the optimization problem in Section 4.3), some unknown bias and random noise is added to the deterministic heat load prediction. The closed-loop performance is then evaluated for different levels of this stochastic disturbance.

For the robustness analysis an approximated Pareto front is computed for a fixed set of weights $Q, R(t+k), S, T$, as introduced in Section 4.1 and varying α between $[0, 1]$. Fig. 9(a)–(d) shows the approximated Pareto fronts and the convex hulls for different lengths of *Np*. For all simulation runs a stratified storage tank volume of 39 m³ is chosen.

Since the MI-MPC optimization problem is generally non-convex, [22], the approximation of the Pareto front is not necessarily convex either. Furthermore, this approximated Pareto front is only *one* among a family of curves, each corresponding to a certain set of fixed weights, nevertheless not yielding the effective Pareto front. Identifying the global Pareto front is a global optimization problem; its solution would be available by e.g. executing a genetic algorithm to find the optimal set of weights. Initially a set of randomly chosen genomes would have to be evaluated according to

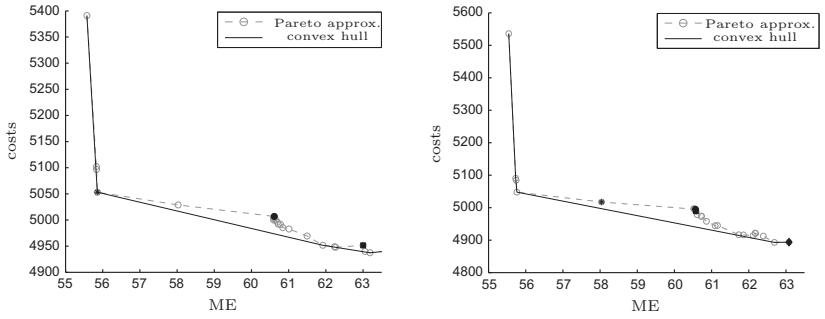

(a) Approximated Pareto front for MI-MPC with Np=8

(b) Approximated Pareto front for MI-MPC with Np=12

(c) Approximated Pareto front for MI-MPC with Np=16

(d) Approximated Pareto front for MI-MPC with Np=24

Fig. 9. Approximated Pareto fronts for Np = 8, Np = 12, Np = 16 and Np = 24.

their fitness, i.e. their contribution to the optimal Pareto front. In an iterative process, the successive ones would have to be modified and again evaluated in order to achieve the best combination of weights.

Secondly, the deterministic output reference $y_{\text{ref}}^{\text{det}}$ is overlaid with a fixed bias over the entire simulation period and a randomly generated white noise in order to get a disturbed reference trajectory $y_{\text{ref}}^{\text{dist}}$. The bias is given by the sine of the low pass filtered reference trajectory $y_{\text{ref}}^{\text{lpf}}$, while the white noise is randomly generated offline for each step over the prediction horizon Np with an amplitude of one tenth of the standard deviation σ of the deterministic standard trajectory $y_{\text{ref}}^{\text{det}}$:

$$y_{\text{ref}}^{\text{dist}}(t+k) = y_{\text{ref}}^{\text{det}}(t+k) + \lambda \cdot \sin(y_{\text{ref}}^{\text{lpf}}(t+k)) + \sigma/10 \cdot \zeta(t+k), \quad (31)$$

where ζ is a random number $\in [0,1]$. In order to show the MI-MPCs robustness, the deterministic reference trajectory is substituted by the disturbed one $y_{\text{ref}}^{\text{dist}}$. The amplitude of the sinus is successively increased in each simulation run by increasing the parameter λ from 1 to 8 at four given levels of α. Fig. 10(a)–(d) shows the results compared to the ones without bias and noise. The symbols, stars, circles, squares and diamonds represent the results for the same level of α. For low α the distances from the disturbed results to the optimal ones on the approximated Pareto front regarding both axes are less than the distances for higher α. In Fig. 10(a)–(c) the results for higher α are widely scattered.

The utilized robustness measure τ is the mean sum of the weighted distances to the corresponding optimal result on the approximated Pareto front in terms of ME and costs. It allows the direct comparison of the results for different prediction horizons Np. τ_i is given by:

$$\tau_i = \frac{1}{N}\sum_{j=1}^{N}\sqrt{(1-\alpha_i)\cdot\left(\text{ME}_{i,j}^{\text{dist}} - \text{ME}_i^{\text{det}}\right)^2 + \alpha_i \cdot \left(\text{costs}_{i,j}^{\text{dist}} - \text{costs}_i^{\text{det}}\right)^2}. \quad (32)$$

Fig. 11 shows the results for τ for the four different prediction horizons as in Figs. 9 and 10. As the robustness analysis is done for $\lambda \in \{1,2,\ldots,8\}$ eight results with increasing white noise are compared to the optimal result. According to the definition of τ in Eq. (32), the MI-MPC becomes the more robust the smaller τ is. It is shown that for a large prediction horizon the MI-MPC shows less distance to the corresponding optimal result on the approximated Pareto front than for smaller prediction horizons. However, if the weighting parameter α is in the interval from 0.1 to 0.45 the MI-MPC is robust even for smaller horizons. If one considers also the absolute costs and the ME as demonstrated in Fig. 10, an α of around 0.1 can be recommended for the given application.

The results considering the system's COP are given in Table 7 in terms of mean value and standard deviation. The two statistical parameters are calculated over the 8 different values of λ at each level of α and different prediction horizons. The highest COP mean value is reached for $\alpha = 0.172$ for all prediction horizons. The system's COP standard deviation is small throughout all simulation runs, although with the variation of λ up to 8 very high disturbance is caused.

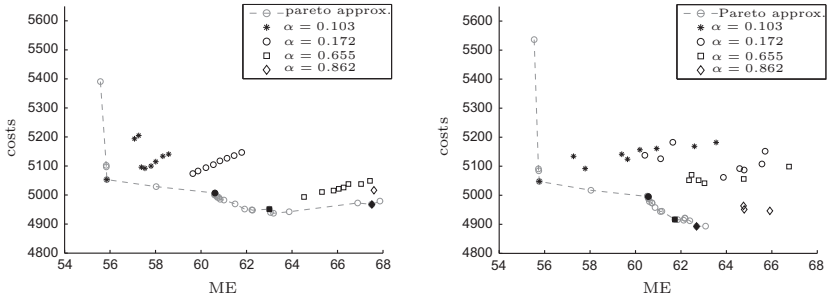

(a) Robustness analysis for MI-MPC with Np=8

(b) Robustness analysis for MI-MPC with Np=12

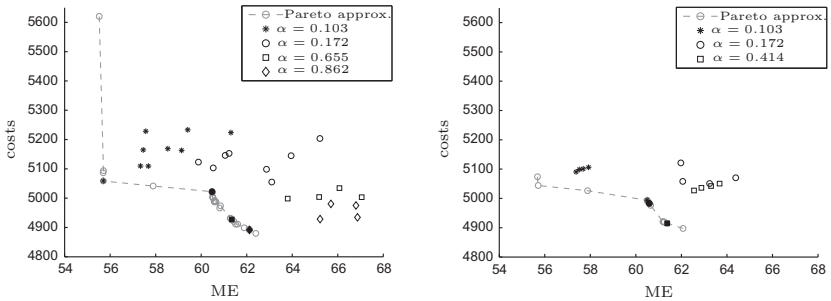

(c) Robustness analysis for MI-MPC with Np=16

(d) Robustness analysis for MI-MPC with Np=24

Fig. 10. Robustness analysis for Np = 8, Np = 12, Np = 16 and Np = 24.

Table 7
COP statistics for robustness analysis.

Np	Metrics	α_1 = **0.103**	α_2 = **0.172**	α_3 = **0.655**	α_4 = **0.862**
8	Mean value	4.8377	4.8422	4.7491	4.7492
	Standard deviation	0.0306	0.0111	0.0220	0.0245
12	Mean value	4.7783	4.8222	4.7530	4.7623
	Standard deviation	0.0271	0.0285	0.0410	0.0392
16	Mean value	4.7378	4.7635	4.7003	4.6376
	Standard deviation	0.0192	0.0238	0.0275	0.0450
		α_1 = **0.103**	α_2 = **0.172**	α_3 = **0.414**	
24	Mean value	4.7328	4.7356	4.6931	
	Standard deviation	0.0365	0.0159	0.0075	

COP statistics for robustness analysis at different levels of the weighting parameter α.

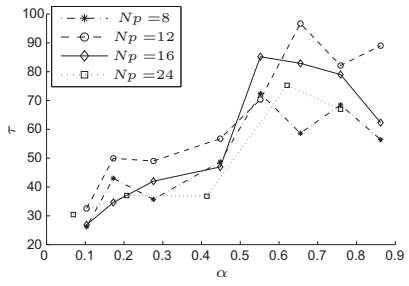

Fig. 11. Robustness metrics for MI-MPC with Np = 8, Np = 12, Np = 16, Np = 24.

6. Conclusion

In this paper a mixed-integer MPC (MI-MPC) has been presented for building heating management with a stratified storage tank. In contrast to other studies in this field, this approach covers the unit commitment problem with switching aggregate, as well as taking their minimum up- and down times into account. The considered stratified storage tank operates in three operation modes, depending on the state of the heat pump. Therefore, the resulting hybrid PWA model, based on first order differential equations, includes discrete and continuous manipulated variables. A validation of the model is currently not possible due to a lack of measurements on the stratified storage tank in the demonstration building. However, for future work the implementation of an appropriate observer is planned in order to substitute the missing plant data. The control strategies are shown in comparison to MPC formulations with a fixed operation tank profile. The simulation results are evaluated according to the mean error, the costs and the system's COP value depending on the volume of the stratified tank. One can see that for small tanks, the MPC with an a priori operation mode profile runs into an infeasible problem, whereas the MI-MPC delivers optimal solutions. Additionally, a robustness analysis has been performed and the approximated Pareto front of the MILP given. For this analysis the originally deterministic heat load reference trajectory has been disturbed. The considered parameter of this analysis was α, putting more emphasis either on the ME or on the costs. Simulation studies with larger prediction horizons have proved beneficial. However, for small α = 0.1 robustness is achieved even for small Np yielding less computational burden than for larger prediction horizons.

7. Acknowledgement

This work was supported by the project "SMART MSR" (FFG, No. 832103) in cooperation with evon GmbH.

Appendix A

The coefficients for the linear system models in (2), (17)–(19) in Sections 3.1 and 3.2 are given in Table A.8.

For the time-continuous linear PWA model (22), the system matrices are derived from the linearized physical first order model, (2), (17)–(19) in SubSections 3.1 and 3.2 where the coefficients in Table A.8 give the matrix entries.

$$A_{1,c} = \begin{pmatrix} 0 & 0 \\ c_6 & c_7 \end{pmatrix}$$

$$B_{1,c} = \begin{pmatrix} 0 & \frac{1}{r^2\pi\rho} & -\frac{1}{r^2\pi\rho} & 0 & 0 \\ c_3 & c_4 & c_5 & 0 & 0 \end{pmatrix}$$

$$C_{1,c} =$$

$$D_{1,c} = \begin{pmatrix} c_8 \cdot cp & 0 & c_9 \cdot cp & 0 & 0 \\ 1 & 0 & 0 & 0 & 0 \\ 0 & 0 & 0 & c_1 \cdot cp & c_2 \cdot cp \end{pmatrix}$$

$$A_{2,c} = \begin{pmatrix} 0 & 0 \\ 0 & \frac{-2k}{r\rho \cdot cp} \end{pmatrix}$$

$$B_{2,c} = \begin{pmatrix} 0 & \frac{1}{r^2\pi\rho} & -\frac{1}{r^2\pi\rho} & 0 & 0 \\ 0 & 0 & 0 & 0 & 0 \end{pmatrix}$$

$$C_{2,c} = \begin{pmatrix} 0 & c_{17} \cdot cp \\ 0 & c_{13} \\ 0 & 0 \end{pmatrix}$$

$$D_{2,c} = \begin{pmatrix} c_{14} \cdot cp & c_{15} \cdot cp & c_{16} \cdot cp & 0 & 0 \\ c_{10} & c_{11} & c_{12} & 0 & 0 \\ 0 & 0 & 0 & c_1 \cdot cp & c_2 \cdot cp \end{pmatrix}$$

$$A_{3,c} = \begin{pmatrix} 0 & 0 \\ 0 & \frac{-2k}{r\rho \cdot cp} \end{pmatrix}$$

$$B_{3,c} = \begin{pmatrix} 0 & \frac{1}{r^2\pi\rho} & -\frac{1}{r^2\pi\rho} & 0 & 0 \\ 0 & 0 & 0 & 0 & 0 \end{pmatrix}$$

$$C_{3,c} = \begin{pmatrix} 0 & c_{18} \cdot cp \\ 0 & 1 \\ 0 & 0 \end{pmatrix}$$

$$D_{3,c} = \begin{pmatrix} 0 & 0 & c_{19} \cdot cp & 0 & 0 \\ 0 & 0 & 0 & 0 & 0 \\ 0 & 0 & 0 & c_1 \cdot cp & c_2 \cdot cp \end{pmatrix}$$

The matrices for the time-discrete system are derived by Laplace transformation for $t_s = 1$:

Table A.8
Coefficients of linearized system model.

c_1	$\dot{m}_{FC}\|_o$
c_2	$(T_{FC,s} - T_{FC,r})\|_o$
c_3	$(\dot{m}_{HP} - \dot{m}_{TABS})/(z_h \cdot r^2\pi)\|_o$
c_4	$(T_{HP} - T_h)/(z_h \cdot r^2\pi)\|_o$
c_5	$(T_h - T_{HP})/(z_h \cdot r^2\pi)\|_o$
c_6	$((\dot{m}_{TABS} - \dot{m}_{HP})(T_{HP} - T_h) \cdot r^2\pi)/(z_h \cdot r^2\pi)^2\|_o$
c_7	$((\dot{m}_{TABS} - \dot{m}_{HP})/(z_h \cdot r^2\pi) - (2r\pi \cdot k)/(r^2\pi \cdot cp))\|_o$
c_8	$\dot{m}_{TABS}\|_o$
c_9	$(T_{HP} - T_{TABS,r})\|_o$
c_{10}	$\dot{m}_{HP}/\dot{m}_{TABS}\|_o$
c_{11}	$(T_{HP} - T_h)/\dot{m}_{TABS}\|_o$
c_{12}	$((T_h - T_{HP}) \cdot \dot{m}_{HP})/\dot{m}^2_{TABS}\|_o$
c_{13}	$((\dot{m}_{TABS} - \dot{m}_{HP}) \cdot T_h)/\dot{m}_{TABS}\|_o$
c_{14}	$\dot{m}_{HP}\|_o$
c_{15}	$(T_{HP} - T_h)\|_o$
c_{16}	$(T_h - T_{TABS,r})\|_o$
c_{17}	$(\dot{m}_{TABS} - \dot{m}_{HP})\|_o$
c_{18}	$\dot{m}_{TABS}\|_o$
c_{19}	$(T_h - T_{TABS,r})\|_o$

$$A_i = e^{A_{i,c}t_s}, \tag{A.1}$$

$$B_i = \int_0^{t_s} e^{A_{i,c}\zeta} B_{i,c} d\zeta = \Psi B, \tag{A.2}$$

with (A.3)

$$\Psi = A_{i,c}^{-1}(e^{A_{i,c}t_s} - I), \tag{A.4}$$

$$C_i = C_{i,c}, \tag{A.5}$$

$$D_i = D_{i,c}. \tag{A.6}$$

References

[1] I.E. Agency, Energy efficiency policies for new buildings [cited 2015-01-21]. <http://www.iea.org/publications/freepublications/publication/Building_Codes.pdf>.

[2] Dagdougui H, Minciardi R, Ouammi A, Robba M, Sacile R. Modeling and optimization of a hybrid system for the energy supply of a "green" building. Energy Convers Manage 2012;64:351–63.

[3] Sun Y, Wang S, Xiao F, Gao D. Peak load shifting control using different cold thermal energy storage facilities in commercial buildings: a review. Energy Convers Manage 2013;71:101–14.

[4] Figueiredo J, Martins J. Energy production system management-renewable energy power supply integration with building automation system. Energy Convers Manage 2010;51(6):1120–6.

[5] Prívara S, Vána Z, Cigler J, Oldewurtel F, Komárek J. Role of mpc in building climate control. Comput Aided Chem Eng 2011;29:728–32.

[6] Privara S, Cigler J, Váňa Z, Oldewurtel F, Sagerschnig C, Žáčeková E. Building modeling as a crucial part for building predictive control. Energy Build 2013;56:8–22.

[7] Oldewurtel F, Parisio A, Jones CN, Gyalistras D, Gwerder M, Stauch V, et al. Use of model predictive control and weather forecasts for energy efficient building climate control. Energy Build 2012;45:15–27.

[8] Killian M, Mayer B, Kozek M. Hierachical fuzzy mpc concept for building heating control.

[9] Bemporad A, Morari M. Control of systems integrating logic, dynamics, and constraints. Automatica 1999;35(3):407–27.

[10] Ma Y, Borrelli F, Hencey B, Coffey B, Bengea S, Haves P. Model predictive control for the operation of building cooling systems. IEEE Trans Control Syst Technol 2012;20(3):796–803.

[11] Berkenkamp F, Gwerder M. Hybrid model predictive control of stratified thermal storages in buildings. Energy Build 2014;84:233–40.

[12] Široký J, Oldewurtel F, Cigler J, Prívara S. Experimental analysis of model predictive control for an energy efficient building heating system. Appl Energy 2011;88(9):3079–87.

[13] Parisio A, Rikos E, Glielmo L. A model predictive control approach to microgrid operation optimization. IEEE Trans Control Syst Technol 2014;22(5):1813–27.

[14] Parisio A, Rikos E, Tzamalis G, Glielmo L. Use of model predictive control for experimental microgrid optimization. Appl Energy 2014;115:37–46.

[15] Henze GP, Kalz DE, Felsmann C, Knabe G. Impact of forecasting accuracy on predictive optimal control of active and passive building thermal storage inventory. HVAC&R Res 2004;10(2):153–78.

[16] Mayer B, Killian M, Kozek M. Cooperative and hierarchical fuzzy mpc for building heating control. In: IEEE International conference on fuzzy systems (FUZZ-IEEE), 2014. IEEE; 2014. p. 1054–9.

[17] Mayer B, Killian M, Kozek M. Modeling workflow for a building model for control purposes. In: 3rd International conference on systems and control (ICSC), 2013. IEEE; 2013. p. 551–6.
[18] Camacho EF, Alba CB. Model predictive control. Springer Science & Business Media; 2013.
[19] Vrettos E, Lai K, Oldewurtel F, Andersson G. Predictive control of buildings for demand response with dynamic day-ahead and real-time prices. In: Control conference (ECC), 2013 european. IEEE; 2013. p. 2527–34.
[20] Lofberg J. Yalmip: a toolbox for modeling and optimization in matlab. In: IEEE international symposium on computer aided control systems design, 2004. IEEE; 2004. p. 284–9.
[21] Gurobi optimizer reference manual [online] (2014) [cited 2014-11-02].
[22] Borrelli F, Bemporad A, Morari M. Predictive Control for linear and hybrid systems. Cambridge University Press, In press; 2014 [cited 2014-11-20]. <http://www.mpc.berkeley.edu/mpc-course-material>.

Curriculum Vitae

Personal Information

Name	Dipl.-Ing. Michaela Killian
Date of birth	14th of June, 1988
Birthplace	Korneuburg
Citizenship	Austria
Gender	Female
Adress	Hauptstraße 35, 2000 Stockerau

Education

08/2012 -	Vienna University of Technology Doctoral studies in Mechanical Engineering
10/2006 - 06/2012	Vienna University of Technology Diploma studies in Technical Mathematics Specialization in statistics and mathematical methods in economics Final examination passed on June 12th, 2012
09/2002 - 06/2006	Erzbischöfliches Gymnasium, Hollabrunn (secondary school) Final secondary-school examinations passed on June 7th, 2006

Diploma Thesis

Title	Non-linear incidence functions in mathematical epidemiology
Supervisor	Univ.Prof. Dr.techn. Vladimir Veliov

Honors and Awards

12/2015	Nomination: FEMtech expert of December 2015

Professional Work Experience

08/2012 -	Project assistant at Vienna University of Technology Institute of Mechanics and Mechatronics Division of Control and Process Automation
03/2012 – 06/2012	Student assistant at Vienna University of Technology Institute of Statistics and Mathematical Methods in Economics Division of Econometrics and System Theory
08/2012 – 10/2012	6-week internship at Kapsch CarrierCom AG, Vienna Technical Department for IT-Solutions
07/2011 – 08/2011	4-week internship at Kapsch CarrierCom AG, Vienna Technical Department for IT-Solutions

IT Skills

Operation systems	Windows
Office	Microsoft Office, LaTeX
Programming	Matlab, R
Mathematics	Matlab, R, Maple

Languages

German	native language
English	fluent in written and spoken

Dead languages

Latin

Leisure Interests

Traveling, reading, cooking and baking, horseback riding/equestrian

List of scientific publications

International Journals:

1. M. Killian, B. Mayer, A. Schirrer, M. Kozek. Cooperative Fuzzy Model Predictive Control. *IEEE Transactions on Fuzzy Systems*, 2015, ISSN: 1063-6706, article in press. DOI: 10.1109/TFUZZ.2015.2463674

2. M. Killian, B. Mayer, A. Schirrer, M. Kozek. Verteilte kooperative modellprädiktive Temperaturregelung für komplexe Gebäude. *e&i Elektrotechnik und Informationstechnik, Springer Verlag*, Volume 132, 2015, pages 474–480, ISSN: 1613-7620. DOI: 0.1007/s00502-015-0374-6

3. M. Killian, B. Mayer, M. Kozek. Effective fuzzy black-box modeling for building heating dynamics. *Energy and Buildings* , Volume 96, 2015, pages 175–186, ISSN: 0378-7788. DOI: 10.1016/j.enbuild.2015.02.057

4. B. Mayer, M. Killian, M. Kozek. Management of hybrid energy supply systems in buildings using mixed-integer model predictive control. *Energy Conversion and Management*, Volume 98, 2015, pages 470–483, ISSN: 0196-8904. DOI: 10.1016/j.enconman.2015.02.076

5. M. Killian, B. Mayer, M. Kozek. Cooperative Fuzzy Model Predictive Control for Heating and Cooling of Buildings. *Energy and Buildings*, Volume 112, 2016, pages 130–140, ISSN: 0378-7788. DOI: 10.1016/j.enbuild.2015.12.017

6. B. Mayer, M. Killian, M. Kozek. A branch and bound approach for building cooling supply control with hybrid MPC. *Energy and Buildings*, ISSN: 0378-7788, submitted.

Talks and Presentations on International Conferences:

1. B. Mayer, M. Killian, M. Kozek. Mixed-integer model predictive control for heating and cooling supply in an office building. In Proc. of European Control Conference 2016 (ECC'16), June 29 – July 1, 2016, Aalborg, Denmark, invited paper for special session, submitted.

2. M. Killian, B. Mayer, M. Mayer, M. Kozek. Eine flexible Methodik für die modellbasierte prädiktive Regelung komplexer Gebäude. In Proc. of International Congress e-nova: "Nachhaltige Gebäude", November 26–27, 2015, Pinkafeld, Austria, invited paper for special session, ISBN: 978-3-7011-0350-8.

3. M. Killian, B. Mayer, M. Kozek. Hierarchical Fuzzy MPC Concept for Building Heating Control. In Proc. of *19th IFAC World Congress (IFAC'14)*, August 24–29, 2014, Cape Town, South Africa.
DOI: 10.3182/20140824-6-ZA-1003.00772

4. B. Mayer, M. Killian, M. Kozek. Cooperative and Hierarchical Fuzzy MPC for Building Heating Control. In Proc. of *2014 IEEE World Congress on Computational Intelligence; Fuzz-IEEE*, July 06–11, 2014, Beijing, China.
DOI: 10.1109/FUZZ-IEEE.2014.6891573

5. M. Killian, S. Grosswindhager, M. Kozek, B. Mayer. Pre-processing of Partition Data for Enhancement of LOLIMOT. In Proc. of *8th EUROSIM Congress on Modelling and Simulation (EUROSIM 2013)*, September 10–13, 2013, Cardiff, Wales, UK.
DOI: 10.1109/EUROSIM.2013.56

6. B. Mayer, M. Killian, M. Kozek. Modeling Workflow for a Building Model for Control Purposes. In Proc. of *3rd International Conference on Systems and Control (ICSC'13)*, October 29–31, 2013, Algiers, Algeria.

7. J. Kopriva, J. Kunovsky, M. Drozdova, V. Satek, M. Killian. Parallel system based on the RNS. In Proc. of *12th Conference Informatics'2013*, November 05–07, 2013, Spisská Nová Ves, Slovakia.

Talks and Presentations:

1. M. Mayer, B. Mayer, M. Killian, M. Kozek. Nichtlineare hierarchische modellprädiktive Klimaregelung für komplexe Gebäude.
Vortrag: Mechatroniktag des Instituts für Mechanik und Mechatronik 2015, Wien; 30.09.2015.